

Measurement of the $Y(1S)$, $Y(2S)$, and $Y(3S)$ cross sections in pp collisions at $\sqrt{s} = 7$ TeV

The CMS Collaboration*

Abstract

The $Y(1S)$, $Y(2S)$, and $Y(3S)$ production cross sections are measured using a data sample corresponding to an integrated luminosity of $35.8 \pm 1.4 \text{ pb}^{-1}$ of proton-proton collisions at $\sqrt{s} = 7$ TeV, collected with the CMS detector at the LHC. The Y resonances are identified through their decays to dimuons. Integrated over the Y transverse momentum range $p_T^Y < 50 \text{ GeV}/c$ and rapidity range $|y^Y| < 2.4$, and assuming unpolarized Y production, the products of the Y production cross sections and dimuon branching fractions are

$$\begin{aligned}\sigma(\text{pp} \rightarrow Y(1S)X) \cdot \mathcal{B}(Y(1S) \rightarrow \mu^+\mu^-) &= (8.55 \pm 0.05_{-0.50}^{+0.56} \pm 0.34) \text{ nb}, \\ \sigma(\text{pp} \rightarrow Y(2S)X) \cdot \mathcal{B}(Y(2S) \rightarrow \mu^+\mu^-) &= (2.21 \pm 0.03_{-0.14}^{+0.16} \pm 0.09) \text{ nb}, \\ \sigma(\text{pp} \rightarrow Y(3S)X) \cdot \mathcal{B}(Y(3S) \rightarrow \mu^+\mu^-) &= (1.11 \pm 0.02_{-0.08}^{+0.10} \pm 0.04) \text{ nb},\end{aligned}$$

where the first uncertainty is statistical, the second is systematic, and the third is from the uncertainty in the integrated luminosity. The differential cross sections in bins of transverse momentum and rapidity, and the cross section ratios are presented. Cross section measurements performed within a restricted muon kinematic range and not corrected for acceptance are also provided. These latter measurements are independent of Y polarization assumptions. The results are compared to theoretical predictions and previous measurements.

Published in Physics Letters B as doi:10.1016/j.physletb.2013.10.033.

1 Introduction

No existing theoretical approach successfully reproduces both the differential cross section and the polarization measurements of the J/ψ or Y states [1] in hadron collisions. Studying quarkonium hadroproduction at high center-of-mass energies and over a wide rapidity and transverse momentum range will facilitate significant improvements in our understanding of the processes involved.

Measurements of Y production have been performed by several experiments [1–5]. The first measurement at $\sqrt{s} = 7$ TeV at the Large Hadron Collider (LHC) was reported by the Compact Muon Solenoid (CMS) Collaboration [6], using a data sample corresponding to an integrated luminosity of 3 pb^{-1} . This paper constitutes an extension of that first cross section measurement, using a larger, independent sample, corresponding to an integrated luminosity of $35.8 \pm 1.4 \text{ pb}^{-1}$ collected in 2010.

Two different approaches to the measurement of the $Y(nS)$ production cross sections, where $n=1-3$, are pursued in this paper. In each approach, the Y is reconstructed in the decay $Y \rightarrow \mu^+ \mu^-$. In the first approach, a cross section measurement corrected for detector acceptance and efficiencies is presented, as in Ref. [6]. This cross section measurement depends on the spin alignment of the Y . No net polarization is assumed for the main results. To show the sensitivity of the results to the polarization and to allow for interpolation, we provide measurements for other polarization assumptions. Recently, the CMS Collaboration has measured the polarizations of the $Y(nS)$ in pp collisions at $\sqrt{s} = 7$ TeV, which are found to be small [7]. Cross section measurements are also provided in the Y transverse momentum (p_T^Y) and rapidity (y^Y) ranges matching those of the polarization measurement, and these polarization results are used to estimate the associated systematic uncertainty. The motivation for the second approach, also used by the ATLAS Collaboration [5], is to eliminate the dependence of the measured cross sections on the spin alignment of the Y . In this second approach, a fiducial cross section measurement, corrected for detector efficiencies but not for acceptance, is presented. This cross section is defined within a muon kinematic range.

The paper is organized as follows. Section 2 contains a short description of the CMS detector. Section 3 presents the data collection, the trigger and offline event selections, and the reconstruction of the Y resonances. Section 4 describes the measurement technique. The detector acceptance and efficiencies to reconstruct Y resonances that decay to two muons are discussed in Sections 5 and 6. The evaluation of systematic uncertainties in the measurements is described in Section 7. In Sections 8 and 9, the $Y(nS)$ fiducial and acceptance-corrected cross section results and comparisons to other experiments and to theoretical predictions are presented.

2 CMS detector

The central feature of the CMS apparatus is a superconducting solenoid, of 6 m inner diameter, producing a magnetic field of 3.8 T. Within the superconducting solenoid volume are a silicon pixel and strip tracker, a lead tungstate crystal electromagnetic calorimeter, and a brass/scintillator hadron calorimeter. Muons are detected by three types of gas-ionization detectors embedded in the magnet steel return yoke surrounding the solenoid: drift tubes, cathode strip chambers, and resistive-plate chambers. The muon measurement covers the pseudorapidity range $|\eta^\mu| < 2.4$, where $\eta = -\ln[\tan(\theta/2)]$ and the polar angle θ is measured from the axis pointing along the counterclockwise-beam direction. The muon transverse momentum measurement, p_T^μ , based on information from the silicon tracker alone, has a resolution of about 1% for a typical muon in this analysis. The two-level CMS trigger system selects events

of interest for permanent storage. The first trigger level, composed of custom hardware processors, uses information from the calorimeter and muon detectors to select events in less than $3.2 \mu\text{s}$. The high-level trigger software algorithms, executed on a farm of commercial processors, further reduce the event rate using information from all detector subsystems. A detailed description of the CMS detector can be found in Ref. [8].

3 Data selection and event reconstruction

The data sample was collected in 2010, in low instantaneous luminosity conditions, allowing a less restrictive selection at the trigger level in comparison to subsequent data taking periods. Data are included in the analysis for all periods where the silicon tracker, the muon detectors, and the trigger were performing well and the luminosity information was available. In the first data-taking period, the trigger requires the detection of two muons without an explicit p_{T}^{μ} requirement. The minimum distance between each reconstructed muon trajectory and the average proton-proton interaction point in the transverse plane must be less than 2 cm. In the second data-taking period, characterized by higher LHC instantaneous luminosities, additional requirements are imposed at trigger level: the two muons must have opposite charge and an invariant mass in the mass range $1.5 < M_{\mu\mu} < 14.5 \text{ GeV}/c^2$. All three muon systems take part in the trigger decision. In the first (second) data-taking period the trigger selected about 2 (5) million events.

Simulation is employed to design the offline selection, assess the detector acceptance, and study systematic effects. The $Y(nS)$ events are simulated using PYTHIA 6.412 [9], which generates events based on the leading-order color-singlet and color-octet mechanisms, with nonrelativistic quantum chromodynamics (QCD) matrix elements, tuned by comparing calculations with CDF data [10], and applying the normalization and wave functions recommended in Ref. [11]. The underlying-event simulation uses the CTEQ6L1 parton distribution functions [12]. Since PYTHIA does not provide a simulation of $Y(2S)$ and $Y(3S)$, the predictions for these states are obtained by replacing the $Y(1S)$ mass in the simulation with the $Y(2S)$ and $Y(3S)$ masses, respectively. Contributions from the decays of higher-mass bottomonium states (feed-down) are included in the simulation. For simulating the $Y(2S)$ feed-down component, the masses of the 2P states replace the corresponding 1P states. For the $Y(3S)$ the feed-down is assumed to be small and is not simulated. Final-state radiation (FSR) is implemented using PHOTOS [13, 14]. The response of the CMS detector is simulated with a GEANT4-based [15] Monte Carlo (MC) simulation program. Simulated events are processed with the same reconstruction and trigger algorithms used for data.

The offline selection starts from Y candidates reconstructed from pairs of oppositely charged muons with invariant mass between 7 and $14 \text{ GeV}/c^2$. The muons are required to have one or more reconstructed track segments in the muon systems that are well matched to the extrapolated position of a track reconstructed in the silicon tracker. Quality criteria are applied to the tracks to reject muons from kaon and pion decays. Tracks are required to have at least 11 hits in the silicon tracker, at least one of which must be in the pixel detector, and a track-fit χ^2 per degree of freedom smaller than 5. In addition, tracks are required to extrapolate back to a cylindrical volume of radius 2 mm and length 25 cm, centered on the pp interaction region and parallel to the beam line. After offline confirmation of the trigger selection, muons are required

to satisfy a kinematic threshold that depends on pseudorapidity

$$\begin{aligned}
 p_{\text{T}}^{\mu} > 3.75 \text{ GeV}/c & \quad \text{if} \quad |\eta^{\mu}| < 0.8, \\
 p_{\text{T}}^{\mu} > 3.5 \text{ GeV}/c & \quad \text{if} \quad 0.8 < |\eta^{\mu}| < 1.6, \\
 p_{\text{T}}^{\mu} > 3.0 \text{ GeV}/c & \quad \text{if} \quad 1.6 < |\eta^{\mu}| < 2.4.
 \end{aligned} \tag{1}$$

These kinematic acceptance criteria are chosen to ensure that the trigger and muon reconstruction efficiencies are high and not rapidly changing within the phase space of the analysis. The longitudinal separation between the two muons along the beam axis is required to be less than 2 cm. The two muon helices are fit with a common vertex constraint, and events are retained if the fit χ^2 probability is larger than 0.1%. If multiple dimuon candidates are found in the same event, the candidate with the smallest vertex-fit χ^2 probability is retained; the fraction of Y candidates rejected by this requirement is about 0.6%.

4 Measurement of the inclusive differential cross section

The product of the Y(nS) differential cross section, σ , and the dimuon branching fraction, \mathcal{B} , is determined from the signal yield $N_{\text{Y(nS)}}^{\text{cor}}$, corrected by the acceptance \mathcal{A} and the efficiency ϵ , using

$$\frac{d\sigma(\text{pp} \rightarrow \text{Y(nS)X})}{dp_{\text{T}}^{\text{Y}} dy^{\text{Y}}} \cdot \mathcal{B}(\text{Y(nS)} \rightarrow \mu^+ \mu^-) = \frac{N_{\text{Y(nS)}}^{\text{cor}}(p_{\text{T}}^{\text{Y}}, y^{\text{Y}}; \mathcal{A}, \epsilon)}{\mathcal{L} \cdot \Delta p_{\text{T}}^{\text{Y}} \cdot \Delta y^{\text{Y}}}, \tag{2}$$

where \mathcal{L} is the integrated luminosity of the data set, and $\Delta p_{\text{T}}^{\text{Y}}$ and Δy^{Y} are the bin widths of the Y transverse momentum and rapidity, respectively. The rapidity is defined as $y = \frac{1}{2} \ln\left(\frac{E+p_z c}{E-p_z c}\right)$, where E is the energy and p_z is the momentum component parallel to the beam axis of the muon pair.

The Y(nS) yields are extracted via an extended unbinned maximum-likelihood fit to the dimuon invariant-mass spectrum. The measured mass line shape of each Y state is parametrized by a ‘‘Crystal Ball’’ (CB) [16] function, which consists of a Gaussian core portion and a power-law low-side tail to allow for FSR, with the low-mass tail parameters fixed from MC simulation [6]. The three Y(nS) states are fitted simultaneously since the three resonances overlap in the measured dimuon mass range. The resolution, given by the standard deviation of the Gaussian component of the CB, is a free parameter in the fit, but is constrained to scale with the ratios of the resonance masses. However, the mass resolution varies with Y rapidity. Consequently, a single resolution term in the Gaussian component of the CB is not sufficient to describe the data. For this reason, in the p_{T}^{Y} intervals with sufficient statistical precision, the sum of two CBs with the same mean and FSR tail parameters, but different resolutions, is used for each Y state. The fitted resolution is consistent with expectation from MC at the few percent level. The Y(nS) mass ratios are fixed to their world-average values [17]. The background in the 7–14 GeV/ c^2 mass-fit range is nonpeaking and in some kinematic bins has a turn-on caused by the trigger and offline requirements. In general, the product of an error function and an exponential is chosen to describe the background [18], except when, for bins with poor statistical precision, a single exponential function is used. The dimuon invariant-mass spectra in the Y(nS) region, before accounting for acceptance and efficiencies, are shown in Fig. 1 and in Appendix A.

Following Ref. [6], given the significant p_{T}^{μ} and η^{μ} dependencies of the acceptances and efficiencies of the muons from Y(nS) decays, we correct for them on a candidate-by-candidate basis before performing the mass fit to obtain $N_{\text{Y(nS)}}^{\text{cor}}$ used in Eq. (2). The fiducial differential cross

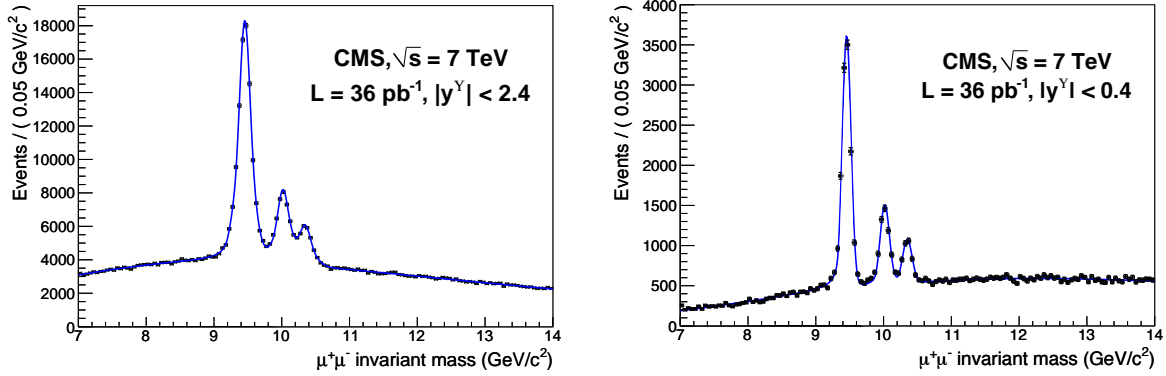


Figure 1: The dimuon invariant-mass distribution in the vicinity of the $Y(nS)$ resonances for $|y^Y| < 2.4$ (left) and for the subset of events where the rapidity of the $Y(nS)$ satisfies $|y^Y| < 0.4$ (right). The solid lines represent the results of the fits to the signal-plus-background functions described in the text.

section is determined from the efficiency-corrected signal yield within the kinematic region defined in Eq. (1).

5 Acceptance

The $Y \rightarrow \mu^+ \mu^-$ acceptance of the CMS detector is the product of two terms. The first is, for a given p_T^Y and y^Y , the fraction of dimuon decays in which both muons are within the phase space specified in Eq. (1). The second is the probability that when there are only two muons in the event both can be reconstructed in the tracker without requiring the quality criteria. Both components are evaluated by simulation and parametrized as a function of p_T^Y and y^Y . The second component is close to unity, as verified in simulation and data.

Following Ref. [6], the acceptance is defined by the ratio

$$\mathcal{A}(p_T^Y, y^Y) = \frac{N^{\text{reco}}(p_T^Y, y^Y | \text{Si tracks satisfying Eq. (1)})}{N^{\text{gen}}(p_T^Y, y^Y)}, \quad (3)$$

and is computed in small bins in (p_T^Y, y^Y) . The parameter N^{gen} is the number of Y particles generated within a given (p_T^Y, y^Y) bin, while N^{reco} is the number of Y particles with reconstructed (p_T^Y, y^Y) values within that bin, and having the silicon tracks satisfying Eq. (1). The (p_T^Y, y^Y) values represent the generated and reconstructed values, respectively in the denominator and the numerator, thus accounting also for the effect of detector resolution in the definition of \mathcal{A} . In addition the numerator requires the two tracks to be reconstructed with opposite charges and have an invariant mass within the Y mass-fit range of 7–14 GeV/c^2 .

The acceptance is evaluated with a signal MC simulation sample in which the Y decay to two muons is generated with the EVTGEN [19] package, including FSR. There are no particles in the event besides the Y , its daughter muons, and the FSR photons. The Y mesons are generated uniformly in p_T^Y and y^Y . This sample is then simulated and reconstructed with the CMS detector simulation software to assess the effects of multiple scattering and finite resolution of the detector. An acceptance map with the assumption of zero Y polarization can be found in Ref. [6]. Systematic uncertainties arising from the dependence of the cross section measurement on the MC simulation description of the p_T spectrum and resolution are evaluated in Section 7. The acceptance is calculated as a two-dimensional grid in p_T^Y and $|y^Y|$ using bin sizes of 0.1 in

rapidity and $0.5 \text{ GeV}/c$ in p_T^Y for $0 < p_T^Y < 2 \text{ GeV}/c$ and $1 \text{ GeV}/c$ for $2 < p_T^Y < 50 \text{ GeV}/c$. The corresponding correction is then performed on a candidate-by-candidate basis. The acceptance depends on the resonance mass; the $Y(3S)$ gives rise to higher-momenta muons which results in a roughly 10% larger acceptance for the $Y(3S)$ than for the $Y(1S)$. Consequently, the corrected yield for each of the $Y(nS)$ resonances is obtained from a fit in which the corresponding $Y(nS)$ acceptance is employed. The acceptance decreases with rapidity, and there are no accepted events beyond $|y^Y| = 2.4$. The acceptance has a minimum near $p_T^Y = 5 \text{ GeV}/c$, as a result of the softer muon failing the p_T^μ cut. The polarization of the Y strongly influences the muon angular distributions and could be a function of p_T^Y . In order to show the sensitivity of the result to the $Y(nS)$ polarization and to allow for interpolation, we provide cross section measurements for unpolarized (default) and 6 polarization scenarios in which the polar anisotropy parameter λ_θ [7] is changed from fully longitudinal to fully transverse polarization, corresponding to $\lambda_\theta = -1, -0.5, -0.25, 0.25, 0.5, 1$, in both the center-of-mass helicity and Collins–Soper [20] reference frames. Cross section measurements for the p_T^Y and y^Y ranges used in Ref. [7] are also provided in Fig. 4. In that case, the polarization results from Ref. [7] are used to estimate the corresponding systematic uncertainty.

6 Efficiency

The total muon efficiency is factorized into the three conditional terms,

$$\varepsilon = \varepsilon(\text{trig}|\text{id}) \times \varepsilon(\text{id}|\text{track}) \times \varepsilon(\text{track}|\text{accepted}) \equiv \varepsilon_{\text{trig}} \times \varepsilon_{\text{id}} \times \varepsilon_{\text{track}}. \quad (4)$$

The tracking efficiency, $\varepsilon_{\text{track}}$, combines the efficiency that the accepted track of a muon from a $Y(nS)$ decay is reconstructed in the presence of additional particles in the silicon tracker, as determined with a track-embedding technique [21], and the efficiency for the track to satisfy the track-quality criteria. The efficiency of the track-quality criteria [21] is nearly uniform in p_T and η and has an average value of $(98.66 \pm 0.05)\%$, as measured in Ref. [6], with negligible dependence on instantaneous luminosity. The muon identification efficiency, ε_{id} , is the probability that the silicon track caused by a muon is correctly identified as a muon. The efficiency that an identified muon satisfies the trigger is denoted by $\varepsilon_{\text{trig}}$. The track quality, muon trigger, and muon identification efficiencies are determined using the tag-and-probe (T&P) technique. The T&P implementation follows Ref. [6], and utilizes a J/ψ data sample as it provides a statistically independent, large-yield dimuon sample.

The Y efficiency is estimated from the product of the single-muon efficiencies. A factor, ρ , is used as a correction to this factorization hypothesis, and to account for possible biases introduced by the T&P efficiency measurement with the J/ψ sample. We define ρ as

$$\rho(p_T^Y, |y^Y|) = \frac{\varepsilon(Y)}{\varepsilon(\mu^+_{J/\psi}) \cdot \varepsilon(\mu^-_{J/\psi})}, \quad (5)$$

where $\varepsilon(Y)$ is the efficiency for a Y to pass the trigger and muon identification selections, and $\varepsilon(\mu^+_{J/\psi})$ and $\varepsilon(\mu^-_{J/\psi})$ are the corresponding efficiencies for positively and negatively charged muons from a J/ψ decay with the same p_T and η as a muon in the Y decay. The Y efficiency is taken from MC simulation generator-level matching, which is performed by associating the two generated muons from the Y with the reconstructed muons or trigger objects. The single-muon efficiencies are from the T&P method utilizing a J/ψ MC simulation sample. Finally, the efficiency of the vertex-fit χ^2 probability requirement is determined from data to be $(99.16 \pm 0.09)\%$ and constant over the entire kinematic range.

7 Systematic uncertainties

Systematic uncertainties in the cross section measurement stem from variations in the acceptance determination, potential residual inaccuracies in the efficiency measurement, the method of yield extraction, and the integrated luminosity. For each uncertainty, we give below in parentheses a representative range of values corresponding to the variation with p_T^Y . The acceptance is varied in the dimuon invariant-mass fit coherently by ± 1 standard deviation, reflecting the uncertainty from the finite MC simulation statistics (0.3–1%). The acceptance is sensitive to biases in track momentum and differences in resolution between simulation and data. To determine the effect on the Y acceptance, we introduce a track p_T bias of 0.2%, chosen based on the momentum scale biases seen in simulation and data [22]. We also vary the transverse momentum resolution by $\pm 10\%$, corresponding to the uncertainty in the resolution measurement using J/ψ in data. This reflects a conservative estimation of resolution effects. The acceptance map as a function of p_T^Y and $|y^Y|$ is then recalculated, and the systematic uncertainty is the difference in the resulting cross sections when using the perturbed acceptance map rather than the nominal one (0.0–0.7%). Imperfect knowledge of the production p_T spectrum of the Y resonances at $\sqrt{s} = 7$ TeV contributes a systematic uncertainty. Using either a flat p_T distribution or the p_T distribution from PYTHIA, which is found to be consistent with the previously measured p_T distribution [6], gives rise to a systematic uncertainty (0.2%). FSR is incorporated into the simulation using the PHOTOS algorithm. To estimate the systematic uncertainty associated with this procedure, the acceptance is calculated without FSR, and 20% of the difference is taken as the uncertainty (0.1–0.8%), based on a study in Ref. [14].

Variation of the measured factorized efficiencies within their uncertainties also gives rise to a systematic uncertainty. The systematic uncertainties for the tracking efficiency (0.3–0.4%), muon identification efficiency (2–4%), and trigger efficiency (1–5%) are evaluated conservatively by coherently varying all bins by ± 1 standard deviation. The systematic uncertainty arising from the choice of bin size for the efficiencies is determined by fitting the efficiency turn-on curves as a function of muon p_T^μ in different $|\eta^\mu|$ regions using a hyperbolic tangent function and taking the muon efficiencies from the function instead of the binned value to compute the cross section (1–4%). The intrinsic bias from the T&P method, including possible bias in the T&P technique and differences in the J/ψ and Y kinematics, as well as the possible misestimation of the double-muon Y efficiency as the product of the single-muon efficiencies, are all included in the correction factor ρ . The average rho factor value is 1.07 and the full range of variation is from 0.92 to 1.20. As a conservative estimate of the systematic uncertainty associated with ρ , the measurements are repeated with a correction factor of unity and half of the variation is taken as the systematic uncertainty (2–5%).

In addition, systematic uncertainties may arise from differences between the dimuon invariant-mass distribution in the data and the probability density functions (PDF) chosen for the signal and background components in the fit. Since the CB parameters, which describe the radiative tail of each signal resonance, are fixed from MC simulation in the fit to the data, we fit the full data set with free tail parameters and use the values obtained to fix the tail parameters for the yield extraction in the $(\Delta p_T^Y, \Delta y^Y)$ bins. The difference in the fit yield is taken as a systematic uncertainty (1–4%). We vary the background PDF by replacing the product of the exponential and error function by a polynomial function, while restricting the fit to the mass range 8–12 GeV/ c^2 (1–5%). The determination of the integrated luminosity is made with an uncertainty of 4% [23]. A summary of systematic uncertainties for the $Y(nS)$ production cross section, integrated over the full transverse momentum (p_T^Y) and rapidity (y^Y) ranges, is shown in Table 1. The largest sources of systematic uncertainty arise from the statistical precision of the efficiency measurements determined from data, the efficiency correction factor ρ , and from

the measurement of the integrated luminosity.

The cross section measurement uses acceptance maps corresponding to different Y polarization scenarios. The values of the resulting cross sections vary approximately linearly by about $\pm 5\%$, $\pm 10\%$, and $\pm 20\%$, respectively, assuming $\lambda_\theta = \pm 0.25$, ± 0.5 , and ± 1 , as shown in Table 2. The cross sections are also measured for $10 < p_T^Y < 50 \text{ GeV}/c$ and $|y^Y| < 1.2$ using the measured $Y(nS)$ polarizations [7] to compute the acceptance corrections. The three anisotropy parameters in the center-of-mass helicity and Collins–Soper frames are varied coherently by ± 1 standard deviation, and the largest positive and negative variations with respect to the nominal (no polarization) case are taken as systematic uncertainties. These are listed in Table 4. They are comparable to, or smaller than, the result of varying the longitudinal or transverse polarizations by setting λ_θ to ± 0.25 for the $Y(1S)$ case, while they are between the results obtained by setting λ_θ to ± 0.25 and ± 0.5 for the $Y(2S)$ and $Y(3S)$. The fiducial cross sections do not depend on the acceptance, the assumed Y polarization, or the associated uncertainties. The definition of the acceptance in Eq. (3) includes reconstructed quantities. The variation in the cross section using only generator-level quantities is less than 1%.

Table 1: Relative systematic uncertainties in the $Y(nS)$ production cross section, integrated over the rapidity range $|y^Y| < 2.4$, times the dimuon branching fraction, in percent. The symbols \mathcal{A} , $\epsilon_{T\&P}$, ϵ_ρ , and PDF refer to the systematic uncertainties arising from the acceptance, tag-and-probe efficiencies, correction factor ρ , and signal-and-background PDF. The remaining systematic uncertainties are summed in the “other” category. The integrated luminosity uncertainty of 4% is not shown. The numbers in parentheses are negative variations.

	p_T (GeV/ c)	\mathcal{A}	$\epsilon_{T\&P}$	ϵ_ρ	PDF	other
Y(1S)	0–50	1.0 (1.0)	5.2 (4.3)	3.4	1.8	0.4 (0.3)
Y(2S)	0–42	1.1 (1.1)	5.5 (4.1)	3.7	2.6	0.4 (0.4)
Y(3S)	0–38	1.2 (1.1)	6.7 (4.9)	4.0	3.8	0.6 (0.5)

Table 2: The fractional change in percent to the central value of the $Y(nS)$ cross section integrated over the rapidity range $|y^Y| < 2.4$, relative to the unpolarized value, for six polarization scenarios in the center-of-mass helicity and Collins–Soper frames. The polarization assumption changes from fully longitudinal to fully transverse polarization as λ_θ changes from -1 to 1 .

	p_T (GeV/ c)	Helicity Frame λ_θ						Collins–Soper Frame λ_θ					
		1	0.5	0.25	-0.25	-0.5	-1	1	0.5	0.25	-0.25	-0.5	-1
Y(1S)	0–50	+19	+10	+5	-5	-11	-24	+16	+8	+4	-5	-9	-19
Y(2S)	0–42	+14	+5	+3	-7	-12	-24	+13	+6	+2	-6	-10	-20
Y(3S)	0–38	+16	+9	+5	-4	-9	-21	+14	+8	+5	-3	-7	-17

8 Differential fiducial cross section measurement and comparison to theory

The fiducial $Y(nS)$ cross sections are determined from the efficiency-corrected signal yields within the muon kinematic range specified by Eq. (1), using Eq. (2) with the acceptance term set to unity. The resulting total fiducial $Y(nS)$ cross sections times dimuon branching fractions at $\sqrt{s} = 7 \text{ TeV}$ for $|y^Y| < 2.4$ are

$$\begin{aligned} \sigma(\text{pp} \rightarrow Y(1S)X) \cdot \mathcal{B}(Y(1S) \rightarrow \mu^+\mu^-) &= (3.06 \pm 0.02_{-0.18}^{+0.20} \pm 0.12) \text{ nb}, \\ \sigma(\text{pp} \rightarrow Y(2S)X) \cdot \mathcal{B}(Y(2S) \rightarrow \mu^+\mu^-) &= (0.910 \pm 0.011_{-0.046}^{+0.055} \pm 0.036) \text{ nb}, \\ \sigma(\text{pp} \rightarrow Y(3S)X) \cdot \mathcal{B}(Y(3S) \rightarrow \mu^+\mu^-) &= (0.490 \pm 0.010_{-0.029}^{+0.029} \pm 0.020) \text{ nb}, \end{aligned}$$

where the first uncertainty is statistical, the second is systematic, and the third is associated with the estimation of the integrated luminosity of the data sample. The integrated results are obtained from the sum of the differential p_T^Y results. The measured cross sections include feed-down from higher-mass bottomonium states.

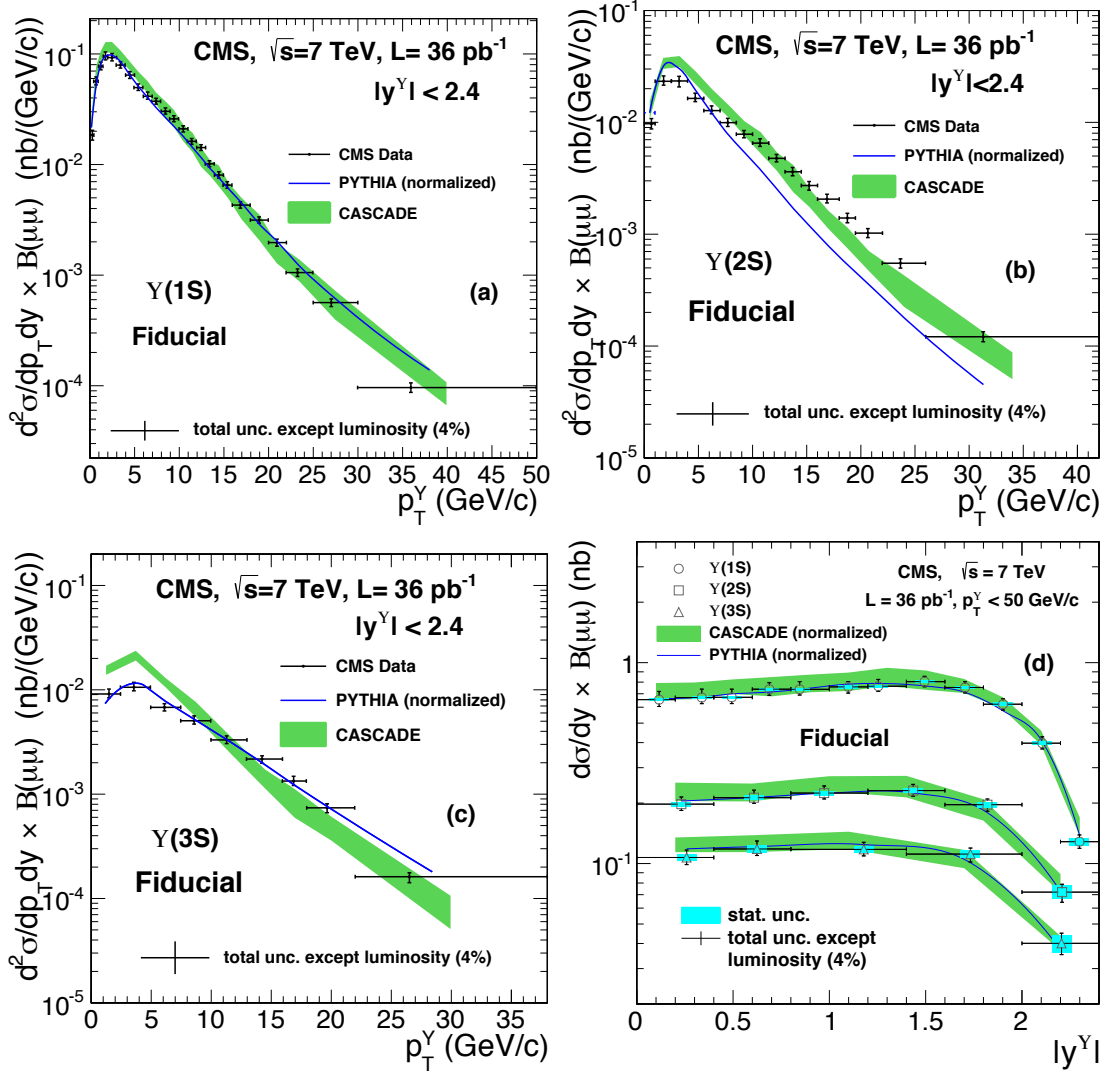


Figure 2: Differential fiducial cross section of (a) Y(1S), (b) Y(2S), and (c) Y(3S) as a function of p_T^Y in the rapidity range $|y^Y| < 2.4$, and comparison to the predictions from CASCADE and PYTHIA. (d) Differential fiducial cross section of the Y(nS) as a function of rapidity and comparison to the predictions from CASCADE and PYTHIA. The PYTHIA prediction is normalized to the measured total cross section, in order to facilitate the comparison of the shape of the dependences. The full CASCADE prediction is shown in (a), (b), and (c); the normalised CASCADE prediction is shown in (d). The bands indicate the estimated uncertainties in the CASCADE prediction.

The Y(nS) differential p_T fiducial cross sections are summarized in Table 3 and plotted in Fig. 2 (a,b,c) and Appendix A. In the figures, $B(Y(nS) \rightarrow \mu^+\mu^-)$ is denoted as $B(\mu\mu)$. The results are also given for six rapidity intervals in Appendix A. Here, and throughout the paper, in figures illustrating differential cross sections, the data points are plotted at the average p_T (or rapidity) of the data in each bin. The p_T^Y dependence of the cross sections has the same trend for all six rapidity intervals. The Y(nS) p_T -integrated, differential rapidity fiducial cross sections,

plotted in Fig. 2 (d) and Appendix A, are all roughly constant from $|y^Y| = 0$ to about 1.6, where they then fall quickly. The ratios of the $Y(nS)$ differential p_T fiducial cross sections, also shown in Appendix A, increase with p_T^Y .

Table 3: The product of the fiducial or acceptance-corrected $Y(nS)$ production cross sections, σ , integrated and differential in p_T^Y , and the respective dimuon branching fraction, \mathcal{B} , integrated over the rapidity range $|y^Y| < 2.4$. The cross sections assume the $Y(nS)$ are unpolarized. The fiducial $Y(nS)$ cross sections are independent of the $Y(nS)$ polarization. The statistical uncertainty (stat.), the sum of the systematic uncertainties in quadrature ($\Sigma_{\text{syst.}}$), and the total uncertainty ($\Delta\sigma$; including stat., $\Sigma_{\text{syst.}}$, and the uncertainty in the integrated luminosity) are in percent. The numbers in parentheses are negative variations.

			Fiducial Cross Section				Cross Section			
	p_T (GeV/c)	mean	$\sigma \cdot \mathcal{B}$ (nb)	stat. σ	$\Sigma_{\text{syst.}}$ σ	$\Delta\sigma$ σ	$\sigma \cdot \mathcal{B}$ (nb)	stat. σ	$\Sigma_{\text{syst.}}$ σ	$\Delta\sigma$ σ
Y(1S)	0–0.5	0.33	0.0440	5.4	8 (8)	11 (11)	0.0859	5.4	8 (7)	11 (10)
	0.5–1	0.77	0.133	3.1	8 (8)	10 (10)	0.263	3.3	8 (7)	9 (9)
	1–1.5	1.26	0.182	2.5	8 (8)	9 (9)	0.374	2.6	8 (8)	9 (9)
	1.5–2	1.75	0.228	2.4	8 (8)	10 (9)	0.505	2.4	9 (8)	10 (9)
	2–3	2.49	0.442	1.6	8 (7)	9 (8)	1.16	1.6	8 (10)	9 (11)
	3–4	3.48	0.374	1.8	6 (6)	8 (7)	1.21	2.1	7 (6)	9 (8)
	4–5	4.48	0.302	1.8	7 (7)	8 (8)	1.084	2.1	7 (6)	8 (8)
	5–6	5.49	0.236	2.0	7 (6)	8 (7)	0.879	1.9	7 (9)	8 (10)
	6–7	6.49	0.195	2.0	8 (7)	9 (9)	0.680	2.6	6 (6)	8 (7)
	7–8	7.49	0.174	2.1	5 (5)	7 (6)	0.556	2.0	6 (5)	7 (7)
	8–9	8.48	0.144	2.3	6 (5)	7 (7)	0.419	2.2	5 (5)	7 (7)
	9–10	9.48	0.1235	2.4	5 (4)	7 (6)	0.331	2.3	5 (4)	7 (6)
	10–11	10.48	0.0988	2.5	6 (5)	8 (7)	0.238	2.5	5 (4)	7 (6)
	11–12	11.49	0.0759	2.8	4 (4)	7 (6)	0.179	2.9	5 (4)	7 (6)
	12–13	12.49	0.0670	2.9	4 (4)	7 (6)	0.145	2.9	5 (4)	7 (7)
	13–14	13.47	0.0477	3.3	5 (4)	7 (7)	0.0990	3.2	4 (5)	7 (7)
	14–15	14.49	0.0381	3.6	5 (5)	7 (7)	0.0750	3.6	5 (5)	8 (7)
	15–16	15.48	0.0312	4.0	5 (4)	8 (7)	0.0595	3.8	5 (5)	7 (7)
	16–18	16.91	0.0412	3.5	5 (5)	7 (7)	0.0732	3.4	5 (5)	7 (7)
	18–20	18.98	0.0296	4.0	5 (4)	7 (7)	0.0500	3.8	5 (4)	7 (7)
20–22	20.94	0.0187	5.1	4 (4)	8 (8)	0.0302	5.1	5 (4)	8 (8)	
22–25	23.30	0.0148	5.8	4 (4)	8 (8)	0.0237	5.6	5 (4)	8 (8)	
25–30	27.03	0.0133	6.1	4 (4)	8 (8)	0.0205	6.0	5 (4)	9 (8)	
30–50	35.97	0.00923	7.8	6 (6)	11 (10)	0.0123	7.4	6 (6)	10 (10)	
0–50	5.34	3.06	0.6	6 (6)	8 (7)	8.55	0.6	7 (6)	8 (7)	
Y(2S)	0–1	0.66	0.0467	6.3	7 (8)	10 (11)	0.0829	5.9	9 (8)	11 (11)
	1–2.5	1.79	0.168	3.4	8 (8)	10 (10)	0.331	3.3	11 (10)	12 (12)
	2.5–4	3.21	0.169	3.1	8 (11)	9 (12)	0.409	3.1	9 (8)	10 (9)
	4–5.5	4.71	0.118	3.3	8 (7)	10 (9)	0.362	3.3	8 (7)	9 (9)
	5.5–7	6.22	0.0917	3.6	6 (5)	8 (8)	0.286	3.6	7 (6)	9 (8)
	7–8.5	7.71	0.0716	3.4	7 (7)	9 (9)	0.212	3.9	7 (7)	9 (9)
	8.5–10	9.21	0.0564	4.0	5 (5)	8 (8)	0.146	4.0	6 (6)	9 (8)
	10–11.5	10.69	0.0470	4.1	6 (5)	8 (8)	0.1123	4.1	6 (6)	9 (8)
	11.5–13	12.21	0.0343	4.6	4 (4)	7 (8)	0.0765	4.6	5 (5)	8 (8)
	13–14.5	13.70	0.0260	5.2	5 (5)	8 (8)	0.0519	5.1	5 (5)	8 (8)
	14.5–16	15.22	0.0196	5.7	4 (6)	8 (9)	0.0376	5.7	5 (7)	9 (10)
	16–18	16.88	0.0198	5.5	6 (5)	9 (8)	0.0373	5.3	6 (5)	9 (8)
	18–19.5	18.76	0.01005	7.5	4 (5)	9 (10)	0.0159	7.4	5 (4)	10 (9)
	19.5–22	20.65	0.0123	6.8	5 (5)	9 (9)	0.0204	6.6	5 (5)	9 (9)
	22–26	23.69	0.0104	7.4	4 (5)	9 (10)	0.0158	7.2	5 (4)	10 (9)
	26–42	31.30	0.00930	8.0	5 (5)	10 (10)	0.0126	7.7	6 (5)	10 (10)
	0–42	5.32	0.910	1.2	6 (5)	7 (7)	2.21	1.2	7 (6)	8 (7)
Y(3S)	0–2.5	1.54	0.107	5.3	7 (7)	10 (10)	0.203	5.3	8 (8)	11 (10)
	2.5–5	3.62	0.125	4.5	8 (8)	10 (10)	0.287	4.5	10 (11)	12 (12)
	5–7.5	6.15	0.0801	4.7	6 (6)	9 (8)	0.227	4.6	9 (8)	11 (10)
	7.5–10	8.62	0.0604	4.8	9 (8)	11 (10)	0.157	4.8	11 (10)	12 (12)
	10–13	11.31	0.0476	4.5	6 (7)	8 (9)	0.113	4.3	7 (5)	9 (8)
	13–16	14.30	0.0308	5.1	5 (6)	8 (9)	0.0617	5.0	5 (5)	8 (8)
	16–18	16.94	0.0127	7.5	6 (5)	10 (10)	0.0227	7.4	6 (5)	10 (10)
	18–22	19.72	0.0140	6.9	7 (7)	11 (11)	0.0229	7.0	7 (6)	10 (10)
	22–38	26.51	0.0124	7.4	9 (9)	12 (12)	0.0185	7.6	13 (13)	15 (15)
	0–38	5.31	0.490	2.0	6 (6)	8 (7)	1.11	2.0	9 (8)	10 (9)

A comparison between the fiducial cross section measurement and theoretical predictions is shown in Fig. 2. Each of the predictions is made with the assumption of unpolarized $Y(nS)$ production. The comparison is made to the *CASCADE* [24] MC generator in the fixed-order-plus-next-to-leading-log (FONLL) framework, including feed-down from $\chi_b(1P)$, $\chi_b(2P)$, $\chi_b(3P)$ [25], and other higher-mass Y states, and to *PYTHIA* [11] including feed-down for the $Y(1S)$ and $Y(2S)$ from the P-wave states with the same principal quantum number. The p_T dependence of the cross section predicted by *CASCADE* agrees with the data for the $Y(1S)$, is marginally consistent for the $Y(2S)$ but does not describe the $Y(3S)$ spectrum, where it predicts a softer p_T spectrum. For each resonance, the total cross section predicted by *PYTHIA* is higher, by factors of about 2, than the measured cross section. In Fig. 2, for each resonance the *PYTHIA* prediction is normalized to the measured total cross section, in order to facilitate the comparison of the cross section dependences with the predictions. The *PYTHIA* prediction of the p_T dependence agrees with data for the $Y(1S)$ and $Y(3S)$, but not for the $Y(2S)$. Both *CASCADE* and *PYTHIA* provide a good description of the shape of the rapidity dependence for the three states. Complete tables of results for the differential fiducial cross sections for the three Y states are available in Appendix A.

9 Acceptance-corrected differential cross section measurement and comparison to theory

The acceptance-corrected $Y(nS)$ production cross sections times the dimuon branching fractions at $\sqrt{s} = 7$ TeV for $|y^Y| < 2.4$ are measured to be

$$\begin{aligned}\sigma(\text{pp} \rightarrow Y(1S)X) \cdot \mathcal{B}(Y(1S) \rightarrow \mu^+ \mu^-) &= (8.55 \pm 0.05^{+0.56}_{-0.50} \pm 0.34) \text{ nb}, \\ \sigma(\text{pp} \rightarrow Y(2S)X) \cdot \mathcal{B}(Y(2S) \rightarrow \mu^+ \mu^-) &= (2.21 \pm 0.03^{+0.16}_{-0.14} \pm 0.09) \text{ nb}, \\ \sigma(\text{pp} \rightarrow Y(3S)X) \cdot \mathcal{B}(Y(3S) \rightarrow \mu^+ \mu^-) &= (1.11 \pm 0.02^{+0.10}_{-0.08} \pm 0.04) \text{ nb},\end{aligned}\tag{6}$$

where the first uncertainty is statistical, the second is systematic, and the third is from the estimation of the integrated luminosity. These results assume unpolarized $Y(nS)$ production. The $Y(1S)$ integrated production cross section in the restricted rapidity range $|y^Y| < 2.0$ is 7.496 ± 0.052 (stat.) nb, which is consistent with the previous CMS result of 7.37 ± 0.13 (stat.) nb [6], measured in the same rapidity range. The results of the $Y(nS)$ production cross sections for the same p_T^Y and y^Y ranges used for the measurement of the $Y(nS)$ polarizations in Ref. [7] are shown in Table 4.

Table 4: The product of the acceptance-corrected $Y(nS)$ production cross sections, σ , and the dimuon branching fraction, \mathcal{B} , integrated over the rapidity range $|y^Y| < 1.2$, and the p_T^Y range from 10 to 50 GeV/ c , as used in Ref. [7] for the measurement of the Y polarizations. The cross sections assume the $Y(nS)$ are unpolarized. The statistical uncertainty (stat.), the sum in quadrature of the systematic uncertainties ($\Sigma_{\text{syst.}}$), excluding the contribution from the polarization uncertainty, the systematic uncertainties from the polarization (pol.), and the total uncertainty ($\Delta\sigma$; including stat., $\Sigma_{\text{syst.}}$, pol., and the uncertainty in the integrated luminosity) are in percent. The numbers in parentheses are negative variations.

	$\sigma \cdot \mathcal{B}$ (nb)	$\frac{\text{stat.}}{\sigma}$	$\frac{\Sigma_{\text{syst.}}}{\sigma}$	$\frac{\text{pol.}}{\sigma}$	$\frac{\Delta\sigma}{\sigma}$
Y(1S)	0.558	1.3	6 (5)	4 (2)	8 (7)
Y(2S)	0.213	2.4	5 (5)	7 (3)	10 (8)
Y(3S)	0.127	3.2	7 (5)	7 (3)	11 (8)

The acceptance-corrected $Y(nS)$ differential p_T cross sections for the rapidity range $|y^Y| < 2.4$ are plotted in Fig. 3 and summarized in Table 3. Figure 4 shows the same for the ranges $10 < p_T^Y < 50 \text{ GeV}/c$, $|y^Y| < 1.2$ used in Ref. [7] and includes the systematic uncertainties from the polarization measurement of Ref. [7], as explained in Section 7. The $Y(nS)$ differential p_T cross sections for six different rapidity bins are given in Appendix A. The p_T^Y dependence of the cross section in the six exclusive rapidity intervals shows a similar trend within the uncertainties. The $Y(nS)$ p_T -integrated, differential rapidity cross section results are shown in Fig. 5. Similar to the fiducial differential rapidity cross sections, the acceptance-corrected cross sections are approximately flat from $|y^Y| = 0$ to about 2.0, where they then begin to fall. In Fig. 5, a comparison with similar results from the LHCb Collaboration [4] is also shown. The two sets of measurements are complementary in their rapidity coverage and consistent within the uncertainties in the region of overlap. The fiducial cross sections and the acceptance-corrected cross sections exhibit similar p_T^Y and $|y^Y|$ dependencies. However, the decrease in the cross section at large values of the rapidity is greater for the fiducial cross section than for the acceptance-corrected cross section because the acceptance also decreases with rapidity. A comparison to the normalized differential p_T cross section results from CDF [2] and D0 [3], provided in Appendix A, indicates a harder spectrum at the LHC. Comparisons to results from ATLAS [5], shown also in Appendix A, show good agreement. The ratios of the $Y(nS)$ differential p_T cross sections are plotted in Fig. 6, along with comparisons to the CASCADE and PYTHIA predictions. The ratios increase with p_T^Y , as they do for the fiducial cross sections. The predictions for the ratios from CASCADE have relatively large uncertainty bands; this arises as a consequence of the asymmetric variation of the uncertainty of the predictions in Fig. 2 as a function of p_T^Y . The CASCADE prediction is consistent with the $Y(2S)/Y(1S)$ and $Y(3S)/Y(2S)$ measurements, while it disagrees with the $Y(3S)/Y(1S)$ results at low p_T . The PYTHIA prediction agrees with the measured $Y(3S)/Y(1S)$ values, but is inconsistent with the $Y(2S)/Y(1S)$ and $Y(3S)/Y(2S)$ results.

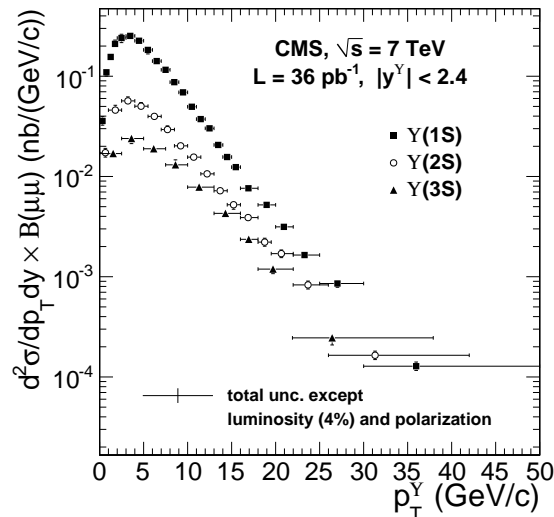


Figure 3: Acceptance-corrected differential cross sections as a function of p_T^Y in the rapidity range $|y^Y| < 2.4$.

The acceptance-corrected differential p_T and rapidity $Y(nS)$ cross sections and the theoretical predictions are shown in Fig. 7. The measurements and predictions in Figs. 7 (a,b,c) are for $|y^Y| < 2.0$ and assume unpolarized $Y(nS)$ production. Comparisons are made to the CASCADE MC generator; the normalized PYTHIA (as explained in Section 8); the color-evaporation model (CEM) [26] with feed-down not included; nonrelativistic QCD (NRQCD) to next-to-leading

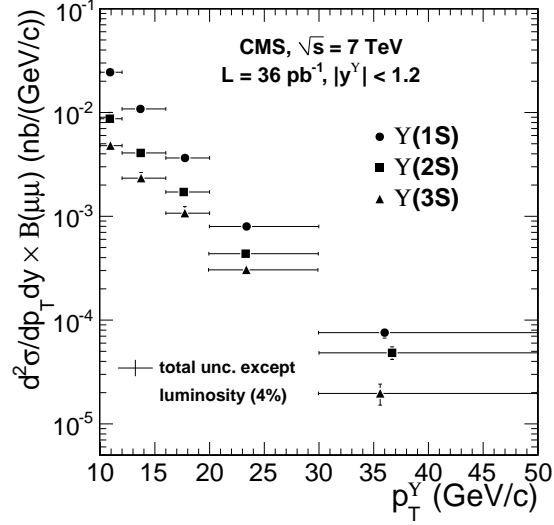


Figure 4: Acceptance-corrected differential cross sections as a function of p_T^Y for $|y^Y| < 1.2$. The error bars represent the total uncertainties, including the systematic uncertainties from the measurement of the $Y(nS)$ polarization [7], but not the uncertainty (4%) in the integrated luminosity.

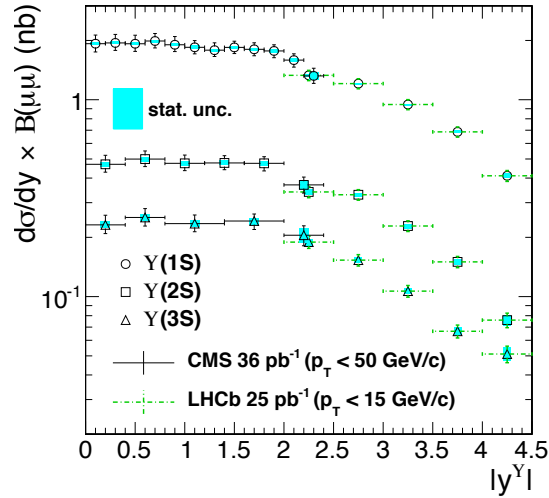


Figure 5: Acceptance-corrected differential production cross sections as a function of rapidity, and comparison with LHCb results [4]. The bands represent the statistical uncertainty and the error bars represent the total uncertainty, except for those from the $Y(nS)$ polarization.

order (NLO) including feed-down, as described in Ref. [27]; the color-singlet model (CSM) to NLO and NNLO* [28], with feed-down accounted for by scaling the $Y(1S)$ and $Y(2S)$ direct-production cross sections by factors 2 and 1.43, respectively [28], and no feed-down for the $Y(3S)$. The theoretical predictions are based on published models for $Y(nS)$ production, and, except for NRQCD [27], are made for lower \sqrt{s} [24, 26, 28]. These models have been updated by their respective authors to $\sqrt{s} = 7$ TeV when relevant. The updates are unpublished and are in the form of private communications. Our measured $Y(1S)$ cross section is in good agreement with NRQCD, for the prediction provided for p_T in 8–30 GeV/ c . The CEM predictions for the three states are, within their uncertainties, also compatible with the data. The data agree with CASCADE for the $Y(1S)$ and $Y(2S)$, but the agreement is not as satisfactory for the $Y(3S)$ when

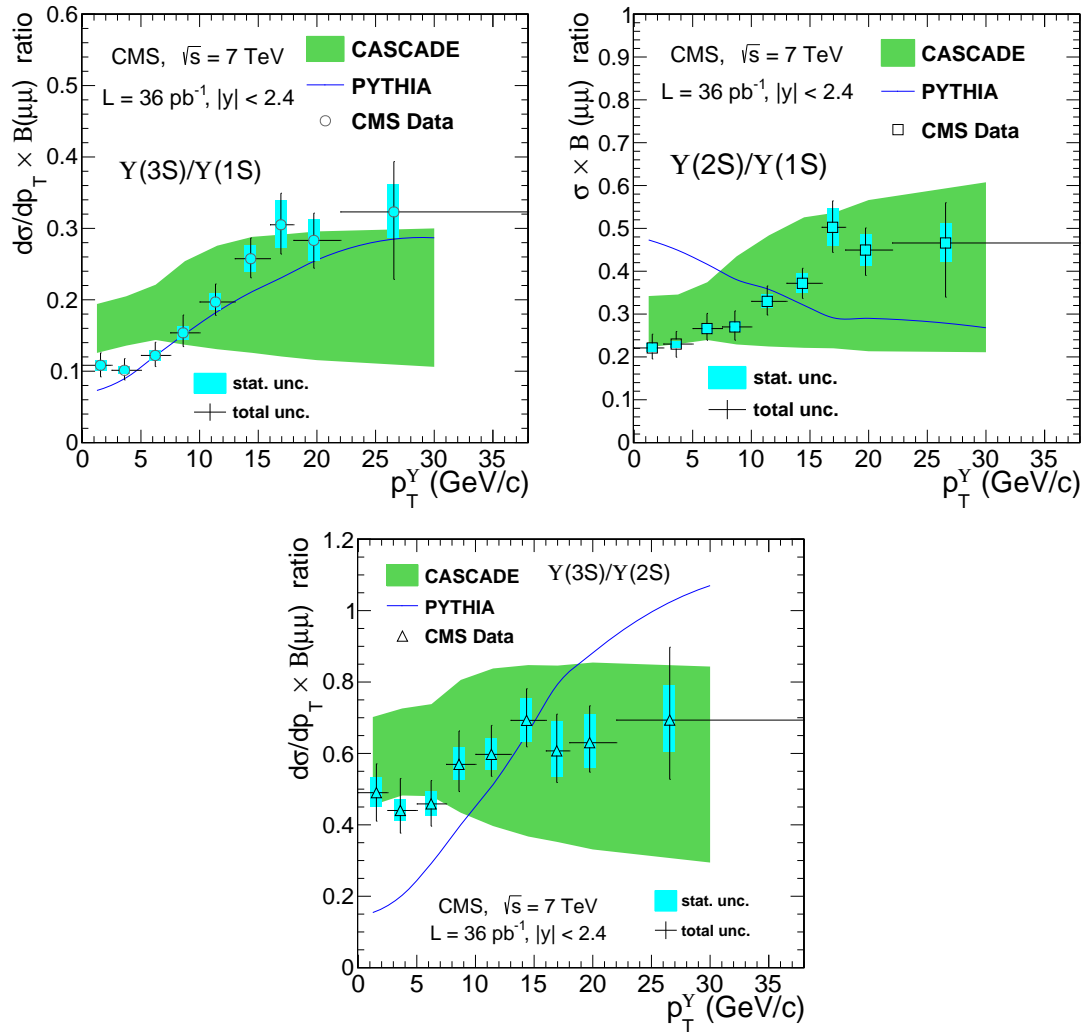


Figure 6: Ratios of acceptance-corrected differential cross sections as a function of p_T^Y in the rapidity range $|y^Y| < 2.4$, along with predictions from CASCADE (bands) and PYTHIA (lines), for the $Y(3S)/Y(1S)$, $Y(2S)/Y(1S)$ and $Y(3S)/Y(2S)$. The width of a band indicates an estimate of the uncertainty in the prediction.

judged on the basis of the smaller uncertainties quoted by this prediction. The NLO CSM does not describe the data, while the NNLO* CSM shows improved agreement within the large uncertainties. The total cross section predicted by PYTHIA is higher than the measured cross section by about a factor 2; in Fig. 7, the PYTHIA predictions are for this reason normalized to the measured $Y(nS)$ cross sections. The p_T dependence of the cross section predicted by PYTHIA agrees with the data for the $Y(1S)$ and $Y(3S)$ but not for the $Y(2S)$. CASCADE and PYTHIA also describe the rapidity dependence over the range of the measurement, as shown in Fig. 7 (d). Complete tables of results for the differential cross sections for the three Y states are available in Appendix A, including variations for extreme polarization scenarios.

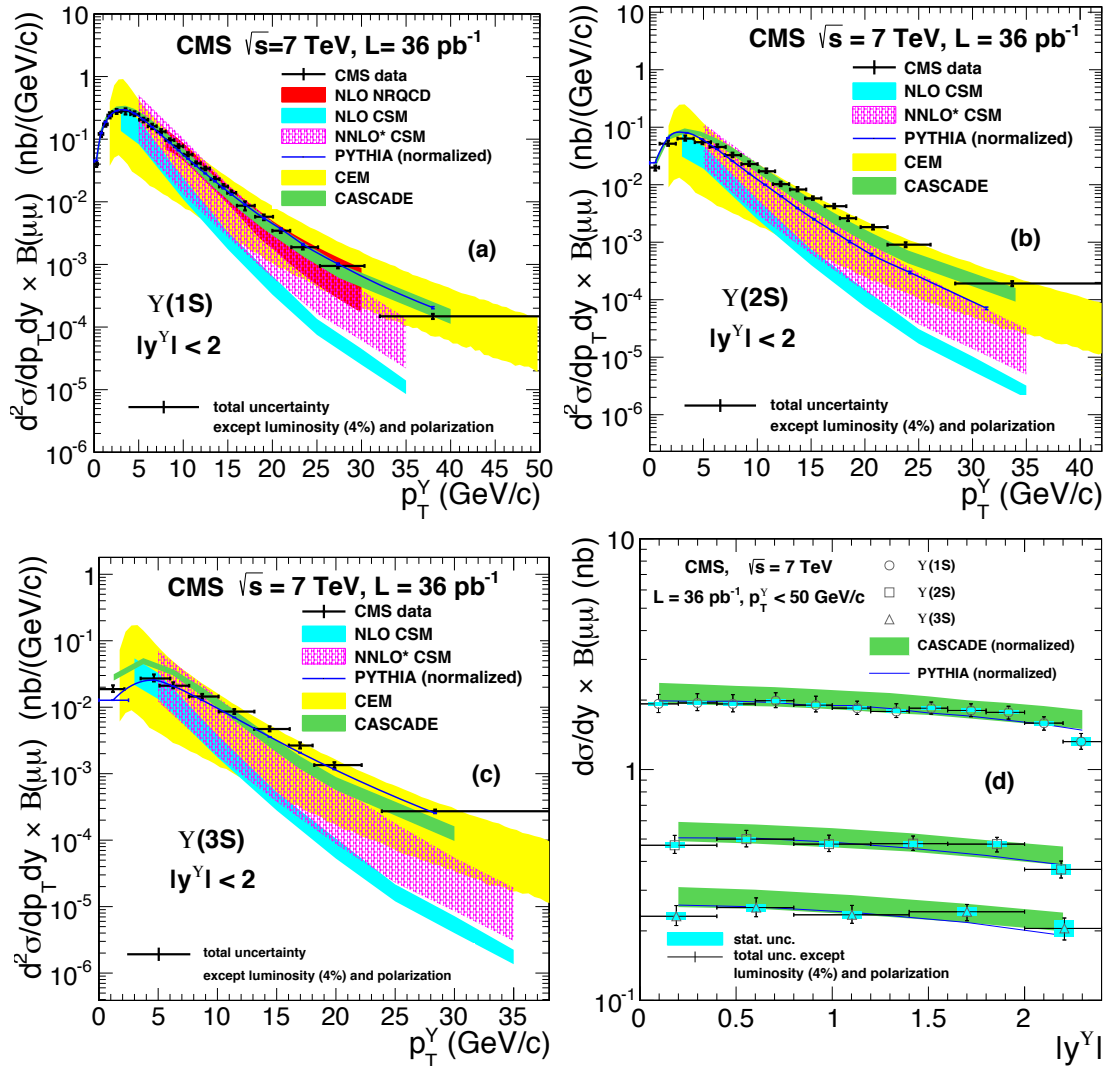


Figure 7: Acceptance-corrected differential cross sections of (a) $Y(1S)$, (b) $Y(2S)$, and (c) $Y(3S)$ as a function of p_T^Y in the rapidity range $|y^Y| < 2$, and comparison to various theoretical predictions. (d) Acceptance-corrected differential cross section of the $Y(nS)$ as a function of rapidity and comparison to CASCADE and PYTHIA. The PYTHIA prediction is normalized to the measured total cross section, in order to facilitate the comparison of the shape of the dependences; for the rapidity differential results (d), the normalized CASCADE prediction is also shown. The width of a band indicates an estimate of the uncertainty in the prediction by the author of the prediction.

10 Summary

Measurements of the $Y(nS)$ differential and total production cross sections from proton-proton collisions at $\sqrt{s} = 7\text{ TeV}$ with the CMS detector have been presented. The results have been shown in two ways: as acceptance-corrected cross sections, and fiducial cross sections in which both muons from the $Y(nS)$ decay are within the detector acceptance. The latter cross sections are independent of the assumed $Y(nS)$ polarizations. The differential cross sections have been given as a function of p_T^Y and $|y^Y|$, and compared to theoretical predictions. The differential cross sections as a function of p_T^Y and y^Y for each $Y(nS)$ state have also been measured and compared to theoretical predictions. Finally, the Y cross section ratios have been given. The dominant sources of systematic uncertainty in the cross section measurements arise from the determination of the muon identification and trigger efficiencies, and the integrated luminosity.

The measurements are consistent with previous CMS results based on less than 10% of the integrated luminosity analyzed here. These earlier measurements have been extended in terms of both the precision attained and the kinematic reach. In addition, this paper expands upon the previous result by the inclusion of fiducial cross section measurements and the polarization systematics, utilizing the recent Y polarization results from CMS. The results are compared to the ATLAS and LHCb Collaborations' measurements, and are found to be consistent in the regions of overlap. Comparisons to measurements by the CDF, D0, and LHCb Collaborations also illustrate the achieved extension in kinematic coverage. The results presented here will allow for a more precise determination of the parameters of the various bottomonium production models.

Acknowledgements

We congratulate our colleagues in the CERN accelerator departments for the excellent performance of the LHC and thank the technical and administrative staffs at CERN and at other CMS institutes for their contributions to the success of the CMS effort. In addition, we gratefully acknowledge the computing centres and personnel of the Worldwide LHC Computing Grid for delivering so effectively the computing infrastructure essential to our analyses. Finally, we acknowledge the enduring support for the construction and operation of the LHC and the CMS detector provided by the following funding agencies: BMWF and FWF (Austria); FNRS and FWO (Belgium); CNPq, CAPES, FAPERJ, and FAPESP (Brazil); MEYS (Bulgaria); CERN; CAS, MoST, and NSFC (China); COLCIENCIAS (Colombia); MSES (Croatia); RPF (Cyprus); MoER, SF0690030s09 and ERDF (Estonia); Academy of Finland, MEC, and HIP (Finland); CEA and CNRS/IN2P3 (France); BMBF, DFG, and HGF (Germany); GSRT (Greece); OTKA and NKTH (Hungary); DAE and DST (India); IPM (Iran); SFI (Ireland); INFN (Italy); NRF and WCU (Republic of Korea); LAS (Lithuania); CINVESTAV, CONACYT, SEP, and UASLP-FAI (Mexico); MSI (New Zealand); PAEC (Pakistan); MSHE and NSC (Poland); FCT (Portugal); JINR (Armenia, Belarus, Georgia, Ukraine, Uzbekistan); MON, RosAtom, RAS and RFBR (Russia); MSTD (Serbia); SEIDI and CPAN (Spain); Swiss Funding Agencies (Switzerland); NSC (Taipei); ThEP-Center, IPST and NSTDA (Thailand); TUBITAK and TAEK (Turkey); NASU (Ukraine); STFC (United Kingdom); DOE and NSF (USA). Individuals have received support from the Marie-Curie programme and the European Research Council and EPLANET (European Union); the Leventis Foundation; the A. P. Sloan Foundation; the Alexander von Humboldt Foundation; the Belgian Federal Science Policy Office; the Fonds pour la Formation à la Recherche dans l'Industrie et dans l'Agriculture (FRIA-Belgium); the Agentschap voor Innovatie door Wetenschap en Technologie (IWT-Belgium); the Ministry of Education, Youth and Sports (MEYS) of Czech Republic; the Council of Science and Industrial Research, India; the Compagnia di San

Paolo (Torino); and the HOMING PLUS programme of Foundation for Polish Science, cofinanced from European Union, Regional Development Fund.

References

- [1] N. Brambilla et al., “Heavy quarkonium: progress, puzzles, and opportunities”, *Eur. Phys. J. C* **71** (2011) 1534, doi:10.1140/epjc/s10052-010-1534-9, arXiv:1010.5827.
- [2] CDF Collaboration, “Upsilon production and polarization in $p\bar{p}$ collisions at $\sqrt{s} = 1.8\text{-TeV}$ ”, *Phys. Rev. Lett.* **88** (2002) 161802, doi:10.1103/PhysRevLett.88.161802.
- [3] D0 Collaboration, “Measurement of inclusive differential cross sections for $Y(1S)$ production in $p\bar{p}$ collisions at $\sqrt{s} = 1.96\text{-TeV}$ ”, *Phys. Rev. Lett.* **94** (2005) 232001, doi:10.1103/PhysRevLett.100.049902, arXiv:hep-ex/0502030. And *Erratum*, *Phys. Rev. Lett.* **100** (2008) 049902, doi:10.1103/PhysRevLett.100.049902.
- [4] LHCb Collaboration, “Measurement of Upsilon production in pp collisions at $\sqrt{s} = 7\text{ TeV}$ ”, *Eur. Phys. J. C* **72** (2012) 2025, doi:10.1140/epjc/s10052-012-2025-y, arXiv:1202.6579.
- [5] ATLAS Collaboration, “Measurement of Upsilon production in 7 TeV pp collisions at ATLAS”, *Phys. Rev. D* **87** (2013) 052004, doi:10.1103/PhysRevD.87.052004, arXiv:1211.7255.
- [6] CMS Collaboration, “Upsilon production cross section in pp collisions at $\sqrt{s} = 7\text{ TeV}$ ”, *Phys. Rev. D* **83** (2011) 112004, doi:10.1103/PhysRevD.83.112004, arXiv:1012.5545.
- [7] CMS Collaboration, “Measurement of the $Y(1S)$, $Y(2S)$ and $Y(3S)$ polarizations in pp collisions at $\sqrt{s} = 7\text{ TeV}$ ”, *Phys. Rev. Lett.* **110** (2013) 081802, doi:10.1103/PhysRevLett.110.081802, arXiv:1209.2922.
- [8] CMS Collaboration, “The CMS experiment at the CERN LHC”, *JINST* **3** (2008) S08004, doi:10.1088/1748-0221/3/08/S08004.
- [9] T. Sjöstrand, S. Mrenna, and P. Z. Skands, “PYTHIA 6.4 physics and manual”, *JHEP* **5** (2006) 026, doi:10.1088/1126-6708/2006/05/026, arXiv:hep-ph/0603175.
- [10] M. Krämer, “Quarkonium production at high-energy colliders”, *Prog. Part. Nucl. Phys.* **47** (2001) 141, doi:10.1016/S0146-6410(01)00154-5, arXiv:hep-ph/0106120.
- [11] M. Bargiotti and V. Vagnoni, “Heavy Quarkonia sector in PYTHIA 6.324 : tuning, validation and perspectives at LHC(b)”, LHCb Note LHCb-2007-042, (2007).
- [12] J. Pumplin et al., “New generation of parton distributions with uncertainties from global QCD analysis”, *JHEP* **07** (2002) 012, doi:10.1088/1126-6708/2002/07/012, arXiv:hep-ph/0201195.
- [13] E. Barberio, B. van Eijk, and Z. Waş, “PHOTOS—a universal Monte Carlo for QED radiative corrections in decays”, *Comput. Phys. Commun.* **66** (1991) 115, doi:10.1016/0010-4655(91)90012-A.

- [14] E. Barberio and Z. Was, "PHOTOS—a universal Monte Carlo for QED radiative corrections: version 2.0", *Comput. Phys. Commun.* **79** (1994) 291, doi:10.1016/0010-4655(94)90074-4.
- [15] S. Agostinelli et al., "GEANT4—a simulation toolkit", *Nucl. Instrum. Meth. A* **506** (2003) 250, doi:10.1016/S0168-9002(03)01368-8.
- [16] M. J. Oreglia, "A study of the reactions $\psi' \rightarrow \gamma\gamma\psi$ ". PhD thesis, Stanford University, 1980. SLAC Report SLAC-R-236, see Appendix D.
- [17] Particle Data Group, J. Beringer et al., "Review of Particle Physics", *Phys. Rev. D* **86** (2012) 010001, doi:10.1103/PhysRevD.86.010001.
- [18] CMS Collaboration, "Observation of sequential Y suppression in PbPb collisions", *Phys. Rev. Lett.* **109** (2012) 222301, doi:10.1103/PhysRevLett.109.222301, arXiv:1208.2826.
- [19] D. J. Lange, "The EVTGEN particle decay simulation package", *Nucl. Instrum. Meth. A* **462** (2001) 152, doi:10.1016/S0168-9002(01)00089-4.
- [20] J. C. Collins and D. E. Soper, "Angular Distribution of Dileptons in High-Energy Hadron Collisions", *Phys. Rev. D* **16** (1977) 2219, doi:10.1103/PhysRevD.16.2219.
- [21] CMS Collaboration, "Measurement of Tracking Efficiency", CMS Physics Analysis Summary CMS-PAS-TRK-10-002, (2010).
- [22] CMS Collaboration, "Measurement of Momentum Scale and Resolution using Low-mass Resonances and Cosmic Ray Muons", CMS Physics Analysis Summary CMS-PAS-TRK-10-004, (2010).
- [23] CMS Collaboration, "Measurement of CMS Luminosity", CMS Physics Analysis Summary CMS-PAS-EWK-10-004, (2010).
- [24] H. Jung et al., "The CCFM Monte Carlo generator CASCADE version 2.2.03", *Eur. Phys. J. C* **70** (2010) 1237, doi:10.1140/epjc/s10052-010-1507-z, arXiv:1008.0152.
- [25] S. P. Baranov, "Prompt Y(nS) production at the LHC in view of the k_t -factorization approach", *Phys. Rev. D* **86** (2012) 054015, doi:10.1103/PhysRevD.86.054015.
- [26] A. D. Frawley, T. Ullrich, and R. Vogt, "Heavy flavor in heavy-ion collisions at RHIC and RHIC II", *Phys. Rept.* **462** (2008) 125, doi:10.1016/j.physrep.2008.04.002, arXiv:0806.1013. And private communication.
- [27] K. Wang, Y.-Q. Ma, and K.-T. Chao, "Y(1S) prompt production at the Tevatron and LHC in nonrelativistic QCD", *Phys. Rev. D* **85** (2012) 114003, doi:10.1103/PhysRevD.85.114003, arXiv:1202.6012. And private communication.
- [28] J. P. Lansberg, "J/ ψ production at $\sqrt{s} = 1.96$ and 7 TeV: Color-Singlet Model, NNLO* and polarisation", *J. Phys. G* **38** (2011) 124110, doi:10.1088/0954-3889/38/12/124110, arXiv:1107.0292. And private communication.

A Supplementary Material

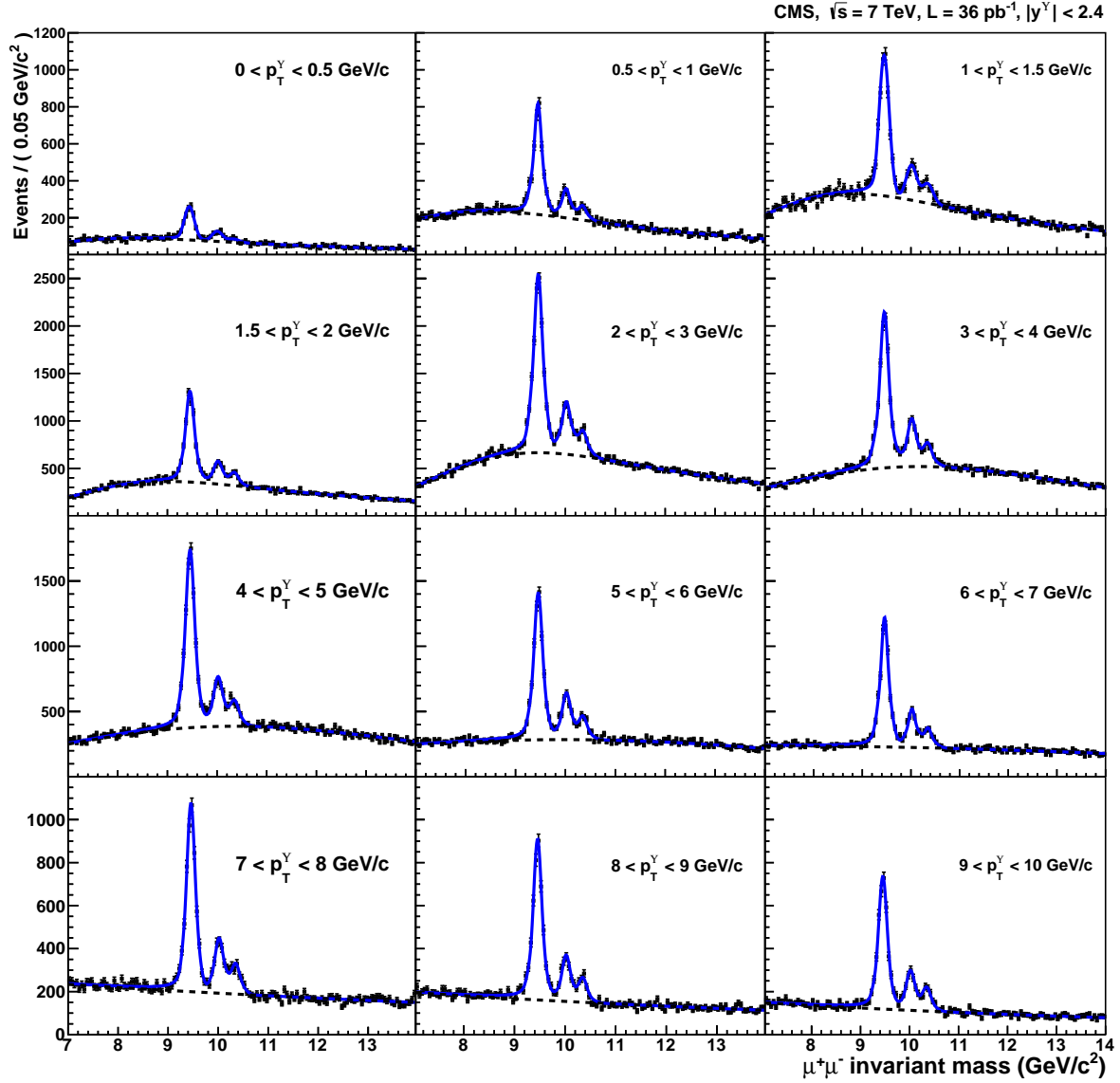


Figure A.1: Fit to the dimuon invariant-mass distribution in the specified p_T regions for $|y| < 2.4$, before accounting for acceptance and efficiency. The solid line shows the result of the fit described in the text, with the dashed line representing the background component.

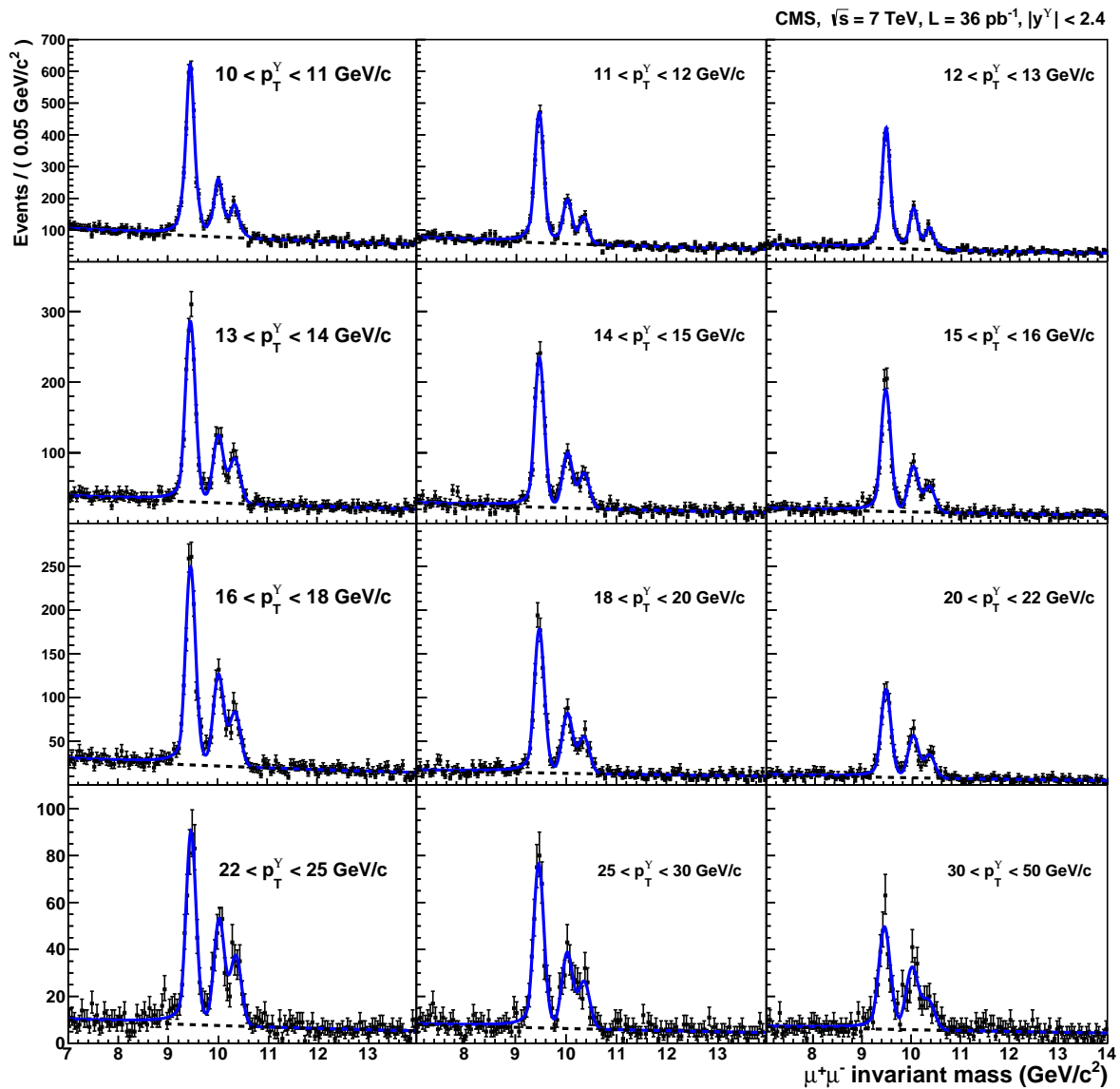


Figure A.2: Fit to the dimuon invariant-mass distribution in the specified p_T regions for $|y| < 2.4$, before accounting for acceptance and efficiency. The solid line shows the result of the fit described in the text, with the dashed line representing the background component.

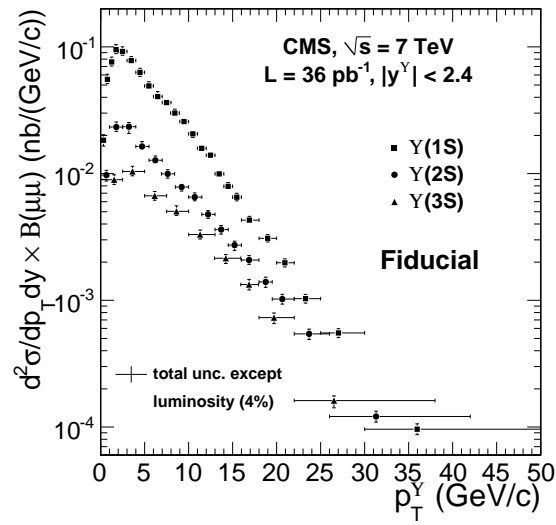


Figure A.3: Measured $Y(nS)$ differential fiducial cross sections as a function of p_T^Y in the rapidity range $|y^Y| < 2.4$. The error bars indicate the total uncertainties, except for the 4% uncertainty in the integrated luminosity.

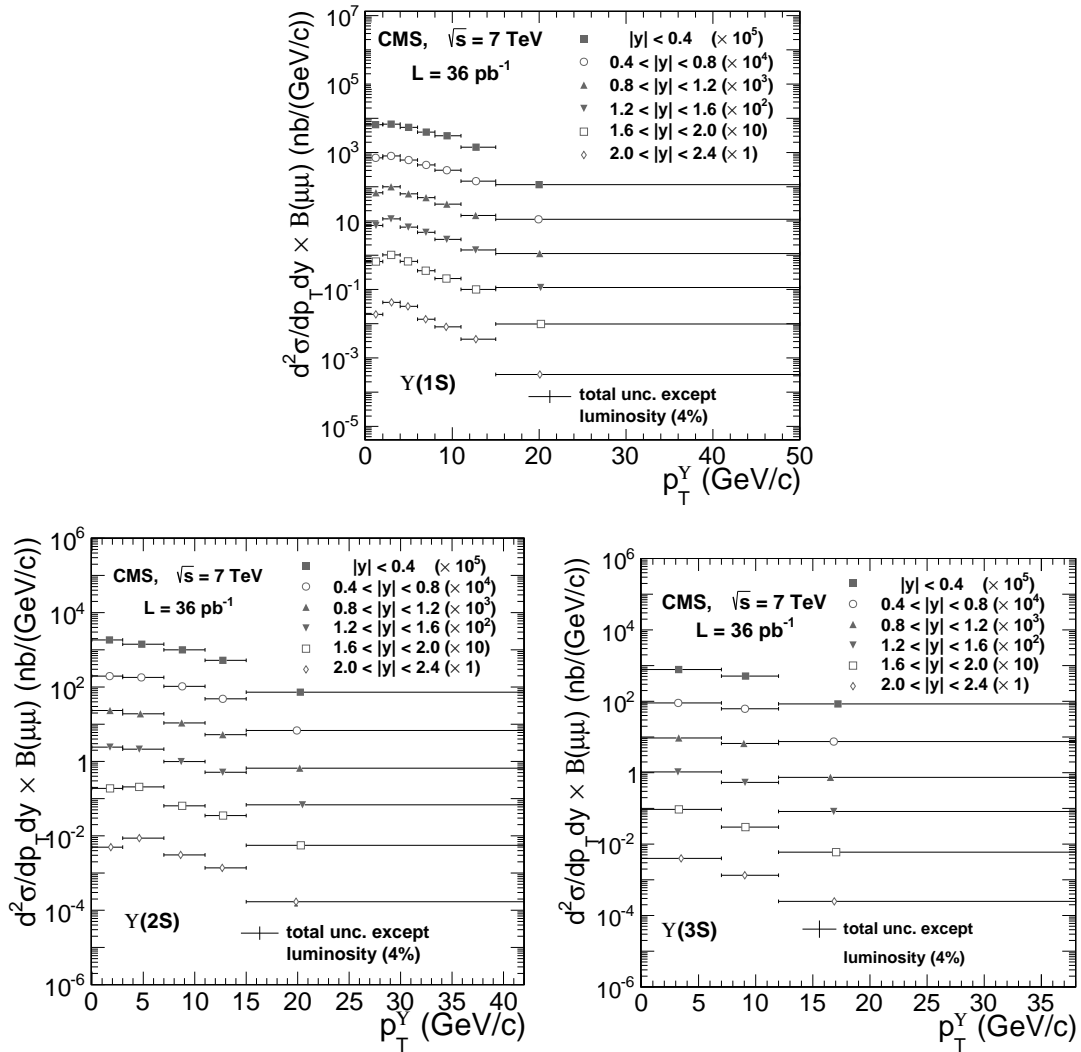


Figure A.4: The $Y(nS)$ differential fiducial cross sections as a function of p_T^Y in six rapidity ranges, scaled for clarity by the factors shown in the figures.

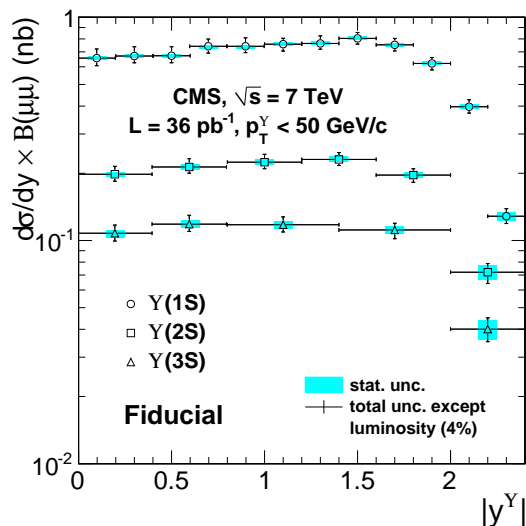


Figure A.5: Differential fiducial cross sections of the $Y(nS)$ as a function of rapidity. The regions show the statistical uncertainties and the error bars show the total uncertainties, except for the 4% uncertainty in the integrated luminosity.

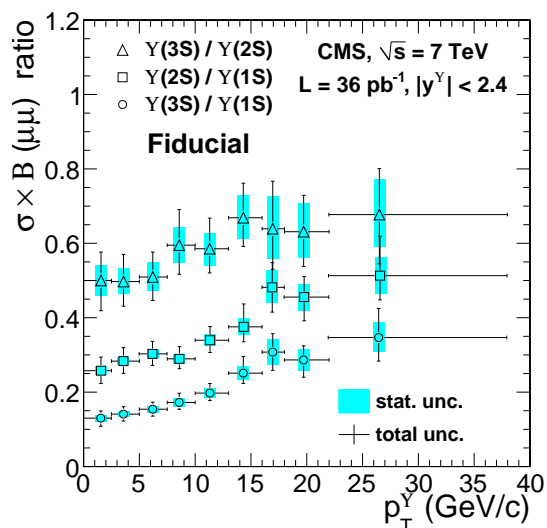


Figure A.6: Ratios of the differential fiducial cross sections for the $Y(nS)$ as a function of p_T^Y in the rapidity range $|y^Y| < 2.4$.

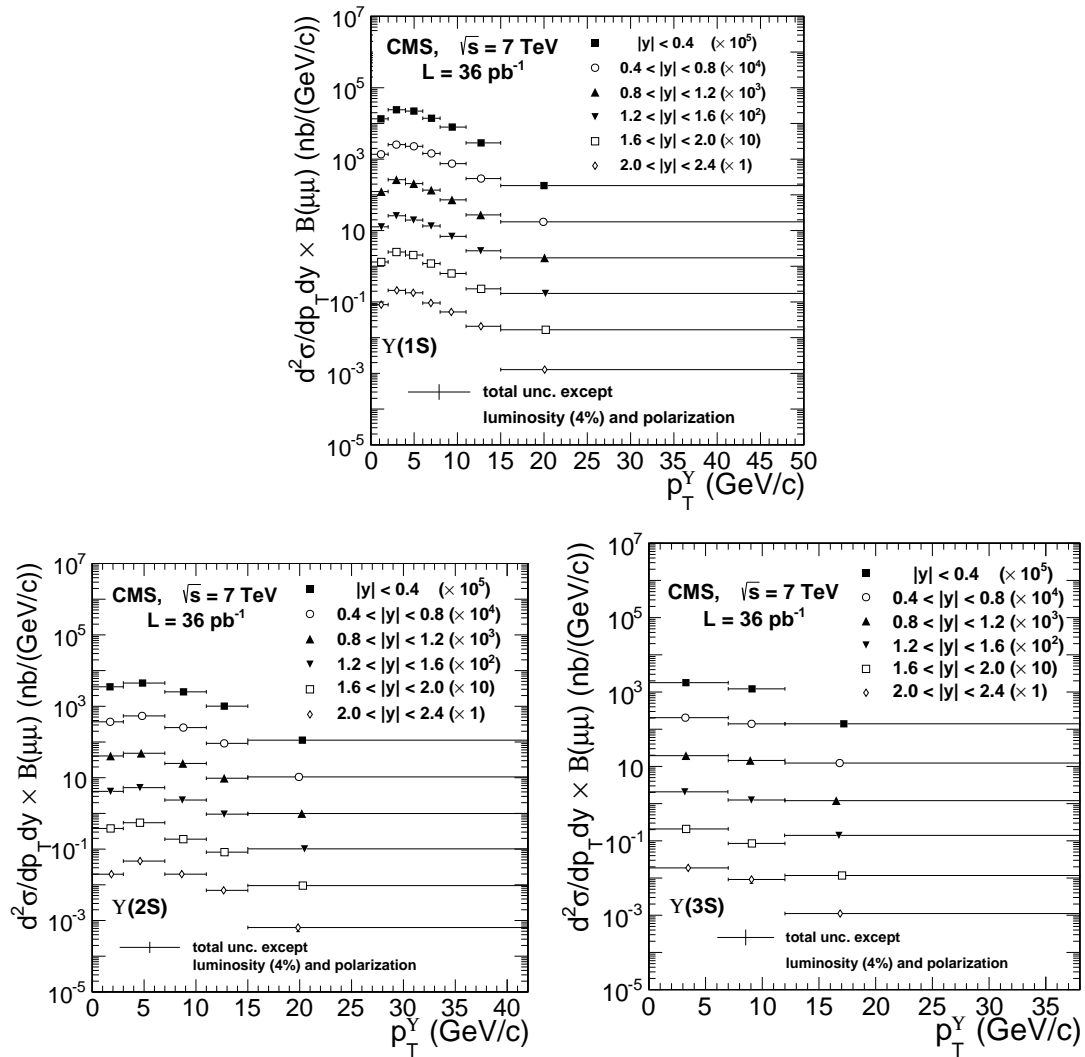


Figure A.7: Differential production cross sections of the $Y(nS)$ as a function of p_T^Y in six rapidity regions. The measurements have been multiplied by the factors shown in the figure for clarity.

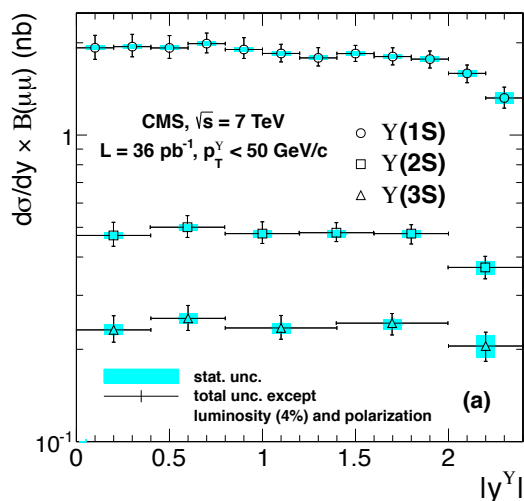


Figure A.8: Acceptance-corrected differential production cross sections as a function of rapidity. The bands represent the statistical uncertainty and the error bars represent the total uncertainty, except for those from the $Y(nS)$ polarization and the integrated luminosity.

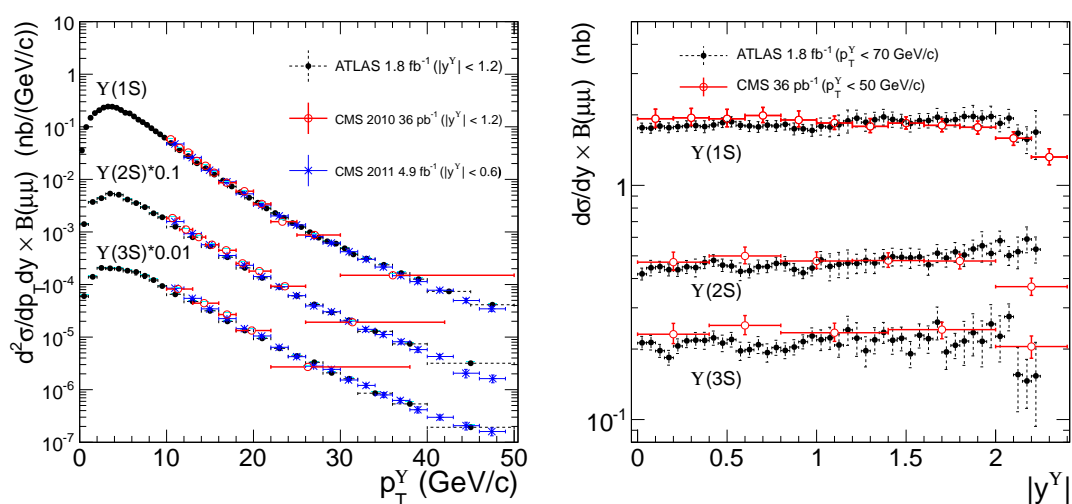


Figure A.9: Comparison of the $Y(nS)$ acceptance-corrected differential cross section results to the ATLAS results, as a function of p_T^Y (left) and y^Y (right).

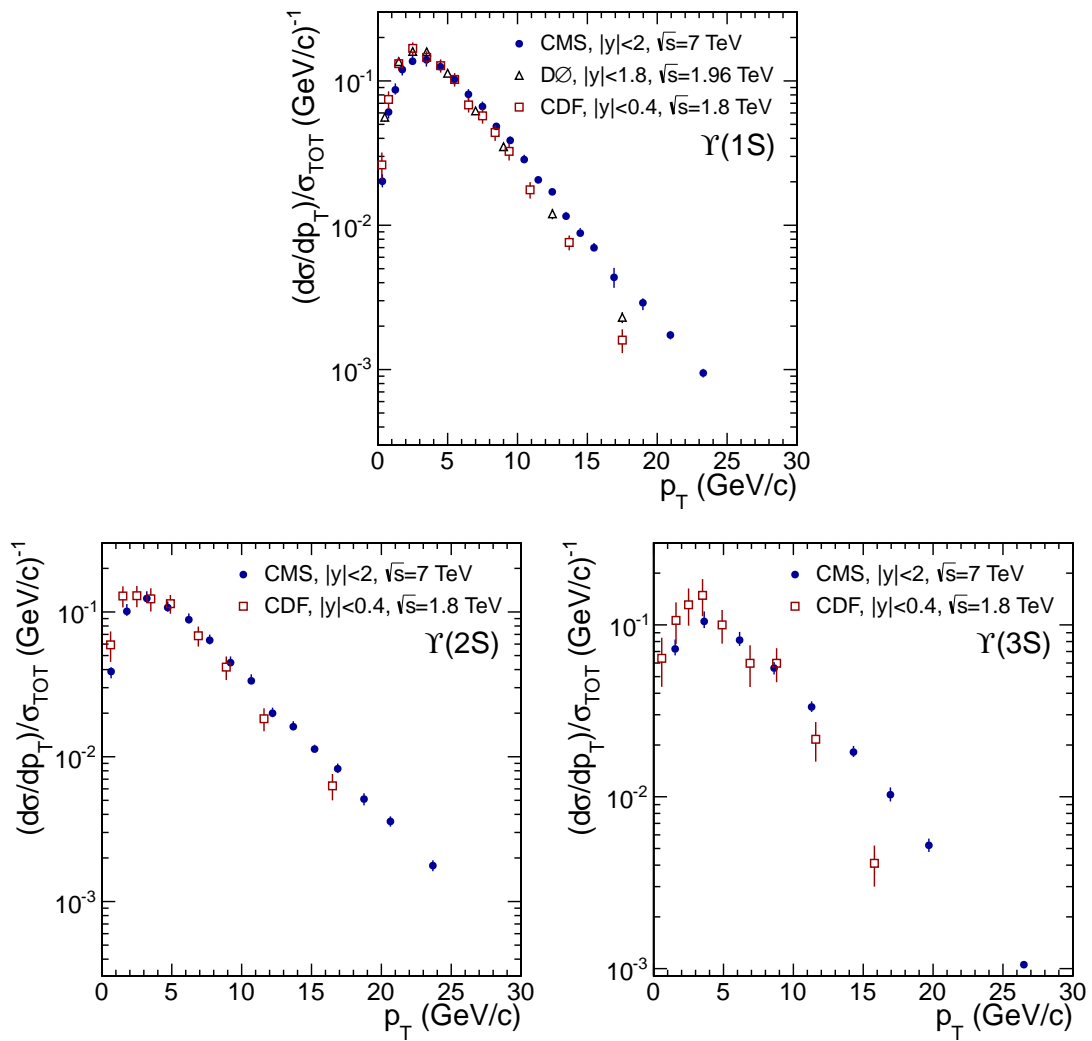


Figure A.10: Comparison of acceptance-corrected differential cross section results, normalized by $\sigma_{TOT} = \sum(d\sigma/dp_T)\Delta p_T$, to the CDF and D0 results, as a function of p_T , for $Y(1S)$ (top), $Y(2S)$ (left), $Y(3S)$ (right).

Table A.1: The product of the fiducial $Y(1S)$ production cross sections, σ , integrated and differential in p_T^Y , and the dimuon branching fraction, \mathcal{B} , integrated over the rapidity range $|y^Y| < 2.4$. The statistical uncertainty (stat.), the sum of the systematic uncertainties in quadrature ($\Sigma_{\text{syst.}}$), and the total uncertainty ($\Delta\sigma$; including stat., $\Sigma_{\text{syst.}}$, and the uncertainty in the integrated luminosity) are in percent. The numbers in parentheses are negative variations.

$ y^Y < 2.4$				
$Y(1S)$				
p_T (GeV/c)	$\sigma \cdot \mathcal{B}$ (nb)	$\frac{\text{stat.}}{\sigma}$	$\frac{\Sigma_{\text{syst.}}}{\sigma}$	$\frac{\Delta\sigma}{\sigma}$
0–0.5	0.0440	5.4	8 (8)	11 (11)
0.5–1	0.133	3.1	8 (8)	10 (10)
1–1.5	0.182	2.5	8 (8)	9 (9)
1.5–2	0.228	2.4	8 (8)	10 (9)
2–3	0.442	1.6	8 (7)	9 (8)
3–4	0.374	1.8	6 (6)	8 (7)
4–5	0.302	1.8	7 (7)	8 (8)
5–6	0.236	2.0	7 (6)	8 (7)
6–7	0.195	2.0	8 (7)	9 (9)
7–8	0.174	2.1	5 (5)	7 (6)
8–9	0.144	2.3	6 (5)	7 (7)
9–10	0.1235	2.4	5 (4)	7 (6)
10–11	0.0988	2.5	6 (5)	8 (7)
11–12	0.0759	2.8	4 (4)	7 (6)
12–13	0.0670	2.9	4 (4)	7 (6)
13–14	0.0477	3.3	5 (4)	7 (7)
14–15	0.0381	3.6	5 (5)	7 (7)
15–16	0.0312	4.0	5 (4)	8 (7)
16–18	0.0412	3.5	5 (5)	7 (7)
18–20	0.0296	4.0	5 (4)	7 (7)
20–22	0.0187	5.1	4 (4)	8 (8)
22–25	0.0148	5.8	4 (4)	8 (8)
25–30	0.0133	6.1	4 (4)	8 (8)
30–50	0.00923	7.8	6 (6)	11 (10)
0–50	3.06	0.6	6 (6)	8 (7)

Table A.2: The product of the fiducial $\Upsilon(2S)$ production cross sections, σ , integrated and differential in p_T^Y , and the dimuon branching fraction, \mathcal{B} , integrated over the rapidity range $|y^Y| < 2.4$. The statistical uncertainty (stat.), the sum of the systematic uncertainties in quadrature ($\Sigma_{\text{syst.}}$), and the total uncertainty ($\Delta\sigma$; including stat., $\Sigma_{\text{syst.}}$, and the uncertainty in the integrated luminosity) are in percent. The numbers in parentheses are negative variations.

$$|y^Y| < 2.4$$

$$\Upsilon(2S)$$

p_T (GeV/c)	$\sigma \cdot \mathcal{B}$ (nb)	$\frac{\text{stat.}}{\sigma}$	$\frac{\Sigma_{\text{syst.}}}{\sigma}$	$\frac{\Delta\sigma}{\sigma}$
0–1	0.0467	6.3	7 (8)	10 (11)
1–2.5	0.168	3.4	8 (8)	10 (10)
2.5–4	0.169	3.1	8 (11)	9 (12)
4–5.5	0.118	3.3	8 (7)	10 (9)
5.5–7	0.0917	3.6	6 (5)	8 (8)
7–8.5	0.0716	3.4	7 (7)	9 (9)
8.5–10	0.0564	4.0	5 (5)	8 (8)
10–11.5	0.0470	4.1	6 (5)	8 (8)
11.5–13	0.0343	4.6	4 (4)	7 (8)
13–14.5	0.0260	5.2	5 (5)	8 (8)
14.5–16	0.0196	5.7	4 (6)	8 (9)
16–18	0.0198	5.5	6 (5)	9 (8)
18–19.5	0.01005	7.5	4 (5)	9 (10)
19.5–22	0.0123	6.8	5 (5)	9 (9)
22–26	0.0104	7.4	4 (5)	9 (10)
26–42	0.00930	8.0	5 (5)	10 (10)
0–42	0.910	1.2	6 (5)	7 (7)

Table A.3: The product of the fiducial $\Upsilon(3S)$ production cross sections, σ , integrated and differential in p_T^Y , and the dimuon branching fraction, \mathcal{B} , integrated over the rapidity range $|y^Y| < 2.4$. The statistical uncertainty (stat.), the sum of the systematic uncertainties in quadrature ($\Sigma_{\text{syst.}}$), and the total uncertainty ($\Delta\sigma$; including stat., $\Sigma_{\text{syst.}}$, and the uncertainty in the integrated luminosity) are in percent. The numbers in parentheses are negative variations.

$$|y^Y| < 2.4$$

$$\Upsilon(3S)$$

p_T (GeV/c)	$\sigma \cdot \mathcal{B}$ (nb)	$\frac{\text{stat.}}{\sigma}$	$\frac{\Sigma_{\text{syst.}}}{\sigma}$	$\frac{\Delta\sigma}{\sigma}$
0–2.5	0.107	5.3	7 (7)	10 (10)
2.5–5	0.125	4.5	8 (8)	10 (10)
5–7.5	0.0801	4.7	6 (6)	9 (8)
7.5–10	0.0604	4.8	9 (8)	11 (10)
10–13	0.0476	4.5	6 (7)	8 (9)
13–16	0.0308	5.1	5 (6)	8 (9)
16–18	0.0127	7.5	6 (5)	10 (10)
18–22	0.0140	6.9	7 (7)	11 (11)
22–38	0.0124	7.4	9 (9)	12 (12)
0–38	0.490	2.0	6 (6)	8 (7)

Table A.4: The product of the fiducial $Y(nS)$ production cross sections, σ , integrated and differential in p_T^Y , and the respective dimuon branching fraction, \mathcal{B} , integrated over the rapidity range $|y^Y| < 0.4$. The statistical uncertainty (stat.), the sum of the systematic uncertainties in quadrature ($\Sigma_{\text{syst.}}$), and the total uncertainty ($\Delta\sigma$; including stat., $\Sigma_{\text{syst.}}$, and the uncertainty in the integrated luminosity) are in percent. The numbers in parentheses are negative variations.

$ y^Y < 0.4$					
	p_T (GeV/c)	$\sigma \cdot \mathcal{B}$ (nb)	stat. $\frac{\sigma}{\sigma}$	$\frac{\Sigma_{\text{syst.}}}{\sigma}$	$\frac{\Delta\sigma}{\sigma}$
Y(1S)	0–2	0.104	3.5	14 (13)	15 (14)
	2–4	0.108	3.1	10 (11)	11 (12)
	4–6	0.0870	2.9	10 (9)	11 (11)
	6–8	0.0632	3.3	14 (14)	15 (15)
	8–11	0.0741	2.9	7 (7)	8 (8)
	11–15	0.0458	3.3	5 (5)	7 (7)
	15–50	0.0323	3.7	4 (5)	7 (7)
Y(2S)	0–3	0.0442	7.0	12 (11)	15 (14)
	3–7	0.0453	4.9	11 (11)	12 (12)
	7–11	0.0320	5.3	8 (7)	10 (10)
	11–15	0.0167	6.1	5 (5)	9 (9)
	15–42	0.0157	5.7	4 (5)	8 (9)
Y(3S)	0–7	0.0434	6.5	14 (12)	16 (15)
	7–12	0.0203	7.5	10 (9)	13 (13)
	12–38	0.0176	5.9	5 (5)	9 (9)

Table A.5: The product of the fiducial $Y(nS)$ production cross sections, σ , integrated and differential in p_T^Y , and the respective dimuon branching fraction, \mathcal{B} , integrated over the rapidity range $0.4 < |y^Y| < 0.8$. The statistical uncertainty (stat.), the sum of the systematic uncertainties in quadrature ($\Sigma_{\text{syst.}}$), and the total uncertainty ($\Delta\sigma$; including stat., $\Sigma_{\text{syst.}}$, and the uncertainty in the integrated luminosity) are in percent. The numbers in parentheses are negative variations.

$0.4 < y^Y < 0.8$					
	p_T (GeV/c)	$\sigma \cdot \mathcal{B}$ (nb)	stat. $\frac{\sigma}{\sigma}$	$\frac{\Sigma_{\text{syst.}}}{\sigma}$	$\frac{\Delta\sigma}{\sigma}$
Y(1S)	0–2	0.112	3.3	12 (12)	13 (13)
	2–4	0.127	3.0	9 (9)	10 (11)
	4–6	0.0967	2.8	8 (8)	9 (9)
	6–8	0.0695	3.3	12 (12)	13 (13)
	8–11	0.0731	2.9	6 (5)	8 (7)
	11–15	0.0467	3.3	6 (6)	8 (8)
	15–50	0.0314	0.8	4 (4)	6 (6)
Y(2S)	0–3	0.0472	7.2	12 (11)	14 (14)
	3–7	0.0580	4.5	8 (8)	10 (10)
	7–11	0.0334	5.2	7 (5)	10 (8)
	11–15	0.0154	6.6	5 (6)	9 (10)
	15–42	0.0147	5.9	4 (5)	8 (8)
Y(3S)	0–7	0.0504	6.8	13 (11)	15 (13)
	7–12	0.0247	6.8	7 (7)	11 (10)
	12–38	0.0155	6.5	5 (5)	9 (9)

Table A.6: The product of the fiducial $Y(nS)$ production cross sections, σ , integrated and differential in p_T^Y , and the respective dimuon branching fraction, \mathcal{B} , integrated over the rapidity range $0.8 < |y^Y| < 1.2$. The statistical uncertainty (stat.), the sum of the systematic uncertainties in quadrature ($\Sigma_{\text{syst.}}$), and the total uncertainty ($\Delta\sigma$; including stat., $\Sigma_{\text{syst.}}$, and the uncertainty in the integrated luminosity) are in percent. The numbers in parentheses are negative variations.

$0.8 < y^Y < 1.2$					
	p_T (GeV/c)	$\sigma \cdot \mathcal{B}$ (nb)	$\frac{\text{stat.}}{\sigma}$	$\frac{\Sigma_{\text{syst.}}}{\sigma}$	$\frac{\Delta\sigma}{\sigma}$
Y(1S)	0–2	0.107	3.7	9 (9)	11 (10)
	2–4	0.160	2.7	9 (9)	10 (10)
	4–6	0.0995	2.9	7 (6)	8 (8)
	6–8	0.0770	3.1	12 (12)	13 (13)
	8–11	0.0746	2.9	5 (8)	7 (9)
	11–15	0.0464	3.4	6 (6)	8 (8)
	15–50	0.0313	3.8	5 (6)	7 (8)
Y(2S)	0–3	0.0561	6.1	11 (10)	13 (12)
	3–7	0.0610	5.0	8 (8)	10 (10)
	7–11	0.0347	5.3	14 (14)	15 (15)
	11–15	0.0168	6.2	6 (7)	9 (10)
	15–42	0.0142	6.2	6 (7)	10 (10)
Y(3S)	0–7	0.0526	7.7	17 (17)	19 (19)
	7–12	0.0264	6.9	11 (14)	14 (17)
	12–38	0.0154	6.8	10 (10)	13 (13)

Table A.7: The product of the fiducial $Y(nS)$ production cross sections, σ , integrated and differential in p_T^Y , and the respective dimuon branching fraction, \mathcal{B} , integrated over the rapidity range $1.2 < |y^Y| < 1.6$. The statistical uncertainty (stat.), the sum of the systematic uncertainties in quadrature ($\Sigma_{\text{syst.}}$), and the total uncertainty ($\Delta\sigma$; including stat., $\Sigma_{\text{syst.}}$, and the uncertainty in the integrated luminosity) are in percent. The numbers in parentheses are negative variations.

$1.2 < y^Y < 1.6$					
	p_T (GeV/c)	$\sigma \cdot \mathcal{B}$ (nb)	$\frac{\text{stat.}}{\sigma}$	$\frac{\Sigma_{\text{syst.}}}{\sigma}$	$\frac{\Delta\sigma}{\sigma}$
Y(1S)	0–2	0.119	3.5	6 (12)	8 (13)
	2–4	0.184	2.4	7 (6)	8 (8)
	4–6	0.1059	2.8	6 (5)	8 (7)
	6–8	0.0747	3.0	5 (6)	7 (7)
	8–11	0.0697	3.0	5 (5)	7 (7)
	11–15	0.0456	3.3	6 (6)	8 (8)
	15–50	0.0319	3.8	7 (8)	9 (10)
Y(2S)	0–3	0.0582	6.2	6 (6)	10 (9)
	3–7	0.0684	4.5	7 (6)	9 (8)
	7–11	0.0317	5.5	5 (6)	9 (9)
	11–15	0.0164	6.5	5 (5)	9 (9)
	15–42	0.0147	6.4	8 (9)	11 (12)
Y(3S)	0–7	0.0589	6.9	6 (5)	10 (10)
	7–12	0.0214	7.7	9 (9)	13 (12)
	12–38	0.0171	6.7	8 (8)	11 (11)

Table A.8: The product of the fiducial $Y(nS)$ production cross sections, σ , integrated and differential in p_T^Y , and the respective dimuon branching fraction, \mathcal{B} , integrated over the rapidity range $1.6 < |y^Y| < 2.0$. The statistical uncertainty (stat.), the sum of the systematic uncertainties in quadrature ($\Sigma_{\text{syst.}}$), and the total uncertainty ($\Delta\sigma$; including stat., $\Sigma_{\text{syst.}}$, and the uncertainty in the integrated luminosity) are in percent. The numbers in parentheses are negative variations.

$1.6 < y^Y < 2.0$					
	p_T (GeV/c)	$\sigma \cdot \mathcal{B}$ (nb)	$\frac{\text{stat.}}{\sigma}$	$\frac{\Sigma_{\text{syst.}}}{\sigma}$	$\frac{\Delta\sigma}{\sigma}$
Y(1S)	0–2	0.105	3.1	9 (8)	10 (9)
	2–4	0.164	2.5	6 (5)	8 (7)
	4–6	0.1058	2.7	5 (4)	7 (6)
	6–8	0.0564	3.2	4 (4)	6 (6)
	8–11	0.0500	3.4	6 (6)	8 (8)
	11–15	0.0321	4.1	5 (5)	8 (8)
	15–50	0.0274	4.4	6 (6)	8 (8)
Y(2S)	0–3	0.0452	6.2	8 (8)	11 (11)
	3–7	0.0661	4.3	7 (7)	9 (9)
	7–11	0.0205	7.0	10 (10)	13 (13)
	11–15	0.0112	8.3	5 (5)	11 (11)
	15–42	0.0120	8.1	6 (5)	11 (11)
Y(3S)	0–7	0.0525	7.2	9 (9)	12 (12)
	7–12	0.0120	10.6	15 (15)	19 (19)
	12–38	0.0124	8.8	6 (6)	11 (12)

Table A.9: The product of the fiducial $Y(nS)$ production cross sections, σ , integrated and differential in p_T^Y , and the respective dimuon branching fraction, \mathcal{B} , integrated over the rapidity range $2.0 < |y^Y| < 2.4$. The statistical uncertainty (stat.), the sum of the systematic uncertainties in quadrature ($\Sigma_{\text{syst.}}$), and the total uncertainty ($\Delta\sigma$; including stat., $\Sigma_{\text{syst.}}$, and the uncertainty in the integrated luminosity) are in percent. The numbers in parentheses are negative variations.

$2.0 < y^Y < 2.4$					
	p_T (GeV/c)	$\sigma \cdot \mathcal{B}$ (nb)	$\frac{\text{stat.}}{\sigma}$	$\frac{\Sigma_{\text{syst.}}}{\sigma}$	$\frac{\Delta\sigma}{\sigma}$
Y(1S)	0–2	0.0299	5.3	9 (9)	11 (11)
	2–4	0.0671	2.8	7 (5)	8 (7)
	4–6	0.0515	3.7	12 (12)	13 (13)
	6–8	0.0216	5.6	6 (7)	9 (10)
	8–11	0.0194	5.8	6 (6)	9 (9)
	11–15	0.0113	7.2	9 (8)	12 (12)
	15–50	0.0092	9.1	13 (12)	16 (16)
Y(2S)	0–3	0.0119	13.2	11 (10)	18 (17)
	3–7	0.0278	7.6	9 (8)	12 (12)
	7–11	0.0098	10.9	9 (8)	14 (14)
	11–15	0.00440	14.7	8 (7)	17 (17)
	15–42	0.00365	20.4	10 (9)	23 (23)
Y(3S)	0–7	0.0223	11.2	10 (9)	16 (15)
	7–12	0.0054	19.3	7 (7)	21 (21)
	12–38	0.00518	15.8	8 (8)	18 (18)

Table A.10: The product of the fiducial $Y(nS)$ production cross sections, σ , integrated and differential in $|y^Y|$, and the respective dimuon branching fraction, \mathcal{B} , integrated over the p_T range $p_T^Y < 50 \text{ GeV}/c$. The statistical uncertainty (stat.), the sum of the systematic uncertainties in quadrature ($\Sigma_{\text{syst.}}$), and the total uncertainty ($\Delta\sigma$; including stat., $\Sigma_{\text{syst.}}$, and the uncertainty in the integrated luminosity) are in percent. The numbers in parentheses are negative variations.

$p_T^Y < 50 \text{ GeV}/c$					
	$ y $	$\sigma \cdot \mathcal{B}$ (nb)	$\frac{\text{stat.}}{\sigma}$	$\frac{\Sigma_{\text{syst.}}}{\sigma}$	$\frac{\Delta\sigma}{\sigma}$
Y(1S)	0–0.2	0.262	1.7	9 (9)	10 (10)
	0.2–0.4	0.268	1.7	9 (9)	10 (10)
	0.4–0.6	0.269	1.7	9 (9)	10 (10)
	0.6–0.8	0.295	1.7	7 (6)	8 (8)
	0.8–1.0	0.295	1.7	8 (8)	9 (9)
	1.0–1.2	0.303	1.8	6 (6)	7 (7)
	1.2–1.4	0.305	1.7	7 (7)	8 (8)
	1.4–1.6	0.322	1.7	5 (4)	7 (6)
	1.6–1.8	0.301	1.7	6 (5)	7 (7)
	1.8–2	0.248	1.9	6 (5)	7 (7)
	2–2.2	0.159	2.3	7 (5)	8 (7)
	2.2–2.4	0.0514	4.3	6 (5)	9 (7)
0–2.4	3.08	0.5	6 (6)	8 (7)	
Y(2S)	0–0.4	0.158	2.4	8 (7)	9 (9)
	0.4–0.8	0.170	2.6	8 (7)	9 (9)
	0.8–1.2	0.179	2.8	7 (7)	9 (9)
	1.2–1.6	0.185	2.7	6 (5)	8 (7)
	1.6–2	0.157	2.9	6 (6)	8 (7)
	2–2.4	0.0577	7.6	7 (6)	11 (11)
	0–2.4	0.907	1.2	6 (5)	7 (7)
Y(3S)	0–0.4	0.0858	3.7	8 (8)	10 (10)
	0.4–0.8	0.0946	4.0	8 (7)	10 (9)
	0.8–1.4	0.141	3.8	7 (7)	9 (9)
	1.4–2	0.134	4.0	7 (7)	9 (9)
	2–2.4	0.0321	10.3	7 (5)	13 (12)
	0–2.4	0.487	2.0	6 (6)	8 (7)

Table A.11: The ratio of $Y(3S)/Y(1S)$ fiducial cross sections, and its p_T dependence, integrated over the rapidity range $|y^Y| < 2.4$, with statistical and systematic uncertainties combined in quadrature. The numbers in parentheses are negative variations.

p_T (GeV/c)	$Y(3S)/Y(1S)$
0–2	0.129 ± 0.009 (0.008) ± 0.017 (0.020)
2–5	0.141 ± 0.008 (0.008) ± 0.018 (0.016)
5–8	0.154 ± 0.009 (0.009) ± 0.016 (0.016)
8–10	0.172 ± 0.011 (0.011) ± 0.022 (0.014)
10–13	0.197 ± 0.012 (0.012) ± 0.022 (0.016)
13–16	0.251 ± 0.019 (0.018) ± 0.037 (0.021)
16–18	0.308 ± 0.035 (0.033) ± 0.031 (0.037)
18–22	0.287 ± 0.029 (0.027) ± 0.023 (0.037)
22–38	0.345 ± 0.042 (0.038) ± 0.055 (0.051)
0–38	0.158 ± 0.004 (0.004) ± 0.016 (0.016)

Table A.12: The ratio of $Y(2S)/Y(1S)$ fiducial cross sections, and its p_T dependence, integrated over the rapidity range $|y^Y| < 2.4$, with statistical and systematic uncertainties combined in quadrature. The numbers in parentheses are negative variations.

p_T (GeV/c)	$Y(2S)/Y(1S)$
0–2	0.258 ± 0.011 (0.011) ± 0.034 (0.032)
2–5	0.283 ± 0.010 (0.010) ± 0.035 (0.031)
5–8	0.302 ± 0.012 (0.012) ± 0.031 (0.028)
8–10	0.289 ± 0.014 (0.013) ± 0.030 (0.022)
10–13	0.339 ± 0.016 (0.016) ± 0.032 (0.029)
13–16	0.376 ± 0.023 (0.022) ± 0.053 (0.034)
16–18	0.481 ± 0.045 (0.042) ± 0.046 (0.053)
18–22	0.454 ± 0.037 (0.035) ± 0.040 (0.053)
22–38	0.511 ± 0.051 (0.047) ± 0.083 (0.046)
0–38	0.296 ± 0.005 (0.005) ± 0.031 (0.029)

Table A.13: The ratio of $Y(3S)/Y(2S)$ fiducial cross sections, and its p_T dependence, integrated over the rapidity range $|y^Y| < 2.4$, with statistical and systematic uncertainties combined in quadrature. The numbers in parentheses are negative variations.

p_T (GeV/c)	$Y(3S)/Y(2S)$
0–2	0.500 ± 0.043 (0.040) ± 0.062 (0.072)
2–5	0.497 ± 0.036 (0.034) ± 0.063 (0.057)
5–8	0.510 ± 0.039 (0.037) ± 0.053 (0.051)
8–10	0.595 ± 0.049 (0.046) ± 0.079 (0.062)
10–13	0.581 ± 0.046 (0.043) ± 0.067 (0.049)
13–16	0.669 ± 0.061 (0.057) ± 0.066 (0.054)
16–18	0.639 ± 0.089 (0.079) ± 0.083 (0.077)
18–22	0.631 ± 0.077 (0.070) ± 0.057 (0.065)
22–38	0.675 ± 0.096 (0.085) ± 0.068 (0.101)
0–38	0.534 ± 0.017 (0.016) ± 0.054 (0.051)

Table A.14: The product of the $Y(1S)$ acceptance-corrected production cross sections, σ , integrated and differential in p_T^Y , and the dimuon branching fraction, \mathcal{B} , measured for four polarization scenarios, in the helicity frame (HX) and Collins–Soper (CS) frame, each for $\lambda_\theta = 1$ and $\lambda_\theta = -1$, integrated over the rapidity range $|y^Y| < 2.4$. The statistical uncertainty (stat.), the sum of the systematic uncertainties in quadrature ($\Sigma_{\text{syst.}}$), and the total uncertainty ($\Delta\sigma$; including stat., $\Sigma_{\text{syst.}}$, and the uncertainty in the integrated luminosity) are in percent. For the four polarization scenarios the fractional change to the central value of the cross section relative to the unpolarized value is given in percent. The numbers in parentheses are negative variations.

					$ y^Y < 2.4$ Y(1S)			
p_T (GeV/c)	$\sigma \cdot \mathcal{B}$ (nb)	$\frac{\text{stat.}}{\sigma}$	$\frac{\Sigma_{\text{syst.}}}{\sigma}$	$\frac{\Delta\sigma}{\sigma}$	HX		CS	
					$\lambda_\theta = 1$	$\lambda_\theta = -1$	$\lambda_\theta = 1$	$\lambda_\theta = -1$
0–0.5	0.0859	5.4	8 (7)	11 (10)	+19	–24	+21	–26
0.5–1	0.263	3.3	8 (7)	9 (9)	+22	–24	+23	–25
1–1.5	0.374	2.6	8 (8)	9 (9)	+23	–22	+26	–24
1.5–2	0.505	2.4	9 (8)	10 (9)	+16	–27	+19	–29
2–3	1.16	1.6	8 (10)	9 (11)	+20	–25	+26	–27
3–4	1.21	2.1	7 (6)	9 (8)	+20	–26	+21	–26
4–5	1.084	2.1	7 (6)	8 (8)	+21	–25	+21	–24
5–6	0.879	1.9	7 (9)	8 (10)	+19	–25	+16	–23
6–7	0.680	2.6	6 (6)	8 (7)	+18	–24	+13	–23
7–8	0.556	2.0	6 (5)	7 (7)	+20	–22	+12	–13
8–9	0.419	2.2	5 (5)	7 (7)	+19	–22	+9	–9
9–10	0.331	2.3	5 (4)	7 (6)	+19	–21	+7	–4
10–11	0.238	2.5	5 (4)	7 (6)	+17	–20	+4	–1
11–12	0.179	2.9	5 (4)	7 (6)	+18	–19	+6	+0
12–13	0.145	2.9	5 (4)	7 (7)	+16	–20	+2	+2
13–14	0.0990	3.2	4 (5)	7 (7)	+14	–21	–0	+3
14–15	0.0750	3.6	5 (5)	8 (7)	+15	–20	–1	+5
15–16	0.0595	3.8	5 (5)	7 (7)	+13	–19	–1	+5
16–18	0.0732	3.4	5 (5)	7 (7)	+12	–20	–3	+6
18–20	0.0500	3.8	5 (4)	7 (7)	+13	–18	–2	+7
20–22	0.0302	5.1	5 (4)	8 (8)	+11	–18	–3	+6
22–25	0.0237	5.6	5 (4)	8 (8)	+9	–18	–3	+4
25–30	0.0205	6.0	5 (4)	9 (8)	+10	–16	–1	+4
30–50	0.0123	7.4	6 (6)	10 (10)	+5	–17	–7	+3
0–50	8.55	0.6	7 (6)	8 (7)	+19	–24	+16	–19

Table A.15: The product of the $Y(2S)$ acceptance-corrected production cross sections, σ , integrated and differential in p_T^Y , and the dimuon branching fraction, \mathcal{B} , measured for four polarization scenarios, in the helicity frame (HX) and Collins-Soper (CS) frame, each for $\lambda_\theta = 1$ and $\lambda_\theta = -1$, integrated over the rapidity range $|y^Y| < 2.4$. The statistical uncertainty (stat.), the sum of the systematic uncertainties in quadrature ($\Sigma_{\text{syst.}}$), and the total uncertainty ($\Delta\sigma$; including stat., $\Sigma_{\text{syst.}}$, and the uncertainty in the integrated luminosity) are in percent. For the four polarization scenarios the fractional change to the central value of the cross section relative to the unpolarized value is given in percent. The numbers in parentheses are negative variations.

$ y^Y < 2.4$ Y(2S)								
p_T (GeV/c)	$\sigma \cdot \mathcal{B}$ (nb)	$\frac{\text{stat.}}{\sigma}$	$\frac{\Sigma_{\text{syst.}}}{\sigma}$	$\frac{\Delta\sigma}{\sigma}$	HX		CS	
					$\lambda_\theta = 1$	$\lambda_\theta = -1$	$\lambda_\theta = 1$	$\lambda_\theta = -1$
0–1	0.0829	5.9	9 (8)	11 (11)	+18	–23	+19	–24
1–2.5	0.331	3.3	11 (10)	12 (11)	+14	–23	+18	–25
2.5–4	0.409	3.1	9 (8)	10 (9)	+22	–24	+21	–26
4–5.5	0.362	3.3	8 (7)	9 (9)	+18	–22	+16	–24
5.5–7	0.286	3.6	7 (6)	9 (8)	+17	–23	+15	–20
7–8.5	0.212	3.9	7 (7)	9 (9)	+21	–20	+15	–12
8.5–10	0.146	4.0	6 (6)	9 (8)	+20	–18	+11	–5
10–11.5	0.1123	4.1	6 (6)	9 (8)	+19	–18	+8	–0
11.5–13	0.0765	4.6	5 (5)	8 (8)	+17	–18	+6	+1
13–14.5	0.0519	5.1	5 (5)	8 (8)	+14	–20	+0	+3
14.5–16	0.0376	5.7	5 (7)	9 (10)	+14	–19	+1	+3
16–18	0.0373	5.3	6 (5)	9 (8)	+13	–18	+1	+3
18–19.5	0.0159	7.4	5 (4)	10 (9)	+13	–18	–3	+9
19.5–22	0.0204	6.6	5 (5)	9 (9)	+11	–16	–1	+5
22–26	0.0158	7.2	5 (4)	10 (9)	+11	–16	–3	+7
26–42	0.0126	7.7	6 (5)	10 (10)	+10	–15	–4	+9
0–42	2.21	1.2	7 (6)	8 (7)	+14	–24	+13	–20

Table A.16: The product of the $Y(3S)$ acceptance-corrected production cross sections, σ , integrated and differential in p_T^Y , and the dimuon branching fraction, \mathcal{B} , measured for four polarization scenarios, in the helicity frame (HX) and Collins–Soper (CS) frame, each for $\lambda_\theta = 1$ and $\lambda_\theta = -1$, integrated over the rapidity range $|y^Y| < 2.4$. The statistical uncertainty (stat.), the sum of the systematic uncertainties in quadrature ($\Sigma_{\text{syst.}}$), and the total uncertainty ($\Delta\sigma$; including stat., $\Sigma_{\text{syst.}}$, and the uncertainty in the integrated luminosity) are in percent. For the four polarization scenarios the fractional change to the central value of the cross section relative to the unpolarized value is given in percent. The numbers in parentheses are negative variations.

					$ y^Y < 2.4$			
					$Y(3S)$			
p_T (GeV/c)	$\sigma \cdot \mathcal{B}$ (nb)	$\frac{\text{stat.}}{\sigma}$	$\frac{\Sigma_{\text{syst.}}}{\sigma}$	$\frac{\Delta\sigma}{\sigma}$	HX		CS	
					$\lambda_\theta = 1$	$\lambda_\theta = -1$	$\lambda_\theta = 1$	$\lambda_\theta = -1$
0–2.5	0.203	5.3	8 (8)	11 (10)	+17	–21	+20	–25
2.5–5	0.287	4.5	10 (11)	12 (12)	+17	–22	+20	–25
5–7.5	0.227	4.6	9 (8)	11 (10)	+16	–22	+20	–22
7.5–10	0.157	4.8	11 (10)	12 (12)	+23	–16	+16	–5
10–13	0.113	4.3	7 (5)	9 (8)	+20	–15	+12	–1
13–16	0.0617	5.0	5 (5)	8 (8)	+14	–17	+4	+1
16–18	0.0227	7.4	6 (5)	10 (10)	+12	–18	–1	+4
18–22	0.0229	7.0	7 (6)	10 (10)	+12	–17	–1	+6
22–38	0.0185	7.6	13 (13)	15 (15)	+10	–15	–0	+6
0–38	1.11	2.0	9 (8)	10 (9)	+16	–21	+14	–17

Table A.17: The product of the $Y(nS)$ acceptance-corrected production cross sections, σ , integrated and differential in p_T^Y , and the respective dimuon branching fraction, \mathcal{B} , measured for four polarization scenarios, in the helicity frame (HX) and Collins–Soper (CS) frame, each for $\lambda_\theta = 1$ and $\lambda_\theta = -1$, integrated over the rapidity range $|y^Y| < 0.4$. The statistical uncertainty (stat.), the sum of the systematic uncertainties in quadrature ($\Sigma_{\text{sys.}}$), and the total uncertainty ($\Delta\sigma$; including stat., $\Sigma_{\text{sys.}}$, and the uncertainty in the integrated luminosity) are in percent. For the four polarization scenarios the fractional change to the central value of the cross section relative to the unpolarized value is given in percent. The numbers in parentheses are negative variations.

$ y^Y < 0.4$									
	p_T (GeV/c)	$\sigma \cdot \mathcal{B}$ (nb)	stat. σ	$\Sigma_{\text{sys.}}$ σ	$\frac{\Delta\sigma}{\sigma}$	HX		CS	
						$\lambda_\theta = 1$	$\lambda_\theta = -1$	$\lambda_\theta = 1$	$\lambda_\theta = -1$
Y(1S)	0–2	0.216	3.4	14 (13)	15 (14)	+10	–16	+21	–27
	2–4	0.387	3.2	11 (10)	12 (12)	+15	–22	+20	–26
	4–6	0.355	3.0	10 (10)	11 (11)	+21	–27	+16	–22
	6–8	0.224	3.2	9 (9)	10 (10)	+17	–30	+3	–17
	8–11	0.190	2.9	7 (7)	8 (8)	+22	–27	–0	+1
	11–15	0.0914	3.3	5 (5)	7 (7)	+20	–25	–4	+10
	15–50	0.0509	3.7	4 (4)	7 (7)	+17	–22	–5	+13
Y(2S)	0–3	0.084	6.6	16 (15)	18 (17)	+22	–13	+20	–25
	3–7	0.143	4.9	13 (16)	15 (17)	+27	–16	+15	–19
	7–11	0.0813	5.3	9 (8)	11 (11)	+21	–26	+2	–3
	11–15	0.0323	6.1	6 (5)	9 (9)	+20	–25	–4	+9
	15–42	0.0243	5.7	5 (4)	8 (8)	+16	–21	–5	+12
Y(3S)	0–7	0.100	6.5	15 (14)	17 (16)	+12	–16	+16	–22
	7–12	0.0487	7.5	11 (11)	14 (14)	+20	–25	+2	–3
	12–38	0.0291	5.9	5 (5)	9 (9)	+17	–23	–5	+11

Table A.18: The product of the $Y(nS)$ acceptance-corrected production cross sections, σ , integrated and differential in p_T^Y , and the respective dimuon branching fraction, \mathcal{B} , measured for four polarization scenarios, in the helicity frame (HX) and Collins–Soper (CS) frame, each for $\lambda_\theta = 1$ and $\lambda_\theta = -1$, integrated over the rapidity range $0.4 < |y^Y| < 0.8$. The statistical uncertainty (stat.), the sum of the systematic uncertainties in quadrature ($\Sigma_{\text{syst.}}$), and the total uncertainty ($\Delta\sigma$; including stat., $\Sigma_{\text{syst.}}$, and the uncertainty in the integrated luminosity) are in percent. For the four polarization scenarios the fractional change to the central value of the cross section relative to the unpolarized value is given in percent. The numbers in parentheses are negative variations.

$0.4 < y^Y < 0.8$									
	p_T (GeV/c)	$\sigma \cdot \mathcal{B}$ (nb)	$\frac{\text{stat.}}{\sigma}$	$\frac{\Sigma_{\text{syst.}}}{\sigma}$	$\frac{\Delta\sigma}{\sigma}$	HX		CS	
						$\lambda_\theta = 1$	$\lambda_\theta = -1$	$\lambda_\theta = 1$	$\lambda_\theta = -1$
Y(1S)	0–2	0.220	4.5	13 (12)	14 (13)	+20	–25	+21	–26
	2–4	0.409	3.0	10 (9)	11 (10)	+21	–25	+22	–25
	4–6	0.367	2.9	8 (8)	9 (9)	+20	–25	+16	–21
	6–8	0.231	3.3	7 (6)	9 (8)	+13	–27	+2	–15
	8–11	0.180	2.9	6 (5)	8 (7)	+19	–23	–0	+2
	11–15	0.0915	3.3	6 (6)	8 (8)	+18	–23	–4	+10
	15–50	0.0492	3.8	4 (4)	7 (7)	+15	–20	–5	+13
Y(2S)	0–3	0.088	7.3	14 (13)	16 (15)	+18	–23	+19	–24
	3–7	0.172	4.5	10 (9)	11 (11)	+17	–23	+15	–20
	7–11	0.0811	5.2	6 (6)	9 (9)	+17	–23	+1	–2
	11–15	0.0293	6.6	5 (5)	9 (9)	+17	–22	–4	+9
	15–42	0.0227	5.9	4 (4)	8 (8)	+15	–20	–5	+12
Y(3S)	0–7	0.115	6.7	14 (13)	16 (15)	+16	–22	+16	–21
	7–12	0.0558	6.8	7 (6)	11 (10)	+16	–22	+1	–2
	12–38	0.0257	6.5	5 (5)	9 (9)	+15	–21	–4	+10

Table A.19: The product of the $Y(nS)$ acceptance-corrected production cross sections, σ , integrated and differential in p_T^Y , and the respective dimuon branching fraction, \mathcal{B} , measured for four polarization scenarios, in the helicity frame (HX) and Collins–Soper (CS) frame, each for $\lambda_\theta = 1$ and $\lambda_\theta = -1$, integrated over the rapidity range $0.8 < |y^Y| < 1.2$. The statistical uncertainty (stat.), the sum of the systematic uncertainties in quadrature ($\Sigma_{\text{syst.}}$), and the total uncertainty ($\Delta\sigma$; including stat., $\Sigma_{\text{syst.}}$, and the uncertainty in the integrated luminosity) are in percent. For the four polarization scenarios the fractional change to the central value of the cross section relative to the unpolarized value is given in percent. The numbers in parentheses are negative variations.

$0.8 < y^Y < 1.2$									
	p_T (GeV/c)	$\sigma \cdot \mathcal{B}$ (nb)	$\frac{\text{stat.}}{\sigma}$	$\frac{\Sigma_{\text{syst.}}}{\sigma}$	$\frac{\Delta\sigma}{\sigma}$	HX		CS	
						$\lambda_\theta = 1$	$\lambda_\theta = -1$	$\lambda_\theta = 1$	$\lambda_\theta = -1$
Y(1S)	0–2	0.198	3.7	11 (9)	12 (10)	+20	–25	+20	–24
	2–4	0.426	2.7	9 (9)	10 (10)	+20	–26	+19	–25
	4–6	0.331	2.9	7 (6)	8 (8)	+17	–25	+13	–21
	6–8	0.217	3.4	7 (7)	9 (8)	+22	–18	+12	–7
	8–11	0.174	2.9	5 (5)	7 (7)	+15	–21	–1	+2
	11–15	0.0879	3.4	6 (5)	8 (8)	+15	–21	–4	+9
	15–50	0.0482	3.8	5 (5)	8 (8)	+13	–19	–5	+12
Y(2S)	0–3	0.098	6.2	14 (13)	15 (15)	+18	–23	+17	–23
	3–7	0.155	5.3	11 (8)	13 (10)	+19	–22	+16	–19
	7–11	0.0803	5.3	8 (7)	10 (10)	+14	–20	+1	–2
	11–15	0.0309	6.2	6 (6)	10 (9)	+14	–20	–4	+9
	15–42	0.0214	6.2	6 (6)	10 (9)	+13	–18	–5	+11
Y(3S)	0–7	0.109	7.7	15 (14)	17 (17)	+16	–22	+14	–20
	7–12	0.0579	6.9	9 (9)	12 (12)	+13	–19	+2	–3
	12–38	0.0250	6.8	6 (6)	10 (10)	+13	–19	–4	+10

Table A.20: The product of the $Y(nS)$ acceptance-corrected production cross sections, σ , integrated and differential in p_T^Y , and the respective dimuon branching fraction, \mathcal{B} , measured for four polarization scenarios, in the helicity frame (HX) and Collins-Soper (CS) frame, each for $\lambda_\theta = 1$ and $\lambda_\theta = -1$, integrated over the rapidity range $1.2 < |y^Y| < 1.6$. The statistical uncertainty (stat.), the sum of the systematic uncertainties in quadrature ($\Sigma_{\text{syst.}}$), and the total uncertainty ($\Delta\sigma$; including stat., $\Sigma_{\text{syst.}}$, and the uncertainty in the integrated luminosity) are in percent. For the four polarization scenarios the fractional change to the central value of the cross section relative to the unpolarized value is given in percent. The numbers in parentheses are negative variations.

$1.2 < y^Y < 1.6$									
	p_T (GeV/c)	$\sigma \cdot \mathcal{B}$ (nb)	$\frac{\text{stat.}}{\sigma}$	$\frac{\Sigma_{\text{syst.}}}{\sigma}$	$\frac{\Delta\sigma}{\sigma}$	HX		CS	
						$\lambda_\theta = 1$	$\lambda_\theta = -1$	$\lambda_\theta = 1$	$\lambda_\theta = -1$
Y(1S)	0–2	0.203	3.5	10 (8)	11 (9)	+19	–23	+21	–22
	2–4	0.416	2.4	7 (6)	8 (7)	+20	–26	+18	–25
	4–6	0.315	2.8	6 (5)	8 (7)	+20	–24	+17	–21
	6–8	0.215	3.0	5 (6)	7 (7)	+17	–22	+11	–15
	8–11	0.165	3.0	5 (5)	7 (7)	+13	–19	+2	–4
	11–15	0.0868	3.3	5 (5)	7 (7)	+13	–19	–3	+6
	15–50	0.0485	3.8	4 (4)	7 (7)	+12	–18	–5	+11
Y(2S)	0–3	0.099	6.2	11 (11)	13 (13)	+18	–24	+18	–23
	3–7	0.161	4.5	7 (6)	9 (9)	+18	–23	+17	–22
	7–11	0.0758	5.5	7 (6)	10 (9)	+14	–19	+6	–9
	11–15	0.0305	6.5	5 (5)	9 (9)	+12	–18	–2	+5
	15–42	0.0219	6.4	5 (4)	9 (9)	+11	–17	–4	+10
Y(3S)	0–7	0.113	6.8	7 (7)	11 (10)	+17	–23	+16	–22
	7–12	0.0480	7.7	10 (10)	13 (13)	+13	–18	+5	–8
	12–38	0.0276	6.7	8 (7)	11 (11)	+11	–17	–3	+7

Table A.21: The product of the $Y(nS)$ acceptance-corrected production cross sections, σ , integrated and differential in p_T^Y , and the respective dimuon branching fraction, \mathcal{B} , measured for four polarization scenarios, in the helicity frame (HX) and Collins-Soper (CS) frame, each for $\lambda_\theta = 1$ and $\lambda_\theta = -1$, integrated over the rapidity range $1.6 < |y^Y| < 2.0$. The statistical uncertainty (stat.), the sum of the systematic uncertainties in quadrature ($\Sigma_{\text{syst.}}$), and the total uncertainty ($\Delta\sigma$; including stat., $\Sigma_{\text{syst.}}$, and the uncertainty in the integrated luminosity) are in percent. For the four polarization scenarios the fractional change to the central value of the cross section relative to the unpolarized value is given in percent. The numbers in parentheses are negative variations.

$1.6 < y^Y < 2.0$									
	p_T (GeV/c)	$\sigma \cdot \mathcal{B}$ (nb)	$\frac{\text{stat.}}{\sigma}$	$\frac{\Sigma_{\text{syst.}}}{\sigma}$	$\frac{\Delta\sigma}{\sigma}$	HX		CS	
						$\lambda_\theta = 1$	$\lambda_\theta = -1$	$\lambda_\theta = 1$	$\lambda_\theta = -1$
Y(1S)	0–2	0.211	3.1	7 (6)	9 (8)	+22	–26	+23	–27
	2–4	0.401	2.5	6 (4)	7 (6)	+22	–26	+24	–27
	4–6	0.330	2.6	5 (4)	7 (6)	+20	–25	+23	–27
	6–8	0.191	3.2	4 (4)	7 (6)	+18	–22	+20	–24
	8–11	0.151	3.4	5 (4)	7 (7)	+15	–20	+15	–19
	11–15	0.0746	4.1	5 (5)	8 (7)	+10	–16	+5	–9
	15–50	0.0465	4.4	6 (6)	9 (8)	+9	–14	–1	+3
Y(2S)	0–3	0.091	6.8	8 (8)	11 (11)	+21	–25	+22	–27
	3–7	0.175	4.4	7 (6)	9 (9)	+19	–24	+23	–27
	7–11	0.0608	7.0	7 (6)	10 (10)	+14	–20	+17	–22
	11–15	0.0263	8.3	5 (5)	11 (10)	+10	–15	+7	–11
	15–42	0.0205	8.1	6 (5)	11 (11)	+8	–13	–0	+1
Y(3S)	0–7	0.117	7.2	9 (9)	13 (12)	+19	–23	+23	–26
	7–12	0.0341	10.6	18 (18)	22 (21)	+13	–19	+16	–21
	12–38	0.0243	8.8	6 (6)	11 (11)	+8	–13	+4	–6

Table A.22: The product of the $Y(nS)$ acceptance-corrected production cross sections, σ , integrated and differential in p_T^Y , and the respective dimuon branching fraction, \mathcal{B} , measured for four polarization scenarios, in the helicity frame (HX) and Collins-Soper (CS) frame, each for $\lambda_\theta = 1$ and $\lambda_\theta = -1$, integrated over the rapidity range $2.0 < |y^Y| < 2.4$. The statistical uncertainty (stat.), the sum of the systematic uncertainties in quadrature ($\Sigma_{\text{syst.}}$), and the total uncertainty ($\Delta\sigma$; including stat., $\Sigma_{\text{syst.}}$, and the uncertainty in the integrated luminosity) are in percent. For the four polarization scenarios the fractional change to the central value of the cross section relative to the unpolarized value is given in percent. The numbers in parentheses are negative variations.

$2.0 < y^Y < 2.4$									
	p_T (GeV/c)	$\sigma \cdot \mathcal{B}$ (nb)	$\frac{\text{stat.}}{\sigma}$	$\frac{\Sigma_{\text{syst.}}}{\sigma}$	$\frac{\Delta\sigma}{\sigma}$	HX		CS	
						$\lambda_\theta = 1$	$\lambda_\theta = -1$	$\lambda_\theta = 1$	$\lambda_\theta = -1$
Y(1S)	0–2	0.135	5.3	8 (7)	11 (9)	+30	–31	+32	–31
	2–4	0.338	2.8	7 (6)	9 (8)	+23	–28	+30	–32
	4–6	0.289	4.1	8 (6)	10 (9)	+27	–21	+38	–28
	6–8	0.150	5.8	7 (6)	10 (9)	+23	–21	+34	–29
	8–11	0.126	5.8	7 (5)	10 (9)	+18	–20	+31	–29
	11–15	0.0667	7.2	8 (7)	12 (11)	+14	–18	+28	–29
	15–50	0.0356	9.1	9 (9)	14 (13)	+6	–13	+18	–24
Y(2S)	0–3	0.0475	13.2	9 (8)	16 (16)	+27	–30	+30	–32
	3–7	0.148	7.5	7 (5)	11 (10)	+20	–25	+31	–32
	7–11	0.0636	10.9	8 (7)	14 (13)	+16	–22	+29	–31
	11–15	0.0224	14.7	9 (8)	18 (17)	+12	–18	+26	–29
	15–42	0.0137	20.4	11 (11)	24 (23)	+9	–14	+20	–24
Y(3S)	0–7	0.105	11.2	8 (6)	14 (13)	+22	–28	+30	–32
	7–12	0.0366	19.3	11 (9)	22 (22)	+14	–20	+29	–31
	12–38	0.0231	15.8	9 (8)	19 (18)	+9	–14	+24	–27

Table A.23: The product of the $Y(nS)$ acceptance-corrected production cross sections, σ , integrated and differential in p_T^Y , and the respective dimuon branching fraction, \mathcal{B} , measured for four polarization scenarios, in the helicity frame (HX) and Collins–Soper (CS) frame, each for $\lambda_\theta = 1$ and $\lambda_\theta = -1$, integrated over the p_T range $p_T^Y < 50 \text{ GeV}/c$. The statistical uncertainty (stat.), the sum of the systematic uncertainties in quadrature ($\Sigma_{\text{syst.}}$), and the total uncertainty ($\Delta\sigma$; including stat., $\Sigma_{\text{syst.}}$ and the uncertainty in the integrated luminosity) are in percent. For the four polarization scenarios the fractional change to the central value of the cross section relative to the unpolarized value is given in percent. The numbers in parentheses are negative variations.

$p_T^Y < 50 \text{ GeV}/c$									
	$ y $	$\sigma \cdot \mathcal{B}$ (nb)	$\frac{\text{stat.}}{\sigma}$	$\frac{\Sigma_{\text{syst.}}}{\sigma}$	$\frac{\Delta\sigma}{\sigma}$	HX		CS	
						$\lambda_\theta = 1$	$\lambda_\theta = -1$	$\lambda_\theta = 1$	$\lambda_\theta = -1$
Y(1S)	0–0.2	0.770	1.7	10 (9)	11 (10)	+27	–16	+22	–9
	0.2–0.4	0.777	1.7	9 (9)	10 (10)	+19	–25	+12	–16
	0.4–0.6	0.770	1.7	9 (9)	10 (10)	+20	–18	+13	–15
	0.6–0.8	0.795	1.7	8 (8)	9 (9)	+20	–24	+13	–15
	0.8–1.0	0.761	1.7	9 (8)	10 (9)	+18	–24	+12	–15
	1.0–1.2	0.738	1.8	6 (5)	7 (7)	+18	–24	+11	–16
	1.2–1.4	0.714	1.7	7 (7)	8 (8)	+18	–23	+12	–16
	1.4–1.6	0.738	1.7	5 (4)	7 (6)	+18	–23	+14	–18
	1.6–1.8	0.721	1.7	6 (5)	7 (7)	+19	–23	+18	–21
	1.8–2	0.708	1.9	6 (5)	7 (6)	+20	–24	+23	–26
	2–2.2	0.636	2.3	6 (5)	8 (7)	+20	–24	+28	–30
	2.2–2.4	0.528	4.2	7 (5)	9 (8)	+22	–26	+32	–32
0–2.4	8.66	0.6	7 (6)	8 (7)	+19	–24	+16	–19	
Y(2S)	0–0.4	0.376	2.5	10 (9)	11 (11)	+16	–21	+10	–13
	0.4–0.8	0.400	2.5	9 (8)	10 (9)	+17	–23	+10	–13
	0.8–1.2	0.380	2.8	9 (8)	10 (9)	+16	–22	+10	–13
	1.2–1.6	0.382	2.7	7 (6)	8 (8)	+16	–22	+12	–16
	1.6–2	0.380	2.9	7 (6)	8 (8)	+17	–22	+19	–23
	2–2.4	0.295	5.1	7 (5)	9 (8)	+19	–24	+29	–31
	0–2.4	2.21	1.3	8 (7)	9 (8)	+26	–16	+23	–12
Y(3S)	0–0.4	0.185	3.9	11 (10)	12 (12)	+15	–20	+9	–11
	0.4–0.8	0.202	3.9	10 (9)	11 (11)	+16	–22	+9	–11
	0.8–1.4	0.282	3.8	9 (9)	11 (10)	+15	–21	+8	–11
	1.4–2	0.290	4.0	7 (7)	9 (9)	+16	–21	+16	–20
	2–2.4	0.164	8.3	7 (6)	12 (11)	+18	–23	+29	–31
	0–2.4	1.12	2.1	8 (7)	10 (8)	+16	–21	+14	–17

Table A.24: The ratio of $Y(3S)/Y(1S)$ acceptance-corrected cross sections, and its p_T dependence, integrated over the rapidity range $|y^Y| < 2.4$, for the unpolarized scenario, with statistical and systematic uncertainties. The numbers in parentheses are negative variations.

p_T (GeV/c)	$Y(3S)/Y(1S)$
0–2	0.108 ± 0.007 (0.007) ± 0.015 (0.015)
2–5	0.101 ± 0.006 (0.006) ± 0.015 (0.012)
5–8	0.122 ± 0.007 (0.007) ± 0.016 (0.014)
8–10	0.154 ± 0.010 (0.009) ± 0.022 (0.017)
10–13	0.197 ± 0.012 (0.011) ± 0.020 (0.015)
13–16	0.258 ± 0.019 (0.018) ± 0.021 (0.019)
16–18	0.305 ± 0.034 (0.032) ± 0.027 (0.026)
18–22	0.283 ± 0.030 (0.028) ± 0.022 (0.027)
22–38	0.323 ± 0.039 (0.036) ± 0.050 (0.089)
0–38	0.129 ± 0.003 (0.003) ± 0.018 (0.015)

Table A.25: The ratio of $Y(2S)/Y(1S)$ acceptance-corrected cross sections, and its p_T dependence, integrated over the rapidity range $|y^Y| < 2.4$, for the unpolarized scenario, with statistical and systematic uncertainties. The numbers in parentheses are negative variations.

p_T (GeV/c)	$Y(2S)/Y(1S)$
0–2	0.221 ± 0.010 (0.009) ± 0.030 (0.024)
2–5	0.230 ± 0.008 (0.008) ± 0.028 (0.030)
5–8	0.266 ± 0.011 (0.010) ± 0.033 (0.025)
8–10	0.270 ± 0.012 (0.012) ± 0.034 (0.029)
10–13	0.330 ± 0.016 (0.015) ± 0.029 (0.028)
13–16	0.372 ± 0.023 (0.022) ± 0.025 (0.028)
16–18	0.502 ± 0.046 (0.043) ± 0.040 (0.041)
18–22	0.449 ± 0.039 (0.036) ± 0.032 (0.048)
22–38	0.466 ± 0.047 (0.044) ± 0.074 (0.121)
0–38	0.264 ± 0.005 (0.005) ± 0.032 (0.028)

Table A.26: The ratio of $Y(3S)/Y(2S)$ acceptance-corrected cross sections, and its p_T dependence, integrated over the rapidity range $|y^Y| < 2.4$, for the unpolarized scenario, with statistical and systematic uncertainties. The numbers in parentheses are negative variations.

p_T (GeV/c)	$Y(3S)/Y(2S)$
0–2	0.490 ± 0.042 (0.040) ± 0.067 (0.070)
2–5	0.440 ± 0.032 (0.030) ± 0.082 (0.057)
5–8	0.459 ± 0.035 (0.033) ± 0.054 (0.053)
8–10	0.569 ± 0.047 (0.044) ± 0.078 (0.063)
10–13	0.597 ± 0.046 (0.043) ± 0.062 (0.044)
13–16	0.693 ± 0.063 (0.059) ± 0.060 (0.047)
16–18	0.607 ± 0.082 (0.074) ± 0.058 (0.051)
18–22	0.630 ± 0.079 (0.071) ± 0.060 (0.044)
22–38	0.69 ± 0.10 (0.09) ± 0.15 (0.14)
0–38	0.490 ± 0.015 (0.015) ± 0.069 (0.058)

Table A.27: The product of the $Y(nS)$ acceptance-corrected production cross sections, σ , integrated and differential in p_T^Y , and the respective dimuon branching fraction, \mathcal{B} , integrated over the rapidity range $|y^Y| < 1.2$ and the p_T^Y range from 10 to 50 GeV/ c . The cross sections assume the $Y(nS)$ are unpolarized. The statistical uncertainty (stat.), the sum in quadrature of the systematic uncertainties excluding the contribution from the polarization uncertainty ($\Sigma_{\text{syst.}}$), the systematic uncertainties from the polarization (syst.(pol)), and the total uncertainty ($\Delta\sigma$; including stat., $\Sigma_{\text{syst.}}$, syst.(pol), and the uncertainty in the integrated luminosity) are in percent. The numbers in parentheses are negative variations.

		$ y^Y < 1.2$				
	p_T (GeV/ c)	$\sigma \cdot \mathcal{B}$ (nb)	stat. σ	$\Sigma_{\text{syst.}}$ σ	syst.(pol.) σ	$\Delta\sigma$ σ
Y(1S)	10–11	0.139	2.8	8 (7)	5 (1)	10 (9)
	11–12	0.0949	3.4	5 (4)	4 (1)	8 (7)
	12–13	0.0779	3.6	6 (5)	3 (1)	8 (8)
	13–14	0.0540	4.1	5 (4)	3 (1)	8 (7)
	14–15	0.0436	4.4	5 (5)	3 (1)	9 (8)
	15–16	0.0322	5.0	5 (5)	3 (1)	9 (8)
	16–18	0.0415	4.2	5 (4)	2 (2)	8 (8)
	18–20	0.0286	4.9	5 (4)	2 (2)	8 (8)
	20–22	0.0164	6.4	4 (4)	2 (2)	9 (9)
	22–25	0.0113	7.6	5 (4)	2 (2)	10 (10)
25–30	0.0105	7.8	4 (4)	1 (2)	10 (10)	
	30–50	0.00720	9.4	5 (5)	3 (2)	12 (12)
	10–50	0.558	1.3	6 (5)	4 (2)	8 (7)
Y(2S)	10–11.5	0.0661	4.9	8 (8)	9 (3)	13 (10)
	11.5–13	0.0400	5.7	6 (6)	8 (4)	12 (10)
	13–14.5	0.0287	6.3	6 (5)	8 (4)	12 (10)
	14.5–16	0.0206	6.9	6 (6)	7 (4)	12 (11)
	16–18	0.0215	6.4	9 (9)	6 (3)	13 (12)
	18–19.5	0.0091	9.5	6 (5)	5 (3)	13 (12)
	19.5–22	0.0108	8.5	7 (7)	6 (4)	13 (12)
	22–26	0.0089	9.3	9 (8)	7 (4)	15 (14)
	26–42	0.00737	9.7	6 (6)	6 (4)	14 (13)
	10–42	0.213	2.4	5 (5)	7 (3)	10 (8)
Y(3S)	10–13	0.0591	5.2	7 (6)	5 (3)	11 (10)
	13–16	0.0318	6.3	6 (5)	8 (4)	12 (10)
	16–18	0.0129	9.1	10 (10)	9 (5)	17 (15)
	18–22	0.0128	8.4	7 (7)	8 (4)	14 (12)
	22–38	0.0104	8.9	6 (6)	6 (4)	13 (12)
	10–38	0.127	3.2	7 (5)	7 (3)	11 (8)

B The CMS Collaboration

Yerevan Physics Institute, Yerevan, Armenia

S. Chatrchyan, V. Khachatryan, A.M. Sirunyan, A. Tumasyan

Institut für Hochenergiephysik der OeAW, Wien, Austria

W. Adam, E. Aguilo, T. Bergauer, M. Dragicevic, J. Erö, C. Fabjan¹, M. Friedl, R. Frühwirth¹, V.M. Ghete, N. Hörmann, J. Hrubec, M. Jeitler¹, W. Kiesenhofer, V. Knünz, M. Krammer¹, I. Krätschmer, D. Liko, I. Mikulec, M. Pernicka[†], D. Rabady², B. Rahbaran, C. Rohringer, H. Rohringer, R. Schöfbeck, J. Strauss, A. Taurok, W. Waltenberger, C.-E. Wulz¹

National Centre for Particle and High Energy Physics, Minsk, Belarus

V. Mossolov, N. Shumeiko, J. Suarez Gonzalez

Universiteit Antwerpen, Antwerpen, Belgium

M. Bansal, S. Bansal, T. Cornelis, E.A. De Wolf, X. Janssen, S. Luyckx, L. Mucibello, S. Ochesanu, B. Roland, R. Rougny, M. Selvaggi, H. Van Haevermaet, P. Van Mechelen, N. Van Remortel, A. Van Spilbeeck

Vrije Universiteit Brussel, Brussel, Belgium

F. Blekman, S. Blyweert, J. D'Hondt, R. Gonzalez Suarez, A. Kalogeropoulos, M. Maes, A. Olbrechts, W. Van Doninck, P. Van Mulders, G.P. Van Onsem, I. Villella

Université Libre de Bruxelles, Bruxelles, Belgium

B. Clerbaux, G. De Lentdecker, V. Dero, A.P.R. Gay, T. Hreus, A. Léonard, P.E. Marage, A. Mohammadi, T. Reis, L. Thomas, C. Vander Velde, P. Vanlaer, J. Wang

Ghent University, Ghent, Belgium

V. Adler, K. Bernaert, A. Cimmino, S. Costantini, G. Garcia, M. Grunewald, B. Klein, J. Lellouch, A. Marinov, J. McCartin, A.A. Ocampo Rios, D. Ryckbosch, M. Sigamani, N. Strobbe, F. Thyssen, M. Tytgat, S. Walsh, E. Yazgan, N. Zaganidis

Université Catholique de Louvain, Louvain-la-Neuve, Belgium

S. Basegmez, G. Bruno, R. Castello, L. Ceard, C. Delaere, T. du Pree, D. Favart, L. Forthomme, A. Giammanco³, J. Hollar, V. Lemaitre, J. Liao, O. Militaru, C. Nuttens, D. Pagano, A. Pin, K. Piotrkowski, J.M. Vizan Garcia

Université de Mons, Mons, Belgium

N. Belyi, T. Caebergs, E. Daubie, G.H. Hammad

Centro Brasileiro de Pesquisas Fisicas, Rio de Janeiro, Brazil

G.A. Alves, M. Correa Martins Junior, T. Martins, M.E. Pol, M.H.G. Souza

Universidade do Estado do Rio de Janeiro, Rio de Janeiro, Brazil

W.L. Aldá Júnior, W. Carvalho, A. Custódio, E.M. Da Costa, D. De Jesus Damiao, C. De Oliveira Martins, S. Fonseca De Souza, H. Malbouisson, M. Malek, D. Matos Figueiredo, L. Mundim, H. Nogima, W.L. Prado Da Silva, A. Santoro, L. Soares Jorge, A. Sznajder, A. Vilela Pereira

Universidade Estadual Paulista ^a, Universidade Federal do ABC ^b, São Paulo, Brazil

T.S. Anjos^b, C.A. Bernardes^b, F.A. Dias^{a,4}, T.R. Fernandez Perez Tomei^a, E.M. Gregores^b, C. Lagana^a, F. Marinho^a, P.G. Mercadante^b, S.F. Novaes^a, Sandra S. Padula^a

Institute for Nuclear Research and Nuclear Energy, Sofia, Bulgaria

V. Genchev², P. Iaydjiev², S. Piperov, M. Rodozov, S. Stoykova, G. Sultanov, V. Tcholakov, R. Trayanov, M. Vutova

University of Sofia, Sofia, Bulgaria

A. Dimitrov, R. Hadjiiska, V. Kozhuharov, L. Litov, B. Pavlov, P. Petkov

Institute of High Energy Physics, Beijing, China

J.G. Bian, G.M. Chen, H.S. Chen, C.H. Jiang, D. Liang, S. Liang, X. Meng, J. Tao, J. Wang, X. Wang, Z. Wang, H. Xiao, M. Xu, J. Zang, Z. Zhang

State Key Laboratory of Nuclear Physics and Technology, Peking University, Beijing, China

C. Asawatangtrakuldee, Y. Ban, Y. Guo, W. Li, S. Liu, Y. Mao, S.J. Qian, H. Teng, D. Wang, L. Zhang, W. Zou

Universidad de Los Andes, Bogota, Colombia

C. Avila, C.A. Carrillo Montoya, J.P. Gomez, B. Gomez Moreno, A.F. Osorio Oliveros, J.C. Sanabria

Technical University of Split, Split, Croatia

N. Godinovic, D. Lelas, R. Plestina⁵, D. Polic, I. Puljak²

University of Split, Split, Croatia

Z. Antunovic, M. Kovac

Institute Rudjer Boskovic, Zagreb, Croatia

V. Brigljevic, S. Duric, K. Kadija, J. Luetic, D. Mekterovic, S. Morovic

University of Cyprus, Nicosia, Cyprus

A. Attikis, M. Galanti, G. Mavromanolakis, J. Mousa, C. Nicolaou, F. Ptochos, P.A. Razis

Charles University, Prague, Czech Republic

M. Finger, M. Finger Jr.

Academy of Scientific Research and Technology of the Arab Republic of Egypt, Egyptian Network of High Energy Physics, Cairo, Egypt

Y. Assran⁶, S. Elgammal⁷, A. Ellithi Kamel⁸, M.A. Mahmoud⁹, A. Mahrous¹⁰, A. Radi^{11,12}

National Institute of Chemical Physics and Biophysics, Tallinn, Estonia

M. Kadastik, M. Müntel, M. Murumaa, M. Raidal, L. Rebane, A. Tiko

Department of Physics, University of Helsinki, Helsinki, Finland

P. Eerola, G. Fedi, M. Voutilainen

Helsinki Institute of Physics, Helsinki, Finland

J. Härkönen, A. Heikkinen, V. Karimäki, R. Kinnunen, M.J. Kortelainen, T. Lampén, K. Lassila-Perini, S. Lehti, T. Lindén, P. Luukka, T. Mäenpää, T. Peltola, E. Tuominen, J. Tuominiemi, E. Tuovinen, D. Ungaro, L. Wendland

Lappeenranta University of Technology, Lappeenranta, Finland

K. Banzuzi, A. Karjalainen, A. Korpela, T. Tuuva

DSM/IRFU, CEA/Saclay, Gif-sur-Yvette, France

M. Besancon, S. Choudhury, M. Dejardin, D. Denegri, B. Fabbro, J.L. Faure, F. Ferri, S. Ganjour, A. Givernaud, P. Gras, G. Hamel de Monchenault, P. Jarry, E. Locci, J. Malcles, L. Millischer, A. Nayak, J. Rander, A. Rosowsky, M. Titov

Laboratoire Leprince-Ringuet, Ecole Polytechnique, IN2P3-CNRS, Palaiseau, France

S. Baffioni, F. Beaudette, L. Benhabib, L. Bianchini, M. Bluj¹³, P. Busson, C. Charlot, N. Daci, T. Dahms, M. Dalchenko, L. Dobrzynski, A. Florent, R. Granier de Cassagnac, M. Haguenaer,

P. Miné, C. Mironov, I.N. Naranjo, M. Nguyen, C. Ochando, P. Paganini, D. Sabes, R. Salerno, Y. Sirois, C. Veelken, A. Zabi

Institut Pluridisciplinaire Hubert Curien, Université de Strasbourg, Université de Haute Alsace Mulhouse, CNRS/IN2P3, Strasbourg, France

J.-L. Agram¹⁴, J. Andrea, D. Bloch, D. Bodin, J.-M. Brom, M. Cardaci, E.C. Chabert, C. Collard, E. Conte¹⁴, F. Drouhin¹⁴, J.-C. Fontaine¹⁴, D. Gelé, U. Goerlach, P. Juillot, A.-C. Le Bihan, P. Van Hove

Centre de Calcul de l'Institut National de Physique Nucleaire et de Physique des Particules, CNRS/IN2P3, Villeurbanne, France

F. Fassi, D. Mercier

Université de Lyon, Université Claude Bernard Lyon 1, CNRS-IN2P3, Institut de Physique Nucléaire de Lyon, Villeurbanne, France

S. Beauceron, N. Beaupere, O. Bondu, G. Boudoul, S. Brochet, J. Chasserat, R. Chierici², D. Contardo, P. Depasse, H. El Mamouni, J. Fay, S. Gascon, M. Gouzevitch, B. Ille, T. Kurca, M. Lethuillier, L. Mirabito, S. Perries, L. Sgandurra, V. Sordini, Y. Tschudi, P. Verdier, S. Viret

Institute of High Energy Physics and Informatization, Tbilisi State University, Tbilisi, Georgia

Z. Tsamalaidze¹⁵

RWTH Aachen University, I. Physikalisches Institut, Aachen, Germany

C. Autermann, S. Beranek, B. Calpas, M. Edelhoff, L. Feld, N. Heracleous, O. Hindrichs, R. Jussen, K. Klein, J. Merz, A. Ostapchuk, A. Perieanu, F. Raupach, J. Sammet, S. Schael, D. Sprenger, H. Weber, B. Wittmer, V. Zhukov¹⁶

RWTH Aachen University, III. Physikalisches Institut A, Aachen, Germany

M. Ata, J. Caudron, E. Dietz-Laursonn, D. Duchardt, M. Erdmann, R. Fischer, A. Güth, T. Hebbeker, C. Heidemann, K. Hoepfner, D. Klingebiel, P. Kreuzer, M. Merschmeyer, A. Meyer, M. Olschewski, P. Papacz, H. Pieta, H. Reithler, S.A. Schmitz, L. Sonnenschein, J. Steggemann, D. Teyssier, S. Thüer, M. Weber

RWTH Aachen University, III. Physikalisches Institut B, Aachen, Germany

M. Bontenackels, V. Cherepanov, Y. Erdogan, G. Flügge, H. Geenen, M. Geisler, W. Haj Ahmad, F. Hoehle, B. Kargoll, T. Kress, Y. Kuessel, J. Lingemann², A. Nowack, L. Perchalla, O. Pooth, P. Sauerland, A. Stahl

Deutsches Elektronen-Synchrotron, Hamburg, Germany

M. Aldaya Martin, J. Behr, W. Behrenhoff, U. Behrens, M. Bergholz¹⁷, A. Bethani, K. Borras, A. Burgmeier, A. Cakir, L. Calligaris, A. Campbell, E. Castro, F. Costanza, D. Dammann, C. Diez Pardos, G. Eckerlin, D. Eckstein, G. Flucke, A. Geiser, I. Glushkov, P. Gunnellini, S. Habib, J. Hauk, G. Hellwig, H. Jung, M. Kasemann, P. Katsas, C. Kleinwort, H. Kluge, A. Knutsson, M. Krämer, D. Krücker, E. Kuznetsova, W. Lange, J. Leonard, W. Lohmann¹⁷, B. Lutz, R. Mankel, I. Marfin, M. Marienfeld, I.-A. Melzer-Pellmann, A.B. Meyer, J. Mnich, A. Mussgiller, S. Naumann-Emme, O. Novgorodova, F. Nowak, J. Olzem, H. Perrey, A. Petrukhin, D. Pitzl, A. Raspereza, P.M. Ribeiro Cipriano, C. Riedl, E. Ron, M. Rosin, J. Salfeld-Nebgen, R. Schmidt¹⁷, T. Schoerner-Sadenius, N. Sen, A. Spiridonov, M. Stein, R. Walsh, C. Wissing

University of Hamburg, Hamburg, Germany

V. Blobel, H. Enderle, J. Erfle, U. Gebbert, M. Görner, M. Gosselink, J. Haller, T. Hermanns, R.S. Höing, K. Kaschube, G. Kaussen, H. Kirschenmann, R. Klanner, J. Lange, T. Peiffer,

N. Pietsch, D. Rathjens, C. Sander, H. Schettler, P. Schleper, E. Schlieckau, A. Schmidt, M. Schröder, T. Schum, M. Seidel, J. Sibille¹⁸, V. Sola, H. Stadie, G. Steinbrück, J. Thomsen, L. Vanelderren

Institut für Experimentelle Kernphysik, Karlsruhe, Germany

C. Barth, J. Berger, C. Böser, T. Chwalek, W. De Boer, A. Descroix, A. Dierlamm, M. Feindt, M. Guthoff², C. Hackstein, F. Hartmann², T. Hauth², M. Heinrich, H. Held, K.H. Hoffmann, U. Husemann, I. Katkov¹⁶, J.R. Komaragiri, P. Lobelle Pardo, D. Martschei, S. Mueller, Th. Müller, M. Niegel, A. Nürnberg, O. Oberst, A. Oehler, J. Ott, G. Quast, K. Rabbertz, F. Ratnikov, N. Ratnikova, S. Röcker, F.-P. Schilling, G. Schott, H.J. Simonis, F.M. Stober, D. Troendle, R. Ulrich, J. Wagner-Kuhr, S. Wayand, T. Weiler, M. Zeise

Institute of Nuclear and Particle Physics (INPP), NCSR Demokritos, Aghia Paraskevi, Greece

G. Anagnostou, G. Daskalakis, T. Geralis, S. Kesisoglou, A. Kyriakis, D. Loukas, I. Manolakos, A. Markou, C. Markou, E. Ntomari

University of Athens, Athens, Greece

L. Gouskos, T.J. Mertzimekis, A. Panagiotou, N. Saoulidou

University of Ioánnina, Ioánnina, Greece

I. Evangelou, C. Foudas, P. Kokkas, N. Manthos, I. Papadopoulos, V. Patras

KFKI Research Institute for Particle and Nuclear Physics, Budapest, Hungary

G. Bencze, C. Hajdu, P. Hidas, D. Horvath¹⁹, F. Sikler, V. Veszpremi, G. Vesztergombi²⁰, A.J. Zsigmond

Institute of Nuclear Research ATOMKI, Debrecen, Hungary

N. Beni, S. Czellar, J. Molnar, J. Palinkas, Z. Szillasi

University of Debrecen, Debrecen, Hungary

J. Karancsi, P. Raics, Z.L. Trocsanyi, B. Ujvari

Panjab University, Chandigarh, India

S.B. Beri, V. Bhatnagar, N. Dhingra, R. Gupta, M. Kaur, M.Z. Mehta, N. Nishu, L.K. Saini, A. Sharma, J.B. Singh

University of Delhi, Delhi, India

Ashok Kumar, Arun Kumar, S. Ahuja, A. Bhardwaj, B.C. Choudhary, S. Malhotra, M. Naimuddin, K. Ranjan, V. Sharma, R.K. Shivpuri

Saha Institute of Nuclear Physics, Kolkata, India

S. Banerjee, S. Bhattacharya, S. Dutta, B. Gomber, Sa. Jain, Sh. Jain, R. Khurana, S. Sarkar, M. Sharan

Bhabha Atomic Research Centre, Mumbai, India

A. Abdulsalam, D. Dutta, S. Kailas, V. Kumar, A.K. Mohanty², L.M. Pant, P. Shukla

Tata Institute of Fundamental Research - EHEP, Mumbai, India

T. Aziz, S. Ganguly, M. Guchait²¹, A. Gurtu²², M. Maity²³, G. Majumder, K. Mazumdar, G.B. Mohanty, B. Parida, K. Sudhakar, N. Wickramage

Tata Institute of Fundamental Research - HECR, Mumbai, India

S. Banerjee, S. Dugad

Institute for Research in Fundamental Sciences (IPM), Tehran, Iran

H. Arfaei²⁴, H. Bakhshiansohi, S.M. Etesami²⁵, A. Fahim²⁴, M. Hashemi²⁶, H. Hesari, A. Jafari, M. Khakzad, M. Mohammadi Najafabadi, S. Paktinat Mehdiabadi, B. Safarzadeh²⁷, M. Zeinali

INFN Sezione di Bari ^a, Università di Bari ^b, Politecnico di Bari ^c, Bari, Italy

M. Abbrescia^{a,b}, L. Barbone^{a,b}, C. Calabria^{a,b,2}, S.S. Chhibra^{a,b}, A. Colaleo^a, D. Creanza^{a,c}, N. De Filippis^{a,c,2}, M. De Palma^{a,b}, L. Fiore^a, G. Iaselli^{a,c}, G. Maggi^{a,c}, M. Maggi^a, B. Marangelli^{a,b}, S. My^{a,c}, S. Nuzzo^{a,b}, N. Pacifico^a, A. Pompili^{a,b}, G. Pugliese^{a,c}, G. Selvaggi^{a,b}, L. Silvestris^a, G. Singh^{a,b}, R. Venditti^{a,b}, P. Verwilligen^a, G. Zito^a

INFN Sezione di Bologna ^a, Università di Bologna ^b, Bologna, Italy

G. Abbiendi^a, A.C. Benvenuti^a, D. Bonacorsi^{a,b}, S. Braibant-Giacomelli^{a,b}, L. Brigliadori^{a,b}, P. Capiluppi^{a,b}, A. Castro^{a,b}, F.R. Cavallo^a, M. Cuffiani^{a,b}, G.M. Dallavalle^a, F. Fabbri^a, A. Fanfani^{a,b}, D. Fasanella^{a,b}, P. Giacomelli^a, C. Grandi^a, L. Guiducci^{a,b}, S. Marcellini^a, G. Masetti^a, M. Meneghelli^{a,b,2}, A. Montanari^a, F.L. Navarria^{a,b}, F. Odorici^a, A. Perrotta^a, F. Primavera^{a,b}, A.M. Rossi^{a,b}, T. Rovelli^{a,b}, G.P. Siroli^{a,b}, N. Tosi^{a,b}, R. Travaglini^{a,b}

INFN Sezione di Catania ^a, Università di Catania ^b, Catania, Italy

S. Albergo^{a,b}, G. Cappello^{a,b}, M. Chiorboli^{a,b}, S. Costa^{a,b}, R. Potenza^{a,b}, A. Tricomi^{a,b}, C. Tuve^{a,b}

INFN Sezione di Firenze ^a, Università di Firenze ^b, Firenze, Italy

G. Barbagli^a, V. Ciulli^{a,b}, C. Civinini^a, R. D'Alessandro^{a,b}, E. Focardi^{a,b}, S. Frosali^{a,b}, E. Gallo^a, S. Gonzi^{a,b}, M. Meschini^a, S. Paoletti^a, G. Sguazzoni^a, A. Tropiano^{a,b}

INFN Laboratori Nazionali di Frascati, Frascati, Italy

L. Benussi, S. Bianco, S. Colafranceschi²⁸, F. Fabbri, D. Piccolo

INFN Sezione di Genova ^a, Università di Genova ^b, Genova, Italy

P. Fabbricatore^a, R. Musenich^a, S. Tosi^{a,b}

INFN Sezione di Milano-Bicocca ^a, Università di Milano-Bicocca ^b, Milano, Italy

A. Benaglia^a, F. De Guio^{a,b}, L. Di Matteo^{a,b,2}, S. Fiorendi^{a,b}, S. Gennai^{a,2}, A. Ghezzi^{a,b}, S. Malvezzi^a, R.A. Manzoni^{a,b}, A. Martelli^{a,b}, A. Massironi^{a,b}, D. Menasce^a, L. Moroni^a, M. Paganoni^{a,b}, D. Pedrini^a, S. Ragazzi^{a,b}, N. Redaelli^a, S. Sala^a, T. Tabarelli de Fatis^{a,b}

INFN Sezione di Napoli ^a, Università di Napoli 'Federico II' ^b, Università della Basilicata (Potenza) ^c, Università G. Marconi (Roma) ^d, Napoli, Italy

S. Buontempo^a, N. Cavallo^{a,c}, A. De Cosa^{a,b,2}, O. Dogangun^{a,b}, F. Fabozzi^{a,c}, A.O.M. Iorio^{a,b}, L. Lista^a, S. Meola^{a,d,29}, M. Merola^a, P. Paolucci^{a,2}

INFN Sezione di Padova ^a, Università di Padova ^b, Università di Trento (Trento) ^c, Padova, Italy

P. Azzi^a, N. Bacchetta^{a,2}, D. Bisello^{a,b}, A. Branca^{a,b,2}, R. Carlin^{a,b}, P. Checchia^a, T. Dorigo^a, U. Dosselli^a, F. Gasparini^{a,b}, U. Gasparini^{a,b}, A. Gozzelino^a, K. Kanishchev^{a,c}, S. Lacaprara^a, I. Lazzizzera^{a,c}, M. Margoni^{a,b}, A.T. Meneguzzo^{a,b}, J. Pazzini^{a,b}, N. Pozzobon^{a,b}, P. Ronchese^{a,b}, F. Simonetto^{a,b}, E. Torassa^a, M. Tosi^{a,b}, S. Vanini^{a,b}, P. Zotto^{a,b}, G. Zumerle^{a,b}

INFN Sezione di Pavia ^a, Università di Pavia ^b, Pavia, Italy

M. Gabusi^{a,b}, S.P. Ratti^{a,b}, C. Riccardi^{a,b}, P. Torre^{a,b}, P. Vitulo^{a,b}

INFN Sezione di Perugia ^a, Università di Perugia ^b, Perugia, Italy

M. Biasini^{a,b}, G.M. Bilei^a, L. Fanò^{a,b}, P. Lariccia^{a,b}, G. Mantovani^{a,b}, M. Menichelli^a, A. Nappi^{a,b,†}, F. Romeo^{a,b}, A. Saha^a, A. Santocchia^{a,b}, A. Spiezia^{a,b}, S. Taroni^{a,b}

INFN Sezione di Pisa ^a, Università di Pisa ^b, Scuola Normale Superiore di Pisa ^c, Pisa, Italy
 P. Azzurri^{a,c}, G. Bagliesi^a, J. Bernardini^a, T. Boccali^a, G. Broccolo^{a,c}, R. Castaldi^a,
 R.T. D’Agnolo^{a,c,2}, R. Dell’Orso^a, F. Fiori^{a,b,2}, L. Foà^{a,c}, A. Giassi^a, A. Kraan^a, F. Ligabue^{a,c},
 T. Lomtadze^a, L. Martini^{a,30}, A. Messineo^{a,b}, F. Palla^a, A. Rizzi^{a,b}, A.T. Serban^{a,31}, P. Spagnolo^a,
 P. Squillacioti^{a,2}, R. Tenchini^a, G. Tonelli^{a,b}, A. Venturi^a, P.G. Verdini^a

INFN Sezione di Roma ^a, Università di Roma ^b, Roma, Italy
 L. Barone^{a,b}, F. Cavallari^a, D. Del Re^{a,b}, M. Diemoz^a, C. Fanelli^{a,b}, M. Grassi^{a,b,2}, E. Longo^{a,b},
 P. Meridiani^{a,2}, F. Micheli^{a,b}, S. Nourbakhsh^{a,b}, G. Organtini^{a,b}, R. Paramatti^a, S. Rahatlou^{a,b},
 L. Soffi^{a,b}

INFN Sezione di Torino ^a, Università di Torino ^b, Università del Piemonte Orientale (Novara) ^c, Torino, Italy
 N. Amapane^{a,b}, R. Arcidiacono^{a,c}, S. Argiro^{a,b}, M. Arneodo^{a,c}, C. Biino^a, N. Cartiglia^a,
 S. Casasso^{a,b}, M. Costa^{a,b}, N. Demaria^a, C. Mariotti^{a,2}, S. Maselli^a, G. Mazza^a, E. Migliore^{a,b},
 V. Monaco^{a,b}, M. Musich^{a,2}, M.M. Obertino^{a,c}, N. Pastrone^a, M. Pelliccioni^a, A. Potenza^{a,b},
 A. Romero^{a,b}, R. Sacchi^{a,b}, A. Solano^{a,b}, A. Staiano^a

INFN Sezione di Trieste ^a, Università di Trieste ^b, Trieste, Italy
 S. Belforte^a, V. Candolise^{a,b}, M. Casarsa^a, F. Cossutti^a, G. Della Ricca^{a,b}, B. Gobbo^a,
 M. Marone^{a,b,2}, D. Montanino^{a,b,2}, A. Penzo^a, A. Schizzi^{a,b}

Kangwon National University, Chunchon, Korea

T.Y. Kim, S.K. Nam

Kyungpook National University, Daegu, Korea

S. Chang, D.H. Kim, G.N. Kim, D.J. Kong, H. Park, D.C. Son, T. Son

Chonnam National University, Institute for Universe and Elementary Particles, Kwangju, Korea

J.Y. Kim, Zero J. Kim, S. Song

Korea University, Seoul, Korea

S. Choi, D. Gyun, B. Hong, M. Jo, H. Kim, T.J. Kim, K.S. Lee, D.H. Moon, S.K. Park, Y. Roh

University of Seoul, Seoul, Korea

M. Choi, J.H. Kim, C. Park, I.C. Park, S. Park, G. Ryu

Sungkyunkwan University, Suwon, Korea

Y. Choi, Y.K. Choi, J. Goh, M.S. Kim, E. Kwon, B. Lee, J. Lee, S. Lee, H. Seo, I. Yu

Vilnius University, Vilnius, Lithuania

M.J. Bilinskas, I. Grigelionis, M. Janulis, A. Juodagalvis

Centro de Investigacion y de Estudios Avanzados del IPN, Mexico City, Mexico

H. Castilla-Valdez, E. De La Cruz-Burelo, I. Heredia-de La Cruz, R. Lopez-Fernandez,
 J. Martínez-Ortega, A. Sanchez-Hernandez, L.M. Villasenor-Cendejas

Universidad Iberoamericana, Mexico City, Mexico

S. Carrillo Moreno, F. Vazquez Valencia

Benemerita Universidad Autonoma de Puebla, Puebla, Mexico

H.A. Salazar Ibarguen

Universidad Autónoma de San Luis Potosí, San Luis Potosí, Mexico

E. Casimiro Linares, A. Morelos Pineda, M.A. Reyes-Santos

University of Auckland, Auckland, New Zealand

D. Krofcheck

University of Canterbury, Christchurch, New Zealand

A.J. Bell, P.H. Butler, R. Doesburg, S. Reucroft, H. Silverwood

National Centre for Physics, Quaid-I-Azam University, Islamabad, Pakistan

M. Ahmad, M.I. Asghar, J. Butt, H.R. Hoorani, S. Khalid, W.A. Khan, T. Khurshid, S. Qazi, M.A. Shah, M. Shoaib

National Centre for Nuclear Research, Swierk, Poland

H. Bialkowska, B. Boimska, T. Frueboes, M. Górski, M. Kazana, K. Nawrocki, K. Romanowska-Rybinska, M. Szleper, G. Wrochna, P. Zalewski

Institute of Experimental Physics, Faculty of Physics, University of Warsaw, Warsaw, Poland

G. Brona, K. Bunkowski, M. Cwiok, W. Dominik, K. Doroba, A. Kalinowski, M. Konecki, J. Krolikowski, M. Misiura

Laboratório de Instrumentação e Física Experimental de Partículas, Lisboa, Portugal

N. Almeida, P. Bargassa, A. David, P. Faccioli, P.G. Ferreira Parracho, M. Gallinaro, J. Seixas, J. Varela, P. Vischia

Joint Institute for Nuclear Research, Dubna, Russia

I. Belotelov, P. Bunin, M. Gavrilenko, I. Golutvin, I. Gorbunov, A. Kamenev, V. Karjavin, G. Kozlov, A. Lanev, A. Malakhov, P. Moisenz, V. Palichik, V. Perelygin, S. Shmatov, V. Smirnov, A. Volodko, A. Zarubin

Petersburg Nuclear Physics Institute, Gatchina (St. Petersburg), Russia

S. Evstyukhin, V. Golovtsov, Y. Ivanov, V. Kim, P. Levchenko, V. Murzin, V. Oreshkin, I. Smirnov, V. Sulimov, L. Uvarov, S. Vavilov, A. Vorobyev, An. Vorobyev

Institute for Nuclear Research, Moscow, Russia

Yu. Andreev, A. Dermenev, S. Gninenko, N. Golubev, M. Kirsanov, N. Krasnikov, V. Matveev, A. Pashenkov, D. Tlisov, A. Toropin

Institute for Theoretical and Experimental Physics, Moscow, Russia

V. Epshteyn, M. Erofeeva, V. Gavrilov, M. Kossov, N. Lychkovskaya, V. Popov, G. Safronov, S. Semenov, I. Shreyber, V. Stolin, E. Vlasov, A. Zhokin

P.N. Lebedev Physical Institute, Moscow, Russia

V. Andreev, M. Azarkin, I. Dremin, M. Kirakosyan, A. Leonidov, G. Mesyats, S.V. Rusakov, A. Vinogradov

Skobeltsyn Institute of Nuclear Physics, Lomonosov Moscow State University, Moscow, RussiaA. Belyaev, E. Boos, M. Dubinin⁴, L. Dudko, A. Ershov, A. Gribushin, V. Klyukhin, O. Kodolova, I. Lokhtin, A. Markina, S. Obraztsov, M. Perfilov, S. Petrushanko, A. Popov, L. Sarycheva[†], V. Savrin, A. Snigirev**State Research Center of Russian Federation, Institute for High Energy Physics, Protvino, Russia**I. Azhgirey, I. Bayshev, S. Bitioukov, V. Grishin², V. Kachanov, D. Konstantinov, V. Krychkin, V. Petrov, R. Ryutin, A. Sobol, L. Tourtchanovitch, S. Troshin, N. Tyurin, A. Uzunian, A. Volkov

University of Belgrade, Faculty of Physics and Vinca Institute of Nuclear Sciences, Belgrade, Serbia

P. Adzic³², M. Djordjevic, M. Ekmedzic, D. Krpic³², J. Milosevic

Centro de Investigaciones Energéticas Medioambientales y Tecnológicas (CIEMAT), Madrid, Spain

M. Aguilar-Benitez, J. Alcaraz Maestre, P. Arce, C. Battilana, E. Calvo, M. Cerrada, M. Chamizo Llatas, N. Colino, B. De La Cruz, A. Delgado Peris, D. Domínguez Vázquez, C. Fernandez Bedoya, J.P. Fernández Ramos, A. Ferrando, J. Flix, M.C. Fouz, P. Garcia-Abia, O. Gonzalez Lopez, S. Goy Lopez, J.M. Hernandez, M.I. Josa, G. Merino, J. Puerta Pelayo, A. Quintario Olmeda, I. Redondo, L. Romero, J. Santaolalla, M.S. Soares, C. Willmott

Universidad Autónoma de Madrid, Madrid, Spain

C. Albajar, G. Codispoti, J.F. de Trocóniz

Universidad de Oviedo, Oviedo, Spain

H. Brun, J. Cuevas, J. Fernandez Menendez, S. Folgueras, I. Gonzalez Caballero, L. Lloret Iglesias, J. Piedra Gomez

Instituto de Física de Cantabria (IFCA), CSIC-Universidad de Cantabria, Santander, Spain

J.A. Brochero Cifuentes, I.J. Cabrillo, A. Calderon, S.H. Chuang, J. Duarte Campderros, M. Felcini³³, M. Fernandez, G. Gomez, J. Gonzalez Sanchez, A. Graziano, C. Jorda, A. Lopez Virto, J. Marco, R. Marco, C. Martinez Rivero, F. Matorras, F.J. Munoz Sanchez, T. Rodrigo, A.Y. Rodríguez-Marrero, A. Ruiz-Jimeno, L. Scodellaro, I. Vila, R. Vilar Cortabitarte

CERN, European Organization for Nuclear Research, Geneva, Switzerland

D. Abbaneo, E. Auffray, G. Auzinger, M. Bachtis, P. Baillon, A.H. Ball, D. Barney, J.F. Benitez, C. Bernet⁵, G. Bianchi, P. Bloch, A. Bocci, A. Bonato, C. Botta, H. Breuker, T. Camporesi, G. Cerminara, T. Christiansen, J.A. Coarasa Perez, D. D'Enterria, A. Dabrowski, A. De Roeck, S. Di Guida, M. Dobson, N. Dupont-Sagorin, A. Elliott-Peisert, B. Frisch, W. Funk, G. Georgiou, M. Giffels, D. Gigi, K. Gill, D. Giordano, M. Girone, M. Giunta, F. Glege, R. Gomez-Reino Garrido, P. Govoni, S. Gowdy, R. Guida, S. Gundacker, J. Hammer, M. Hansen, P. Harris, C. Hartl, J. Harvey, B. Hegner, A. Hinzmann, V. Innocente, P. Janot, K. KAADZE, E. Karavakis, K. Kousouris, P. Lecoq, Y.-J. Lee, P. Lenzi, C. Lourenço, N. Magini, T. Mäki, M. Malberti, L. Malgeri, M. Mannelli, L. Masetti, F. Meijers, S. Mersi, E. Meschi, R. Moser, M.U. Mozer, M. Mulders, P. Musella, E. Nesvold, L. Orsini, E. Palencia Cortezon, E. Perez, L. Perrozzi, A. Petrilli, A. Pfeiffer, M. Pierini, M. Pimiä, D. Piparo, G. Polese, L. Quertenmont, A. Racz, W. Reece, J. Rodrigues Antunes, G. Rolandi³⁴, C. Rovelli³⁵, M. Rovere, H. Sakulin, F. Santanastasio, C. Schäfer, C. Schwick, I. Segoni, S. Sekmen, A. Sharma, P. Siegrist, P. Silva, M. Simon, P. Sphicas³⁶, D. Spiga, A. Tsirou, G.I. Veres²⁰, J.R. Vlimant, H.K. Wöhri, S.D. Worm³⁷, W.D. Zeuner

Paul Scherrer Institut, Villigen, Switzerland

W. Bertl, K. Deiters, W. Erdmann, K. Gabathuler, R. Horisberger, Q. Ingram, H.C. Kaestli, S. König, D. Kotlinski, U. Langenegger, F. Meier, D. Renker, T. Rohe

Institute for Particle Physics, ETH Zurich, Zurich, Switzerland

L. Bäni, P. Bortignon, M.A. Buchmann, B. Casal, N. Chanon, A. Deisher, G. Dissertori, M. Dittmar, M. Donegà, M. Dünser, P. Eller, J. Eugster, K. Freudenreich, C. Grab, D. Hits, P. Lecomte, W. Luster mann, A.C. Marini, P. Martinez Ruiz del Arbol, N. Mohr, F. Moortgat, C. Nägeli³⁸, P. Nef, F. Nessi-Tedaldi, F. Pandolfi, L. Pape, F. Pauss, M. Peruzzi, F.J. Ronga, M. Rossini, L. Sala, A.K. Sanchez, A. Starodumov³⁹, B. Stieger, M. Takahashi, L. Tauscher[†], A. Thea, K. Theofilatos, D. Treille, C. Urscheler, R. Wallny, H.A. Weber, L. Wehrli

Universität Zürich, Zurich, Switzerland

C. Amsler⁴⁰, V. Chiochia, S. De Visscher, C. Favaro, M. Ivova Rikova, B. Kilminster, B. Millan Mejias, P. Otiougova, P. Robmann, H. Snoek, S. Tupputi, M. Verzetti

National Central University, Chung-Li, Taiwan

Y.H. Chang, K.H. Chen, C. Ferro, C.M. Kuo, S.W. Li, W. Lin, Y.J. Lu, A.P. Singh, R. Volpe, S.S. Yu

National Taiwan University (NTU), Taipei, Taiwan

P. Bartalini, P. Chang, Y.H. Chang, Y.W. Chang, Y. Chao, K.F. Chen, C. Dietz, U. Grundler, W.-S. Hou, Y. Hsiung, K.Y. Kao, Y.J. Lei, R.-S. Lu, D. Majumder, E. Petrakou, X. Shi, J.G. Shiu, Y.M. Tzeng, X. Wan, M. Wang

Chulalongkorn University, Bangkok, Thailand

B. Asavapibhop, N. Srimanobhas

Cukurova University, Adana, Turkey

A. Adiguzel, M.N. Bakirci⁴¹, S. Cerci⁴², C. Dozen, I. Dumanoglu, E. Eskut, S. Girgis, G. Gokbulut, E. Gurpinar, I. Hos, E.E. Kangal, T. Karaman, G. Karapinar⁴³, A. Kayis Topaksu, G. Onengut, K. Ozdemir, S. Ozturk⁴⁴, A. Polatoz, K. Sogut⁴⁵, D. Sunar Cerci⁴², B. Tali⁴², H. Topakli⁴¹, L.N. Vergili, M. Vergili

Middle East Technical University, Physics Department, Ankara, Turkey

I.V. Akin, T. Aliev, B. Bilin, S. Bilmis, M. Deniz, H. Gamsizkan, A.M. Guler, K. Ocalan, A. Ozpineci, M. Serin, R. Sever, U.E. Surat, M. Yalvac, E. Yildirim, M. Zeyrek

Bogazici University, Istanbul, Turkey

E. Gülmez, B. Isildak⁴⁶, M. Kaya⁴⁷, O. Kaya⁴⁷, S. Ozkorucuklu⁴⁸, N. Sonmez⁴⁹

Istanbul Technical University, Istanbul, Turkey

K. Cankocak

National Scientific Center, Kharkov Institute of Physics and Technology, Kharkov, Ukraine

L. Levchuk

University of Bristol, Bristol, United Kingdom

J.J. Brooke, E. Clement, D. Cussans, H. Flacher, R. Frazier, J. Goldstein, M. Grimes, G.P. Heath, H.F. Heath, L. Kreczko, S. Metson, D.M. Newbold³⁷, K. Nirunpong, A. Poll, S. Senkin, V.J. Smith, T. Williams

Rutherford Appleton Laboratory, Didcot, United Kingdom

L. Basso⁵⁰, K.W. Bell, A. Belyaev⁵⁰, C. Brew, R.M. Brown, D.J.A. Cockerill, J.A. Coughlan, K. Harder, S. Harper, J. Jackson, B.W. Kennedy, E. Olaiya, D. Petyt, B.C. Radburn-Smith, C.H. Shepherd-Themistocleous, I.R. Tomalin, W.J. Womersley

Imperial College, London, United Kingdom

R. Bainbridge, G. Ball, R. Beuselinck, O. Buchmuller, D. Colling, N. Cripps, M. Cutajar, P. Dauncey, G. Davies, M. Della Negra, W. Ferguson, J. Fulcher, D. Futyan, A. Gilbert, A. Guneratne Bryer, G. Hall, Z. Hatherell, J. Hays, G. Iles, M. Jarvis, G. Karapostoli, L. Lyons, A.-M. Magnan, J. Marrouche, B. Mathias, R. Nandi, J. Nash, A. Nikitenko³⁹, J. Pela, M. Pesaresi, K. Petridis, M. Pioppi⁵¹, D.M. Raymond, S. Rogerson, A. Rose, M.J. Ryan, C. Seez, P. Sharp[†], A. Sparrow, M. Stoye, A. Tapper, M. Vazquez Acosta, T. Virdee, S. Wakefield, N. Wardle, T. Whyntie

Brunel University, Uxbridge, United Kingdom

M. Chadwick, J.E. Cole, P.R. Hobson, A. Khan, P. Kyberd, D. Leggat, D. Leslie, W. Martin, I.D. Reid, P. Symonds, L. Teodorescu, M. Turner

Baylor University, Waco, USA

K. Hatakeyama, H. Liu, T. Scarborough

The University of Alabama, Tuscaloosa, USA

O. Charaf, C. Henderson, P. Rumerio

Boston University, Boston, USA

A. Avetisyan, T. Bose, C. Fantasia, A. Heister, P. Lawson, D. Lazic, J. Rohlf, D. Sperka, J. St. John, L. Sulak

Brown University, Providence, USA

J. Alimena, S. Bhattacharya, G. Christopher, D. Cutts, Z. Demiragli, A. Ferapontov, A. Garabedian, U. Heintz, S. Jabeen, G. Kukartsev, E. Laird, G. Landsberg, M. Luk, M. Narain, D. Nguyen, M. Segala, T. Sinthuprasith, T. Speer

University of California, Davis, Davis, USA

R. Breedon, G. Breto, M. Calderon De La Barca Sanchez, S. Chauhan, M. Chertok, J. Conway, R. Conway, P.T. Cox, J. Dolen, R. Erbacher, M. Gardner, R. Houtz, W. Ko, A. Kopecky, R. Lander, O. Mall, T. Miceli, D. Pellett, F. Ricci-Tam, B. Rutherford, M. Searle, J. Smith, M. Squires, M. Tripathi, R. Vasquez Sierra, R. Yohay

University of California, Los Angeles, USA

V. Andreev, D. Cline, R. Cousins, J. Duris, S. Erhan, P. Everaerts, C. Farrell, J. Hauser, M. Ignatenko, C. Jarvis, G. Rakness, P. Schlein[†], P. Traczyk, V. Valuev, M. Weber

University of California, Riverside, Riverside, USA

J. Babb, R. Clare, M.E. Dinardo, J. Ellison, J.W. Gary, F. Giordano, G. Hanson, H. Liu, O.R. Long, A. Luthra, H. Nguyen, S. Paramesvaran, J. Sturdy, S. Sumowidagdo, R. Wilken, S. Wimpenny

University of California, San Diego, La Jolla, USA

W. Andrews, J.G. Branson, G.B. Cerati, S. Cittolin, D. Evans, A. Holzner, R. Kelley, M. Lebourgeois, J. Letts, I. Macneill, B. Mangano, S. Padhi, C. Palmer, G. Petrucciani, M. Pieri, M. Sani, V. Sharma, S. Simon, E. Sudano, M. Tadel, Y. Tu, A. Vartak, S. Wasserbaech⁵², F. Würthwein, A. Yagil, J. Yoo

University of California, Santa Barbara, Santa Barbara, USA

D. Barge, R. Bellan, C. Campagnari, M. D'Alfonso, T. Danielson, K. Flowers, P. Geffert, C. George, F. Golf, J. Incandela, C. Justus, P. Kalavase, D. Kovalskyi, V. Krutelyov, S. Lowette, R. Magaña Villalba, N. Mccoll, V. Pavlunin, J. Ribnik, J. Richman, R. Rossin, D. Stuart, W. To, C. West

California Institute of Technology, Pasadena, USA

A. Apresyan, A. Bornheim, J. Bunn, Y. Chen, E. Di Marco, J. Duarte, M. Gataullin, D. Kcira, Y. Ma, A. Mott, H.B. Newman, C. Rogan, M. Spiropulu, V. Timciuc, J. Veverka, R. Wilkinson, S. Xie, Y. Yang, R.Y. Zhu

Carnegie Mellon University, Pittsburgh, USA

V. Azzolini, A. Calamba, R. Carroll, T. Ferguson, Y. Iiyama, D.W. Jang, Y.F. Liu, M. Paulini, H. Vogel, I. Vorobiev

University of Colorado at Boulder, Boulder, USA

J.P. Cumalat, B.R. Drell, W.T. Ford, A. Gaz, E. Luiggi Lopez, J.G. Smith, K. Stenson, K.A. Ulmer, S.R. Wagner

Cornell University, Ithaca, USA

J. Alexander, A. Chatterjee, N. Eggert, L.K. Gibbons, B. Heltsley, W. Hopkins, A. Khukhunaishvili, B. Kreis, N. Mirman, G. Nicolas Kaufman, J.R. Patterson, A. Ryd, E. Salvati, W. Sun, W.D. Teo, J. Thom, J. Thompson, J. Tucker, J. Vaughan, Y. Weng, L. Winstrom, P. Wittich

Fairfield University, Fairfield, USA

D. Winn

Fermi National Accelerator Laboratory, Batavia, USA

S. Abdullin, M. Albrow, J. Anderson, L.A.T. Bauerdick, A. Beretvas, J. Berryhill, P.C. Bhat, K. Burkett, J.N. Butler, V. Chetluru, H.W.K. Cheung, F. Chlebana, S. Cihangir, V.D. Elvira, I. Fisk, J. Freeman, Y. Gao, D. Green, O. Gutsche, J. Hanlon, R.M. Harris, J. Hirschauer, B. Hooberman, S. Jindariani, M. Johnson, U. Joshi, B. Klima, S. Kunori, S. Kwan, C. Leonidopoulos⁵³, J. Linacre, D. Lincoln, R. Lipton, J. Lykken, K. Maeshima, J.M. Marraffino, S. Maruyama, D. Mason, P. McBride, K. Mishra, S. Mrenna, Y. Musienko⁵⁴, C. Newman-Holmes, V. O'Dell, O. Prokofyev, E. Sexton-Kennedy, S. Sharma, W.J. Spalding, L. Spiegel, L. Taylor, S. Tkaczyk, N.V. Tran, L. Uplegger, E.W. Vaandering, R. Vidal, J. Whitmore, W. Wu, F. Yang, J.C. Yun

University of Florida, Gainesville, USA

D. Acosta, P. Avery, D. Bourilkov, M. Chen, T. Cheng, S. Das, M. De Gruttola, G.P. Di Giovanni, D. Dobur, A. Drozdetskiy, R.D. Field, M. Fisher, Y. Fu, I.K. Furic, J. Gartner, J. Hugon, B. Kim, J. Konigsberg, A. Korytov, A. Kropivnitskaya, T. Kypreos, J.F. Low, K. Matchev, P. Milenovic⁵⁵, G. Mitselmakher, L. Muniz, M. Park, R. Remington, A. Rinkevicius, P. Sellers, N. Skhirtladze, M. Snowball, J. Yelton, M. Zakaria

Florida International University, Miami, USA

V. Gaultney, S. Hewamanage, L.M. Lebolo, S. Linn, P. Markowitz, G. Martinez, J.L. Rodriguez

Florida State University, Tallahassee, USA

T. Adams, A. Askew, J. Bochenek, J. Chen, B. Diamond, S.V. Gleyzer, J. Haas, S. Hagopian, V. Hagopian, M. Jenkins, K.F. Johnson, H. Prosper, V. Veeraraghavan, M. Weinberg

Florida Institute of Technology, Melbourne, USA

M.M. Baarmand, B. Dorney, M. Hohlmann, H. Kalakhety, I. Vodopiyanov, F. Yumiceva

University of Illinois at Chicago (UIC), Chicago, USA

M.R. Adams, I.M. Anghel, L. Apanasevich, Y. Bai, V.E. Bazterra, R.R. Betts, I. Bucinskaite, J. Callner, R. Cavanaugh, O. Evdokimov, L. Gauthier, C.E. Gerber, D.J. Hofman, S. Khalatyan, F. Lacroix, C. O'Brien, C. Silkworth, D. Strom, P. Turner, N. Varelas

The University of Iowa, Iowa City, USA

U. Akgun, E.A. Albayrak, B. Bilki⁵⁶, W. Clarida, F. Duru, S. Griffiths, J.-P. Merlo, H. Mermerkaya⁵⁷, A. Mestvirishvili, A. Moeller, J. Nachtman, C.R. Newsom, E. Norbeck, Y. Onel, F. Ozok⁵⁸, S. Sen, P. Tan, E. Tiras, J. Wetzel, T. Yetkin⁵⁹, K. Yi

Johns Hopkins University, Baltimore, USA

B.A. Barnett, B. Blumenfeld, S. Bolognesi, D. Fehling, G. Giurgiu, A.V. Gritsan, G. Hu, P. Maksimovic, M. Swartz, A. Whitbeck

The University of Kansas, Lawrence, USA

P. Baringer, A. Bean, G. Benelli, R.P. Kenny Iii, M. Murray, D. Noonan, S. Sanders, R. Stringer, G. Tinti, J.S. Wood

Kansas State University, Manhattan, USA

A.F. Barfuss, T. Bolton, I. Chakaberia, A. Ivanov, S. Khalil, M. Makouski, Y. Maravin, S. Shrestha, I. Svintradze

Lawrence Livermore National Laboratory, Livermore, USA

J. Gronberg, D. Lange, F. Rebassoo, D. Wright

University of Maryland, College Park, USA

A. Baden, B. Calvert, S.C. Eno, J.A. Gomez, N.J. Hadley, R.G. Kellogg, M. Kirn, T. Kolberg, Y. Lu, M. Marionneau, A.C. Mignerey, K. Pedro, A. Peterman, A. Skuja, J. Temple, M.B. Tonjes, S.C. Tonwar

Massachusetts Institute of Technology, Cambridge, USA

A. Apyan, G. Bauer, J. Bendavid, W. Busza, E. Butz, I.A. Cali, M. Chan, V. Dutta, G. Gomez Ceballos, M. Goncharov, Y. Kim, M. Klute, K. Krajczar⁶⁰, A. Levin, P.D. Luckey, T. Ma, S. Nahn, C. Paus, D. Ralph, C. Roland, G. Roland, M. Rudolph, G.S.F. Stephans, F. Stöckli, K. Sumorok, K. Sung, D. Velicanu, E.A. Wenger, R. Wolf, B. Wyslouch, M. Yang, Y. Yilmaz, A.S. Yoon, M. Zanetti, V. Zhukova

University of Minnesota, Minneapolis, USA

S.I. Cooper, B. Dahmes, A. De Benedetti, G. Franzoni, A. Gude, J. Haupt, S.C. Kao, K. Klapoetke, Y. Kubota, J. Mans, N. Pastika, R. Rusack, M. Sasseville, A. Singovsky, N. Tambe, J. Turkewitz

University of Mississippi, Oxford, USA

L.M. Cremaldi, R. Kroeger, L. Perera, R. Rahmat, D.A. Sanders

University of Nebraska-Lincoln, Lincoln, USA

E. Avdeeva, K. Bloom, S. Bose, D.R. Claes, A. Dominguez, M. Eads, J. Keller, I. Kravchenko, J. Lazo-Flores, S. Malik, G.R. Snow

State University of New York at Buffalo, Buffalo, USA

A. Godshalk, I. Iashvili, S. Jain, A. Kharchilava, A. Kumar, S. Rappoccio

Northeastern University, Boston, USA

G. Alverson, E. Barberis, D. Baumgartel, M. Chasco, J. Haley, D. Nash, T. Orimoto, D. Trocino, D. Wood, J. Zhang

Northwestern University, Evanston, USA

A. Anastassov, K.A. Hahn, A. Kubik, L. Lusito, N. Mucia, N. Odell, R.A. Ofierzynski, B. Pollack, A. Pozdnyakov, M. Schmitt, S. Stoynev, M. Velasco, S. Won

University of Notre Dame, Notre Dame, USA

L. Antonelli, D. Berry, A. Brinkerhoff, K.M. Chan, M. Hildreth, C. Jessop, D.J. Karmgard, J. Kolb, K. Lannon, W. Luo, S. Lynch, N. Marinelli, D.M. Morse, T. Pearson, M. Planer, R. Ruchti, J. Slaunwhite, N. Valls, M. Wayne, M. Wolf

The Ohio State University, Columbus, USA

B. Bylsma, L.S. Durkin, C. Hill, R. Hughes, K. Kotov, T.Y. Ling, D. Puigh, M. Rodenburg, C. Vuosalo, G. Williams, B.L. Winer

Princeton University, Princeton, USA

E. Berry, P. Elmer, V. Halyo, P. Hebda, J. Hegeman, A. Hunt, P. Jindal, S.A. Koay, D. Lopes

Pegna, P. Lujan, D. Marlow, T. Medvedeva, M. Mooney, J. Olsen, P. Piroué, X. Quan, A. Raval, H. Saka, D. Stickland, C. Tully, J.S. Werner, S.C. Zenz, A. Zuranski

University of Puerto Rico, Mayaguez, USA

E. Brownson, A. Lopez, H. Mendez, J.E. Ramirez Vargas

Purdue University, West Lafayette, USA

E. Alagoz, V.E. Barnes, D. Benedetti, G. Bolla, D. Bortoletto, M. De Mattia, A. Everett, Z. Hu, M. Jones, O. Koybasi, M. Kress, A.T. Laasanen, N. Leonardo, V. Maroussov, P. Merkel, D.H. Miller, N. Neumeister, I. Shipsey, D. Silvers, A. Svyatkovskiy, M. Vidal Marono, H.D. Yoo, J. Zablocki, Y. Zheng

Purdue University Calumet, Hammond, USA

S. Guragain, N. Parashar

Rice University, Houston, USA

A. Adair, B. Akgun, C. Boulahouache, K.M. Ecklund, F.J.M. Geurts, W. Li, B.P. Padley, R. Redjimi, J. Roberts, J. Zabel

University of Rochester, Rochester, USA

B. Betchart, A. Bodek, Y.S. Chung, R. Covarelli, P. de Barbaro, R. Demina, Y. Eshaq, T. Ferbel, A. Garcia-Bellido, P. Goldenzweig, J. Han, A. Harel, D.C. Miner, D. Vishnevskiy, M. Zielinski

The Rockefeller University, New York, USA

A. Bhatti, R. Ciesielski, L. Demortier, K. Goulios, G. Lungu, S. Malik, C. Mesropian

Rutgers, The State University of New Jersey, Piscataway, USA

S. Arora, A. Barker, J.P. Chou, C. Contreras-Campana, E. Contreras-Campana, D. Duggan, D. Ferencek, Y. Gershtein, R. Gray, E. Halkiadakis, D. Hidas, A. Lath, S. Panwalkar, M. Park, R. Patel, V. Rekovic, J. Robles, K. Rose, S. Salur, S. Schnetzer, C. Seitz, S. Somalwar, R. Stone, S. Thomas, M. Walker

University of Tennessee, Knoxville, USA

G. Cerizza, M. Hollingsworth, S. Spanier, Z.C. Yang, A. York

Texas A&M University, College Station, USA

R. Eusebi, W. Flanagan, J. Gilmore, T. Kamon⁶¹, V. Khotilovich, R. Montalvo, I. Osipenkov, Y. Pakhotin, A. Perloff, J. Roe, A. Safonov, T. Sakuma, S. Sengupta, I. Suarez, A. Tatarinov, D. Toback

Texas Tech University, Lubbock, USA

N. Akchurin, J. Damgov, C. Dragoiu, P.R. Duderu, C. Jeong, K. Kovitangoon, S.W. Lee, T. Libeiro, I. Volobouev

Vanderbilt University, Nashville, USA

E. Appelt, A.G. Delannoy, C. Florez, S. Greene, A. Gurrola, W. Johns, P. Kurt, C. Maguire, A. Melo, M. Sharma, P. Sheldon, B. Snook, S. Tuo, J. Velkovska

University of Virginia, Charlottesville, USA

M.W. Arenton, M. Balazs, S. Boutle, B. Cox, B. Francis, J. Goodell, R. Hirosky, A. Ledovskoy, C. Lin, C. Neu, J. Wood

Wayne State University, Detroit, USA

S. Gollapinni, R. Harr, P.E. Karchin, C. Kottachchi Kankanamge Don, P. Lamichhane, A. Sakharov

University of Wisconsin, Madison, USA

M. Anderson, D.A. Belknap, L. Borrello, D. Carlsmith, M. Cepeda, S. Dasu, E. Friis, L. Gray, K.S. Grogg, M. Grothe, R. Hall-Wilton, M. Herndon, A. Hervé, P. Klabbers, J. Klukas, A. Lanaro, C. Lazaridis, R. Loveless, A. Mohapatra, I. Ojalvo, F. Palmonari, G.A. Pierro, I. Ross, A. Savin, W.H. Smith, J. Swanson

†: Deceased

- 1: Also at Vienna University of Technology, Vienna, Austria
- 2: Also at CERN, European Organization for Nuclear Research, Geneva, Switzerland
- 3: Also at National Institute of Chemical Physics and Biophysics, Tallinn, Estonia
- 4: Also at California Institute of Technology, Pasadena, USA
- 5: Also at Laboratoire Leprince-Ringuet, Ecole Polytechnique, IN2P3-CNRS, Palaiseau, France
- 6: Also at Suez Canal University, Suez, Egypt
- 7: Also at Zewail City of Science and Technology, Zewail, Egypt
- 8: Also at Cairo University, Cairo, Egypt
- 9: Also at Fayoum University, El-Fayoum, Egypt
- 10: Also at Helwan University, Cairo, Egypt
- 11: Also at British University in Egypt, Cairo, Egypt
- 12: Now at Ain Shams University, Cairo, Egypt
- 13: Also at National Centre for Nuclear Research, Swierk, Poland
- 14: Also at Université de Haute Alsace, Mulhouse, France
- 15: Also at Joint Institute for Nuclear Research, Dubna, Russia
- 16: Also at Skobeltsyn Institute of Nuclear Physics, Lomonosov Moscow State University, Moscow, Russia
- 17: Also at Brandenburg University of Technology, Cottbus, Germany
- 18: Also at The University of Kansas, Lawrence, USA
- 19: Also at Institute of Nuclear Research ATOMKI, Debrecen, Hungary
- 20: Also at Eötvös Loránd University, Budapest, Hungary
- 21: Also at Tata Institute of Fundamental Research - HECR, Mumbai, India
- 22: Now at King Abdulaziz University, Jeddah, Saudi Arabia
- 23: Also at University of Visva-Bharati, Santiniketan, India
- 24: Also at Sharif University of Technology, Tehran, Iran
- 25: Also at Isfahan University of Technology, Isfahan, Iran
- 26: Also at Shiraz University, Shiraz, Iran
- 27: Also at Plasma Physics Research Center, Science and Research Branch, Islamic Azad University, Tehran, Iran
- 28: Also at Facoltà Ingegneria, Università di Roma, Roma, Italy
- 29: Also at Università degli Studi Guglielmo Marconi, Roma, Italy
- 30: Also at Università degli Studi di Siena, Siena, Italy
- 31: Also at University of Bucharest, Faculty of Physics, Bucuresti-Magurele, Romania
- 32: Also at Faculty of Physics, University of Belgrade, Belgrade, Serbia
- 33: Also at University of California, Los Angeles, USA
- 34: Also at Scuola Normale e Sezione dell'INFN, Pisa, Italy
- 35: Also at INFN Sezione di Roma, Roma, Italy
- 36: Also at University of Athens, Athens, Greece
- 37: Also at Rutherford Appleton Laboratory, Didcot, United Kingdom
- 38: Also at Paul Scherrer Institut, Villigen, Switzerland
- 39: Also at Institute for Theoretical and Experimental Physics, Moscow, Russia
- 40: Also at Albert Einstein Center for Fundamental Physics, Bern, Switzerland
- 41: Also at Gaziosmanpasa University, Tokat, Turkey

-
- 42: Also at Adiyaman University, Adiyaman, Turkey
43: Also at Izmir Institute of Technology, Izmir, Turkey
44: Also at The University of Iowa, Iowa City, USA
45: Also at Mersin University, Mersin, Turkey
46: Also at Ozyegin University, Istanbul, Turkey
47: Also at Kafkas University, Kars, Turkey
48: Also at Suleyman Demirel University, Isparta, Turkey
49: Also at Ege University, Izmir, Turkey
50: Also at School of Physics and Astronomy, University of Southampton, Southampton, United Kingdom
51: Also at INFN Sezione di Perugia; Università di Perugia, Perugia, Italy
52: Also at Utah Valley University, Orem, USA
53: Now at University of Edinburgh, Scotland, Edinburgh, United Kingdom
54: Also at Institute for Nuclear Research, Moscow, Russia
55: Also at University of Belgrade, Faculty of Physics and Vinca Institute of Nuclear Sciences, Belgrade, Serbia
56: Also at Argonne National Laboratory, Argonne, USA
57: Also at Erzincan University, Erzincan, Turkey
58: Also at Mimar Sinan University, Istanbul, Istanbul, Turkey
59: Also at Yildiz Technical University, Istanbul, Turkey
60: Also at KFKI Research Institute for Particle and Nuclear Physics, Budapest, Hungary
61: Also at Kyungpook National University, Daegu, Korea